PHYSICAL MODEL SIMULATION OF SHALLOW OPENINGS IN ROCK MASS UNDER STATIC AND DYNAMIC CONDITIONS

Chatkun Sakulnitichai

A Thesis Submitted in Partial Fulfillment of the Requirements for the

Degree of Master of Engineering in Geotechnology

Suranaree University of Technology

Academic Year 2009

การจำลองทางกายภาพขององุโมงค์ระดับตื้นในมวลหิน ภายใต้สภาวะสถิตยศาสตร์และพลศาสตร์

นายชาติคุณ สกุลนิติชัย

วิทยานิพนธ์นี้เป็นส่วนหนึ่งของการศึกษาตามหลักสูตรปริญญาวิศวกรรมศาสตรมหาบัณฑิต

สาขาวิชาเทคโนโลยีธรณี

มหาวิทยาลัยเทคโนโลยีสุรนารี

ปีการศึกษา 2552

PHYSICAL MODEL SIMULATION OF SHALLOW OPENINGS IN ROCK MASS UNDER STATIC AND DYNAMIC CONDITIONS

Suranaree University of Technology has approved this thesis submitted in partial fulfillment of the requirements for a Master's Degree.

Thesis Examining Committee

_____

(Asst. Prof. Thara Lekuthai)

Chairperson

_____

(Assoc. Prof. Dr. Kittitep Fuenkajorn)

Member (Thesis Advisor)

_____

(Dr. Prachya Tepnarong)

Member

_____

(Prof. Dr. Pairote Sattayatham)

Vice Rector for Academic Affairs

_____

(Assoc. Prof. Dr. Vorapot Khompis)

Dean of Institute of Engineering

ชาติคุณ สกุลนิติชัย : การจำลองทางกายภาพของอุโมงค์ระดับตื้นในมวลหินภายใต้สภาวะสถิตยศาสตร์และพลศาสตร์ (PHYSICAL MODEL SIMULATION OF SHALLOW OPENINGS IN ROCK MASS UNDER STATIC AND DYNAMIC CONDITIONS) อาจารย์ที่ปรึกษา : รองศาสตราจารย์ ดร. กิตติเทพ เฟื่องขจร, 117 หน้า

แบบจำลองทางกายภาพหรือแบบจำลองย่อส่วนได้ถูกใช้อย่างแพร่หลายในห้องปฏิบัติการเพื่อจำลองเสถียรภาพของอุโมงค์ในมวลหิน แบบจำลองเหล่านี้โดยทั่วไปจะถูกใช้เพื่อให้เข้าใจถึงผลกระทบจากคุณลักษณะของมวลหิน สภาวะความเค้นในที่หรือจากรูปทรงเลขาคณิตของอุโมงค์ การจำลองจากสภาวะจริงจะทำให้ง่ายขึ้น โดยการลดคุณลักษณะสภาวะจริงจากสามมิติเป็นสองมิติ เครื่องมือบางชนิดสามารถหาผลกระทบของแรงในเชิงพลศาสตร์ที่กระทำต่อมวลหินได้ ผลจากการจำลองมักนำมาเปรียบเทียบกับผลของระเบียบวิธีเชิงตัวเลขเพื่อที่จะยืนยันผลการคำนวณด้วยวิธีดังกล่าวหรือเพื่อตรวจสอบความแม่นยำของแบบจำลอง นักวิจัยส่วนใหญ่จะเน้นการศึกษาไปที่เสถียรภาพของอุโมงค์ภายใต้สภาวะที่จำกัดสภาวะหนึ่ง ดังนั้นผลจากการจำลองที่สามารถนำมาใช้ได้อย่างแพร่หลายจึงหาได้ยาก

วัตถุประสงค์ของงานวิจัยนี้คือ เพื่อหาผลกระทบของความลึก ระยะห่างระหว่างรอยแตกและทิศทางของรอยแตกต่อความกว้างสูงสุดของอุโมงค์ที่ไม่มีการค้ำยันในระดับตื้นภายใต้สภาวะสถิตยศาสตร์และพลศาสตร์ โดยใช้แบบจำลองทางกายภาพ โดยนำหินทรายจากชุดภูพานมาจัดเตรียมเป็นรูปลูกบาศก์และรูปสี่เหลี่ยมผืนผ้าแล้วนำมาจัดเรียงในโครงทดสอบที่วางตัวอยู่ในแนวดิ่ง เพื่อจำลองภาพตัดขวางของอุโมงค์เดี่ยวรูปสี่เหลี่ยมผืนผ้าในมวลหินแบบสองมิติ โดยรอยต่อระหว่างก้อนตัวอย่างหินได้ใช้เป็นตัวแทนของรอยแตกสองชุดที่มีทิศทางตั้งฉากกันในมวลหิน ผลจากการทดสอบพบว่า ความกว้างสูงสุดที่ไม่มีการค้ำยันของอุโมงค์ต่อระยะห่างระหว่างรอยแตกในแนวดิ่งจะเพิ่มขึ้นอย่างรวดเร็วตามความลึก และจะมีแนวโน้มเท่ากับค่าคงที่ค่าหนึ่งสำหรับแต่ละอัตราส่วนของรอยแตกระหว่างแนวดิ่งและแนวนอน (S_V/S_H) ความกว้างสูงสุดนี้จะมีค่าเพิ่มขึ้นถ้าอัตราส่วนของรอยแตกระหว่างแนวดิ่งและแนวนอนมีค่าลดลงภายใต้ สภาวะที่ระยะห่างระหว่างรอยแตกในแนวดิ่งและแนวนอนมีค่าเท่ากัน การเพิ่มขึ้นของมุมของรอยแตกจาก 0 ถึง 45° จะลดความกว้างสูงสุดของอุโมงค์ลงประมาณร้อยละ 20 สำหรับอุโมงค์ในระดับตื้นคลื่นไหวสะเทือนที่มีความเร่ง 0.225 g จะสามารถลดความกว้างสูงสุดของอุโมงค์ลงประมาณร้อยละ 50

อย่างไรก็ตามผลกระทบของคลื่นไหวสะเทือนจะลดลงถ้าอุโมงค์อยู่ในระดับความลึกที่เพิ่มขึ้น ผลจากการทดสอบภายใต้สภาวะสถิตและคลื่นไหวสะเทือนในงานวิจัยนี้มีผลสอดคล้องอย่างเป็นเหตุเป็นผลต่อผลที่ได้จากการคำนวณด้วยวิธีเชิงตัวเลขโดยใช้โปรแกรม UDEC

สาขาวิชา เทคโนโลยีธรณี ลายมือชื่อนักศึกษา _____

ปีการศึกษา 2552 ลายมือชื่ออาจารย์ที่ปรึกษา _____

CHATKUN SAKULNITICHAI : PHYSICAL MODEL SIMULATION OF SHALLOW OPENINGS IN ROCK MASS UNDER STATIC AND DYNAMIC CONDITIONS. THESIS ADVISOR : ASSOC. PROF. KITTITEP FUENKAJORN, Ph.D., PE., 117 PP.

OPENING/JOINT/FRICTION/DYNAMIC LOAD/ACCELERATION

Physical models or scaled-down models have been widely used in laboratory to simulate stability conditions of underground openings in rock masses. They are commonly used to gain an understanding of the effects of unique rock characteristics, in-situ stress conditions or opening geometries. The simulations usually simplify the actual conditions into two-dimensional problems. Some devices can incorporate the effects of dynamic loading on the rock models. The modeling results are often compared with those obtained from numerical simulations, usually by a discrete element analysis, either to verify the predictive capability of the computed results or to confirm the accuracy of the test models. Most researchers however aim at studying the opening stability under site-specific conditions. Results obtained from the physical test models that can provide a more general solution of the opening stability in rock masses have been rare.

The objective of this research is to determine the effects of depth, joint spacing and orientation on the maximum unsupported span of shallow underground openings under static and dynamic loads by using physical models. Cubical and rectangular blocks of Phu Phan sandstone are arranged in a vertical test frame to simulate a two-dimensional representation of single rectangular openings in rock mass with two mutually perpendicular joint sets. Results indicate that the normalized

maximum span (W/S_V) rapidly increases with the normalized depth (D/S_H), and tends to approach a certain limit for each joint spacing ratio, S_V:S_H. The maximum span increases with decreasing S_V:S_H ratio. Under S_V=S_H condition, increasing the joint angles from 0° to 45° reduces the maximum span by about 20%. At shallow depths the acceleration of 0.225 g can reduce the maximum span by up to 50%. The impact of the dynamic loads however reduces as the depth increases. The test results under both static and dynamic loading compare reasonably well with those calculated from discrete element analyses using the UDEC code.

School of Geotechnology Student's Signature_____

Academic Year 2008 Advisor's Signature_____

ACKNOWLEDGMENTS

I wish to acknowledge the funding support of Suranaree University of Technology (SUT).

I would like to express my sincere thanks to Assoc. Prof. Dr. Kittitep Fuenkajorn, thesis advisor, who gave a critical review and constant encouragement throughout the course of this research. Further appreciation is extended to Asst. Prof. Thara Lekuthai : Chairman, School of Geotechnology and Dr. Prachya Tepnarong, School of Geotechnology, Suranaree University of Technology who are member of my examination committee. Grateful thanks are given to all staffs of Geomechanics Research Unit, Institute of Engineering who supported I work.

Finally, I most gratefully acknowledge my parents and friends for all their supported throughout the period of this research.

Chatkun Sakulnitichai

TABLE OF CONTENTS

Page

ABSTRACT (THAI) I

ABSTRACT (ENGLISH) III

ACKNOWLEDGEMENTS V

TABLE OF CONTENTS VI

LIST OF TABLES IX

LIST OF FIGURES XIII

LIST OF SYMBOLS AND ABBREVIATIONS XVI

CHAPTER

I INTRODUCTION 1

1.1 Background of problems and significance of the study 1

1.2 Research objectives 2

1.3 Research methodology 2

1.3.1 Literature review 2

1.3.2 Sample collection and preparation 3

1.3.3 Modification of the physical model 3

1.3.4 Physical model experiments 3

1.3.5 Comparison 3

1.3.6 Thesis writing and presentation 3

TABLE OF CONTENTS (Continued)

Page

1.4 Scope and limitations of the study 4

1.5 Thesis contents 4

II LITERATURE REVIEW 5

2.1 Introduction 5

2.2 The stability of an underground excavation 5

2.2.1 Engineering rock mass classification 5

2.2.2 Classification of jointed rocks 7

2.3 Effect of seismic load 9

2.4 Previous physical models 13

2.5 Numerical models 20

III TEST PLATFORM 24

3.1 Introduction 24

3.2 Design requirements and components 24

3.3 Calculation of lateral stresses 31

IV MODEL SIMULATIONS 34

4.1 Introduction 34

4.2 Rock models 34

4.3 Test Models under static condition 36

4.4 Maximum spans estimated from Q and RMR systems 44

4.5 Test Models under dynamic condition 48

TABLE OF CONTENTS (Continued)

Page

V DISCRETE ELEMENT ANALYSES 55

5.1 Introduction 55

5.2 Discrete element analysis 55

VI DISCUSSIONS, CONCLUSIONS, AND RECOMMENDATIONS FOR FUTURE STUDIES 64

6.1 Discussions 64

6.2 Conclusions 65

6.3 Recommendations for future studies 65

REFERENCES 67

APPENDICES

APPENDIX A RESULTS OF SHALLOW OPENING UNDER STATIC CONDITION 78

APPENDIX B RESULTS OF SHALLOW OPENING UNDER DYNAMIC CONDITION 83

APPENDIX C SIMULATION RESULTS OF SHALLOW OPENING USING UDEC CODE 89

APPENDIX D TECHNICAL PUBLICATIONS 96

BIOGRAPHY 117

LIST OF TABLES

Table **Page**

2.1 The intensity of ground motion is estimated from the Mercalli scale 14

4.1 Ranges of test parameters and results under static condition 40

4.2 Empirical relations obtained from regression analysis on the test results under static condition 45

4.3 Predictions of maximum unsupported spans (W) using empirical equations and RMR and Q rock mass classification systems 47

4.4 Results of physical models tested under dynamic loads 50

4.5 Empirical relations obtained from regression analysis on the test results under dynamics load at a = 0.132 g and 0.225 g 54

5.1 Summary of UDEC simulations for shallow opening. The sandstone blocks have ψ_b=26º, c=53 Pa, and γ_r=2.38 kN/m^3, under 14000 cycles 59

A.1 Test parameters and results for 4×4 cm block sizes or joint spacing ratio equal to 1:1 under static condition 79

A.2 Test parameters and results for 4×8 cm block sizes or joint spacing ratio equal to 1:2 under static condition 80

A.3 Test parameters and results for 4×8 cm block sizes or joint spacing ratio equal to 2:1 under static condition 80

A.4 Test parameters and results for 4×12 cm block sizes or joint spacing ratio equal to 1:3 under static condition 81

LIST OF TABLES (Continued)

Table **Page**

A.5 Test parameters and results for 4×12 cm block sizes or joint spacing ratio equal to 3:1 under static condition 81

A.6 Test parameters and results for joint spacing ratio equal to 1:1, 1:2, 2:1, 1:3, and 3:1 under static condition at joint angle = 45° 82

B.1 Test parameters and results for joint spacing ratio equal to 1:1 under horizontal pseudo-static acceleration of 0.132 g and 0.225 g 84

B.2 Test parameters and results for joint spacing ratio equal to 1:2 under horizontal pseudo-static acceleration of 0.132 g and 0.225 g 85

B.3 Test parameters and results for joint spacing ratio equal to 2:1 under horizontal pseudo-static acceleration of 0.132 g and 0.225 g 85

B.4 Test parameters and results for joint spacing ratio equal to 1:3 under horizontal pseudo-static acceleration of 0.132 g and 0.225 g 86

B.5 Test parameters and results for joint spacing ratio equal to 3:1 under horizontal pseudo-static acceleration of 0.132 g and 0.225 g 86

B.6 Test parameters and results for joint spacing ratio equal to 1:1, 1:2, 2:1, 1:3, and 3:1 under horizontal pseudo-static acceleration of 0.132 g at joint angle = 45° 87

B.7 Test parameters and results for joint spacing ratio equal to 1:1, 1:2, 2:1, 1:3, and 3:1 under horizontal pseudo-static acceleration of 0.225 g at joint angle = 45° 88

LIST OF TABLES (Continued)

Table **Page**

C.1 UDEC simulation results for shallow opening of sandstone blocks under static condition at ψ_b=26º, c=53 Pa, and γ_r=2.38 kN/m^3 90

C.2 UDEC simulation results for shallow opening of sandstone blocks under dynamic condition at ψ_b=26º, c=53 Pa, and γ_r=2.38 kN/m^3 93

LIST OF FIGURES

Figure **Page**

2.1 Three-dimensional tunnel test: scheme of the right portion of the experimental model, with respect to vertical plane through the tunnel axis, and locations of the surface settlement transducers h1 to h9 16

2.2 Three-dimensional tunnel test: shear surface at failure 16

2.3 Photos of the Xiluodu 3-D geo-mechanical model test platform 17

2.4 The model tests of underground openings on the shaking table 19

2.5 Horizontal bedded model after test 21

2.6 A post-test view of the model with bedding planes inclined at an angle of 60° and non-persistent joint 21

2.7 The dimension of physical model test 22

2.8 Physical model testing set up 22

3.1 Front view schematic drawing of test platform for physical model 25

3.2 Schematic drawing of test platform for physical model 26

3.3 Test platform used to simulate shallow openings in rock mass 27

3.4 Test platform with rock block samples placed inside the test frame 29

3.5 Crank arm and flywheel used to induce dynamic loading to the test platform 30

3.6 Variables used in physical model simulations and analysis. Joint inclination can be set at any angle by tilting the rock blocks in the model 32

LIST OF FIGURES (Continued)

Figure **Page**

4.1 Nearly 1000 blocks of Phu Phan sandstone prepared for testing and block size are 4×4, 4×8 and 4×12 cm 35

4.2 Rock samples for 4×8 and 4×12 cm blocks at joint angle of 45° load inside the test frame and the joint angle are controlled by triangle timbers 38

4.3 The inclined joint angles are obtained by placing triangle timbers at the bottom of the rock blocks 39

4.4 Examples of physical models showing roof failure after opening widths exceed their maximum unsupported spans. Top: openings in rock mass model formed by 4×4 blocks. Bottom: openings in rock mass model formed by 4×12 blocks 41

4.5 Normalized maximum span (W/S_V) as a function of normalized depth (D/S_H) for joint spacing ratios of 1:1 (a), 1:2 (b), and 1:3 (c) under static condition 42

4.6 Normalized maximum span (W/S_V) as a function of normalized depth (D/S_H) for various joint spacing ratios and joint orientations. The empirical relations of the results are given in Table 4.2 43

4.7 Normalized maximum span (W/S_V) as a function of normalized depth (D/S_H) for joint spacing ratios of 1:1, 1:2, and 1:3 under acceleration of 0.132 g (a) and 0.225 g (b) 51

LIST OF FIGURES (Continued)

Figure **Page**

4.8 Normalized maximum span as a function of normalized depth under pseudo-static accelerations of 0.132 g (b) and 0.225 g (c) compared with the results under static condition (a) for vertical and horizontal joint sets with various spacing ratios 52

4.9 Normalized maximum span as a function of normalized depth under pseudo-static accelerations of 0.132 g (b) and 0.225 g (c) compared with the results under static condition (a) for 45º -inclined joint sets 53

5.1 UDEC simulation results for joint spacing ratios of 1:1 (a), 2:1 (b) and 3:1 (c) under static condition 60

5.2 UDEC simulation results for joint spacing ratios of 1:2 (a) and 1:3 (b) under static condition 61

5.3 Comparisons of UDEC simulations with test models for various spacing ratios 62

5.4 Comparisons of UDEC simulations with test models under pseudo-static acceleration of 0.225 g 63

LIST OF SYMBOLS AND ABBREVIATIONS

a_H	=	horizontal static acceleration
C_p	=	P-wave velocity
D	=	opening depth
D/S_H	=	normalized depth
ESR	=	excavation support ratio
g	=	gravitational acceleration
H	=	model height
$H(\tau)$	=	step function
J_a	=	the joint alteration number
J_n	=	the joint set number
J_r	=	the joint roughness number
J_V	=	sum of the number of joints per unit length for all joint (discontinuity) sets
J_w	=	the water reduction factor
K_a	=	the axial stiffness
m	=	mass
m_o	=	source strength
Q	=	quality index
R	=	radius of wheel
S_H	=	horizontal joint spacing

LIST OF SYMBOLS AND ABBREVIATIONS (Continued)

SRF	=	the stress reduction factor
S_V	=	vertical joint spacing
S_V/S_H	=	joint spacing ratio
T	=	duration of flywheel rotation
t	=	time
u	=	velocity
UCS	=	the uniaxial compressive strength of rock material
W	=	maximum span or maximum unsupported span
W/S_V	=	normalized maximum span
y	=	length of crack arm
ΔF_a	=	an incremental change in axial force
Δu_a	=	an incremental change in axial displacement
$\Delta\sigma_{ij}^{e}$	=	the elastic increments of the stress tensor
$\Delta\in_{ij}$	=	the incremental strains
$\Delta\in_{\upsilon}$	=	the increment of volumetric strain
α	=	velocity of pressure wave
β	=	velocity of shear wave
γ	=	dimensionless bonding parameter
δ_{ij}	=	the Kronecker delta function
ρ	=	density
ϕ	=	angle of friction
ω	=	angular velocity

CHAPTER I

INTRODUCTION

1.1 Background of problems and significance of the study

Physical test models or scaled-down models have been widely used in the laboratory to simulate the stability conditions of underground openings in rock mass (Lama and Vutukuri, 1978; Stimpson, 1979; Bakhtar et al., 1986; Adhikary and Dyskin, 1997). They are commonly used to gain an understanding of the effects of unique rock characteristics, in-situ stress conditions or opening geometries (Zhu and Zhao, 2004). The simulations usually simplify the actual conditions into two-dimensional problem. Recently some researchers have developed sophisticated devices to allow a three-dimensional simulation for tunnel stability in rock mass under high stresses (e.g., Sterpi and Cividini, 2004; Li et al., 2005; Liu et al., 2006). As a result the failure conditions of the joints and intact rocks around the openings can be simulated simultaneously. Some devices can incorporate the effects of dynamic loading on the rock models (Bakhtar, 1997; Ma and Brady, 1999). The modeling results are often compared with those from numerical simulations, usually by a discrete element analysis, either to verify the predictive capability of the computed results or to confirm the accuracy of the test models (Bhasin and Hoeg, 1998; Zhu et al. (2006). Most researchers however concentrate on studying the opening stability under site-specific conditions. Results from the physical test models that can provide a more general solution to the opening stability in rock mass have been rare.

1.2 Research objectives

The objectives of the proposed research are to perform physical model tests to assess the effects of depth, joint spacing and orientation on the maximum unsupported span of shallow underground openings under static and dynamic loads. A vertical test platform will be used to support the rock mass model formed by cubical and rectangular blocks of Phu Phan sandstone. The models will simulate two-dimensional sections of single rectangular openings in rock mass with two mutually perpendicular joint sets. The vertical and horizontal joint spacings will vary from 4, 8 to 12 cm. The stability condition under horizontal pseudo-static accelerations of 0.132 g and 0.225 g is investigated. Empirical relations between the observed maximum span, opening depth and joint spacings will be derived. They will be used to predict the maximum span under shallow depths. The static and dynamic test results will be compared with those simulated from discrete element analyses using UDEC code.

1.3 Research methodology

The research effort is divided into six tasks, including the literature review, sample collection and preparation, modification of the physical model, physical model testing, discrete element analyses, comparisons, and thesis writing and presentation.

1.3.1 Literature review

Literature review is carried out to study the shallow openings and case studies in Thailand and abroad, opening stability, and the earthquake vibration. The sources of information are from journals, technical reports and conference papers. A summary of the literature review is given in the thesis.

1.3.2 Sample collection and preparation

Rock with uniform texture and properties is selected for the model testing. The block specimen dimensions primarily are 4×4×4 cm, 4×4×8 cm, and 4×4×12 cm. Up to about 1,000 blocks are prepared.

1.3.3 Modification of the physical model

The test platform for physical model test (Pangpetch & Fuenkajorn, 2007) is modified for shallow opening simulation in jointed rock mass in Geomechanical Laboratory in Suranaree University of Technology. The testing space (area) is about 1.2×1.2 m. A lateral lithostatic pressure is applied on both sides of the model using a column of crystal balls with a diameter of 16 mm packed in the gap between the model and the test frame.

1.3.4 Physical model experiments

Shallow opening models are simulated for various depths and maximum spans. Video camera of the opening movement is recorded for further analysis and comparisons.

1.3.5 Comparison

Results obtained from the simulations are compared with the solutions from the deterministic methods and with the computer simulations.

1.3.6 Thesis writing and presentation

All research activities, methods, and results are documented and compiled in the thesis.

1.4 Scope and limitations of the study

Scaled-down of shallow opening models are simulated in two dimensions. The shallow opening models have a maximum depth of 1.2 m under various maximum spans. Failure of shallow opening model is induced by real gravitational force. Continuous monitoring of the failure process is made during the test. The effect of submerging condition are studied. The effect of earthquake will be studied in horizontal direction normal to the strike of the openings. Phu Phan sandstone is used to prepare the block specimens.

1.5 Thesis contents

Chapter I introduces the thesis by briefly describing the background of problems and significance of the study. The research objectives, methodology, scope and limitations are identified. **Chapter II** summarizes results of the literature review. **Chapter III** describes the design procedure for physical model modification. **Chapter IV** presents the results obtained from the laboratory testing. The experiments are divided into 2 tests, including 1) shallow opening failure tests under static condition and 2) shallow opening failure tests under dynamic loads. **Chapter V** presents the results obtained from discrete element analyses. **Chapter VI** concludes the research results, and provides recommendations for future research studies.

CHAPTER II

LITERATURE REVIEW

2.1 Introduction

This chapter summarizes the results of literature review carried out to improve an understanding of simulation of shallow opening failure using physical model. The topics reviewed here include the stability of an underground excavation, joint shear strength, effect of seismic load, physical models, and numerical methods.

2.2 The stability of an underground excavation

The stability of an underground excavation depends upon the structural conditions in the rock mass and also upon the relationship between the stress in the rock and the strength of the rock (Hoek and Brown, 1980). Rock mass classification schemes have been developed for over 100 year. Hoek et al. (2000) state that most of multi-parameter classification schemes (Wickham et al., 1972, Bieniawski, 1973, 1989, and Barton et al., 1974) were developed from civil engineering case histories in which all of the components of the engineering geological characters of the rock mass were included.

2.2.1 Engineering rock mass classification

Summaries of some engineering rock mass classification involve with Terzaghi's rock load classification, classification involving stand-up time, and rock quality designation index (RQD). Hoek and Brown (1980) state that the earliest reference to the use of rock mass classification for the design of tunnel support is in a

paper by Terzaghi (1946) in which in rock loads, carried by steel sets, are estimated on the basis of a descriptive classification. He described various types of ground and based upon his experience in steel-supported railroad tunnels in the Alps, he assigned ranges of rock loads for various ground conditions. This very important paper, in which Terzaghi attempted to quantify his experience in such a way that it could be used by others, has been widely used in tunnelling in north America ever since it was published.

The stand-up time for an unsupported span is related to the quality of the rock mass in which the span is excavation. The significance of the stand-up time concept is that an increase in the span of the tunnel leads to a significant reduction in the time available for the installation of support (Lauffer, 1958).

The Rock Quality Designation index (RQD) was developed by Deere (Deere et al., 1967) to provide a quantitative estimate of rock mass quality from drill core logs. RQD is defined as the percentage of intact core pieces longer than 100 mm (4 inches) in the total length of core. Palmstrom (1982) suggested that, when no core is available but discontinuity traces are visible in surface exposures or exploration adits, the RQD may be estimated from the number of discontinuities per unit volume. The suggested relationship for clay-free rock masses is:

$$RQD = 115 - 3.3J_V \quad (1)$$

where J_V is the sum of the number of joints per unit length for all joint (discontinuity) sets known as the volumetric joint count. Hoek et al. (2000) state that RQD is a directionally dependent parameter and its value may change significantly, depending

upon the borehole orientation. The use of the volumetric joint count can be quite useful in reducing this directional dependence.

2.2.2 Classification of Jointed Rocks

Terzaghi's (1946) descriptive rock mass classification has been useful to estimate rock load for tunnels with steel rib support system; it could not be adopted for rock foundations and slopes. Most commonly used and numerically expressed rock mass classifications, RMR (Bieniawski, 1973) and Q-system (Barton et al., 1974) have been developed basically for the stability of tunnels and choice of their support system.

Bieniawski (1974) introduces the Geomechanical Classification System that provides a general rock mass rating (RMR) increasing with rock quality from 0 to 100. The rating system is based on experience from shallow tunnels in sedimentary rock. Bieniawski (1989) state that the reason for using this classification system is the ease of use and the versatility in engineering practice. The RMR system has been calibrated using experience from coalmines, civil engineering excavation and tunnels at shallow depth. RMR is based upon five basic parameter include uniaxial compressive strength of intact rock material, rock quality designation (RQD), ground water conditions, joint or discontinuity spacing, and joint characteristics. A sixth parameters, orientation of joints, can be used for specific application in tunnlling, mining and for foundations (Toyra, 2004).

The Q system or the Rock Mass Quality-system created by Barton et al. (1974) was developed at the Geotechnical Institute of Norway. Updating of the Q-system has taken place on several occasions and was in 1993 based on over 1000 case records. The original parameters of the Q system have never been changed, but

the rating for the stress reduction factor (SRF) has been altered by Grimstad and Barton (1993) and Barton (2002).

The Q-system and the RMR system include somewhat different parameters and can not there fore be strictly correlated. An attempt to compare them was proposed by Bieniawski (1976).

$$RMR = 9\log Q + 44 \tag{2}$$

Milne et al. (1998) discussed some of the potential problems when using the Q and RMR systems. The problems that can be encountered are outlined below:

a) More than one relationship has been suggested for relating joint spacing to RQD. These approaches do not all agree and the users should use more than one method. An estimate within 5% is more than adequate for RQD.

b) Practitioners sometimes estimate one classification and then derive a second classification from empirical relationships. Relating Q and RMR makes for an interesting comparison between classifications and may improve our understanding of the rock mass, however, the two systems should always be derived independently. There are many published relationships between Q and RMR, however, it is likely that no one relationship would work for all rock mass conditions.

c) Care must be taken when using classification systems with empirical design methods. The user must be sure that the classification system used matches the approach taken for the development of the empirical design method.

d) Mining applications of the Q and RMR system have tended to simplify classification systems to only included factors dependent on the rock mass, ignoring environmental and loading conditions.

Despite their limitations, the reviewed classification systems are still in use as they provide an invaluable reference to past experience.

The displacements and geometry of the rock blocks and the properties of the structure play an important role in the stability of tunnels. The necessary condition for the loss of the stability of tunnel roof is the falling of the key blocks. Therefore the key point for the analysis of the stability is the determination of the position, size and geometry of the key blocks (Chengzhi et al., 2008)

2.3 Effect of seismic load

The evaluation of ground response to shaking can be divided into two groups (1) ground failure and (2) ground shaking and deformation. Ground failure as a result of seismic shaking includes liquefaction, slope instability, and fault displacement. Ground failure is particularly prevalent at tunnel portals and in shallow tunnels. Special design considerations are required for cases where ground failure is involved (Hashash et al., 2001).

Guler et al. (2001) studied repeated dynamic loading, the subject of this study, is directly linked to seismicity and the effects of seismic events. While it is impossible to quantify exactly the associated movements, certain relationships between magnitude, relative location and induced movements and associated forces exist. Owen and Scholl (1981) discussed a review of the past performance of 127 underground openings during earthquakes indicates that underground structures in

general are less severely affected than surface structures at the same geographic location. However, some severe damage, including collapse, has been reported. Stability of tunnels during seismic motion is affected by peak ground motion parameters, earthquake duration, and type of support, ground conditions, and in-situ stresses. Siad (2003) considered gravity and inertial forces developed in the rock mass by the passage of seismic waves are the external forces. The rock mass is crossed by two sets of fractures which are considered to be planar and persistent. The stability factor is very sensitive to variations of horizontal seismic coefficient. It is reduced due to seismic effect. However, the value flattens as friction angle of fracture increases. Daisuke et al. (2003) state that generally, underground caverns are highly resistant to earthquake. However, the underground cavern for the public use will be constructed in the ground with shallow overburden for convenience of access to the cavern. Therefore, in construction of underground rock cavern, influence of earthquake must be considered.

Stiros and Kontogianni (2009) studied the Coulomb stress changes from earthquakes to underground excavation failures. Evidence from shallow tunnels and mines indicates that, in certain cases, deformation and failure are not confined to the vicinity of the excavation front, as is widely believed.

There are some researchers studied earthquake related problems such as fault rupture mechanism, seismic site effects, and rock structure interaction by earthquake modeling laboratory (e.g. Brune and Anooshehpoor, 1991; Madariaga et al., 1998; Hashimoto and Matsu'ura, 2000; Ohtani et al., 2003; Pakbaz and Yareevand, 2005) and computer simulation (e.g. Matsu'ura et al., 2002; Kim et al., 2003; Wang et al., 2006).

Console et al. (2006) studied the phenomenon of earthquake clustering, i.e., the increase of occurrence probability for seismic events close in space and time to other previous earthquakes, has been modeled both by statistical and physical processes. They state that the new model incorporating the physical concept of the rate-and-state theory performs not worse than the purely stochastic model with two free parameters only.

The examples of horizontal ground acceleration that they had affect to geotechnical engineering works as; the Dead Sea valley and Mount Masada bedrock have been classified as a region in which earthquake induced peak horizontal ground acceleration (PGA) exceeding 0.2 g. The deep bedrock acceleration certainly exceeding 0.1 g and probably even exceeding 0.2 g (Hatzor et al., 2004). The Western Alboran Basin earthquake induced ground accelerations between 0.16 and 0.43 g (Baraza et al., 1992). Silva et al., 2006 state that the horizontal ground acceleration varied from 0.07 g – 0.16 g for the Neotectonic fault at the Gbraltar Strait tunnel area, Bolonia Bay (South Spain). Peak horizontal ground accelerations measured in the area Loma Prieta earthquake ranged between 0.1 and 0.25 g (EERI, 1990).

Hatzon et al. (2004) analyzed dynamic stability of jointed rock slopes using the DDA method. The peak horizontal ground acceleration (PGA) for DDA computation varied from 0.06 to 0.2 g. Genis and Aydan (2002) evaluated the dynamic response and stability of shallow underground openings in discontinuous rock masses using model tests. They state that the amplitude of acceleration was greater at the ground surface than that in the opening the maximum horizontal acceleration was 250 gal (0.255 g) in the opening when the shaking table acceleration ranged between 50-70 gal (0.051-0.071 g). Furthermore, the vertical acceleration

was 225 gal (0.229 g) at the ground surface while it was 160 gal (0.163 g) in the opening. Jin and Zhang (2008) state that when the horizontal earthquake acceleration are 0.191 and 0.440 g or the longitudinal earthquake acceleration is 0.141 g and their combined action, the initial support of tunnel would be damaged and the local lining would have partial damage.

Barton and Hansteen (1979) used two-dimensional finite element continuum analyses and discontinuous physical models (20,000 discrete blocks) to compared the deformation resulting from excavation of very large openings. They varied both the joint orientations and the model horizontal stress levels were varied. Some models were dynamically loaded to simulate earthquakes (0.2-0.7 g). They state that high horizontal stress caused surface heave when joint orientations were favorable for arch stability. Joint orientations also determined whether the pillars between parallel openings were in a state of compression or tension. Maugeri et al., (2000) tested the failure of a shallow foundation subjected to an acceleration load by shaking table which the peak acceleration of the sine dwell motion was gradually increased up from ±0.1 to ±0.35 g. Riley et al. (2006) studied the terrace tunnel approach walls, Wallington by seismic performance. They state that the walls were designed by the ministry of works and development in the early to mid 1970's. A designed pseudo static acceleration of 0.2 g was adopted for the working load analysis and checked to ensure ultimate limit capacity at a pseudo static acceleration of 0.25 g. The U.S. Department of Homeland Security (2005) states that the peak bedrock accelerations are 0.2 g or less for analyses the effect of earthquake loading to a concrete dam on a rock foundation.

Earthquake intensity scales are designed to describe the effects of earthquakes on man, structures, and their surroundings. Although certain instruments have been occasionally employed in determination of the severity of shaking (e.g. Medvedev, 1953; Richter, 1958; Arias, 1970; Blume, 1970, Trifunac and Brady, 1975; Wald et al., 1999), a majority of intensity scales used today still represent subjective description of human response to shaking and the description of associated building damage (e.g. Karim and Yamazaki, 2002; Davenport, 2003).

For historical earthquakes with no seismograph records, seismologists can estimate the intensity of ground motion from the Mercalli scale (Table 2.1), using the information as a kind of crude seismograph. If intensity information is available for enough different places, a rough estimate of the earthquake magnitude can be made (Gendzwill, 2008).

2.4 Previous physical models

Physical test models or scaled-down models have been widely used in the laboratory to simulate the stability conditions of underground openings in rock masses (Lama and Vutukuri, 1978; Stimpson, 1979; Bakhtar et al., 1986; Adhikary and Dyskin, 1997). They are commonly used to gain an understanding of the effects of unique rock characteristics, in-situ stress conditions or opening geometries (Zhu and Zhao, 2004).

The simulations usually simplify the actual conditions into two-dimensional problems. Cement mixed with sand, plaster or wooden blocks are commonly such as Adhikary and Dyskin (1997) used ilmenite sand and gypsum mixtures for two small-scale models simulating an opening. Recently some researchers have developed

Table 2.1 The intensity of ground motion is estimated from the Mercalli scale (Adapted from Richter, 1958 and Wald et al, 1999)

Modified Mercalli Intensity	Acceleration (g)	Description of Intensity Level
I	<0.0017	Not felt except by a very few under especially favorable circumstances.
II	0.0017	Felt only by a few persons at rest, especially on upper floors of buildings. Delicately suspended objects may swing.
III	0.014	Felt quite noticeably by persons indoors, especially on upper floors of buildings. Many people do not recognize it as an earthquake. Standing motor cars may rock slightly. Vibration similar to the passing of a truck. Duration estimated.
IV	0.014 – 0.039	Felt indoors by many, outdoors by few during the day. At night, some awakened. Dishes, windows, doors disturbed; walls make cracking sound. Sensation like heavy truck striking building. Standing motor cars rocked noticeably.
V	0.039 – 0.092	Felt by nearly everyone; many awakened. Some dishes, windows broken. Unstable objects overturned. Pendulum clocks may stop.
VI	0.092 – 0.18	Felt by all; many frightened. Some heavy furniture moved; a few instances of fallen plaster. Damage slight.
VII	0.18 – 0.34	Damage negligible in building of good design and construction; slight to moderate in well-built ordinary structures; considerable damage in poorly built or badly designed structures; some chimneys broken. Noticed by persons driving motorcars.
VIII	0.34 – 0.65	Damage slight in specially designed structures; considerable in ordinary substantial buildings with partial collapse. Damage great in poorly built structures. Fall of chimneys, factory stacks, columns, monuments, walls. Heavy furniture overturned.
IX	0.65 – 1.24	Damage considerable in specially designed structures; well-designed frame structures thrown out of plumb. Damage great in substantial buildings, with partial collapse. Buildings shifted off foundations.
X	> 1.24	Some well-built wooden structures destroyed; most masonry and frame structures destroyed with foundations. Rails bent.
XI	> 1.24	Few, if any (masonry) structures remain standing. Bridges destroyed. Rails bent greatly.
XII	> 1.24	Damage total. Lines of sight and level distorted. Objects thrown into the air.

sophisticated devices to allow a three-dimensional simulation for tunnel stability in rock mass under high stresses.

The modeling results are often compared with those from numerical simulations, usually by a discrete element analysis, either to verify the predictive capability of the computed results or to confirm the accuracy of the test models.

Sterpi and Cividini (2004) studied the behaviour up to failure of shallow underground openings on the basis of some laboratory, small-scale model tests (Figure 2.1 and 2.2) and of finite element simulation. The experimental results were obtained from two-dimensional (plane strain) and three-dimensional tunnel models tested under standard gravity conditions. The laboratory tests have been simulated by means of a series of plane strain and three-dimensional finite element analyses accounting for the gradual reduction of the shear resistance of the cohesionless medium with increasing plastic strains. They concluded that the adopted procedure for strain softening analysis has a potential for application to actual tunnelling problems. In particular, it could be used to evaluate the minimum radial pressure required for stabilizing the contour of shallow tunnels (2D case) or the minimum fluid pressure necessary to stabilize the tunnel face when excavating, for instance, by means of an Earth Pressure Balance Machine (3D case).

Li et al. (2005) applied of numerical analysis principles and key technology for high fidelity simulation to 3-D physical model tests for underground caverns (Figure 2.3). The comparison of the two methods showed that the effect of the physical model test was satisfactory, and that some geological weak structures are difficult to simulate numerically and easier to simulate using a physical model.

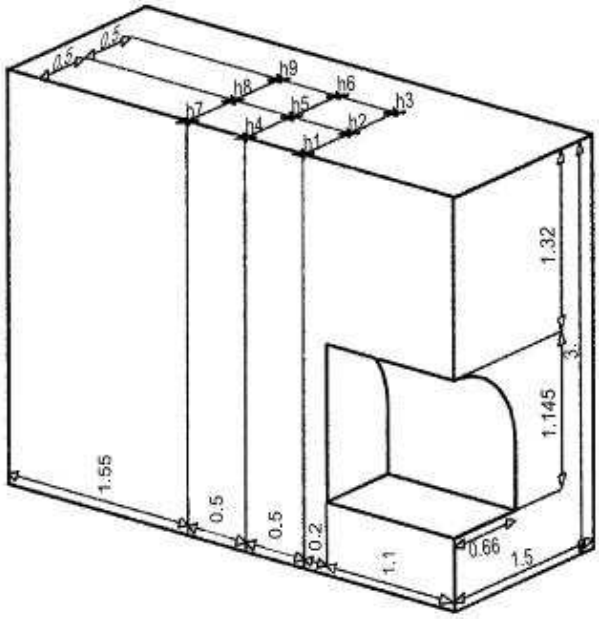

Figure 2.1 Three-dimensional tunnel test: scheme of the right portion of the experimental model, with respect to vertical plane through the tunnel axis, and locations of the surface settlement transducers h1 to h9 by Sterpi and Cividini (2004).

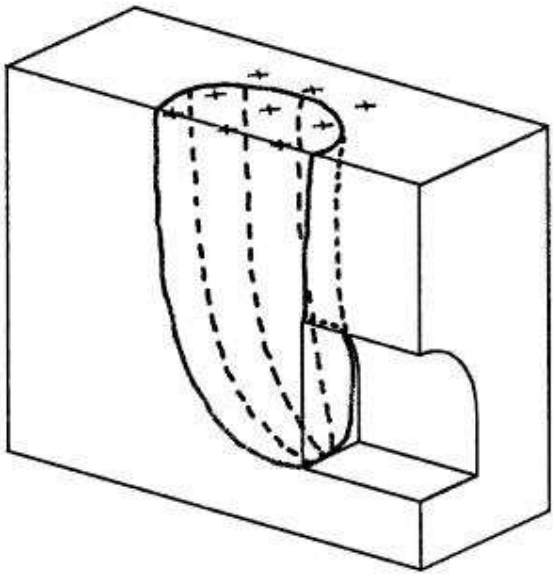

Figure 2.2 Three-dimensional tunnel test: shear surface at failure Sterpi and Cividini (2004).

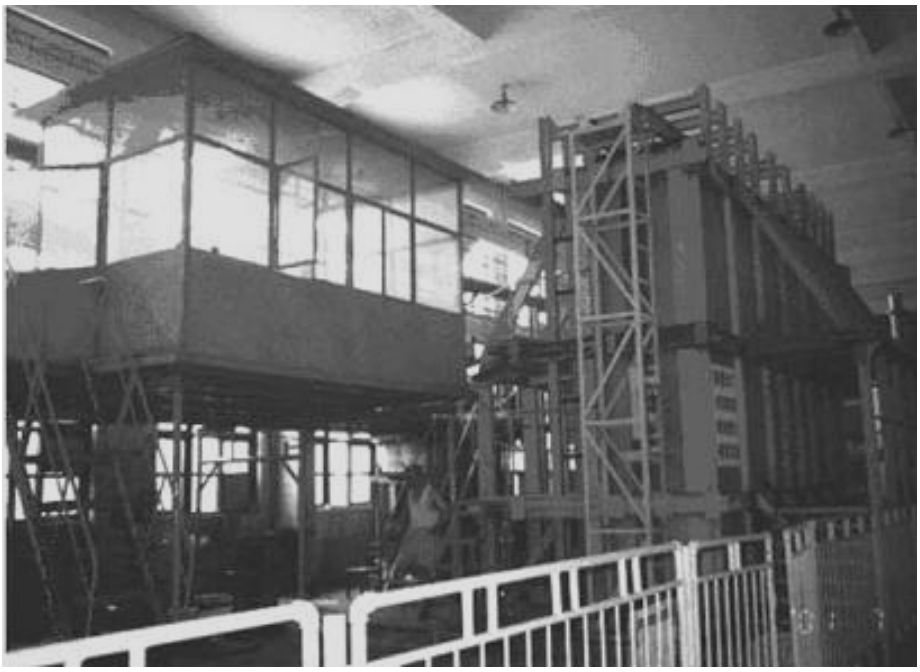

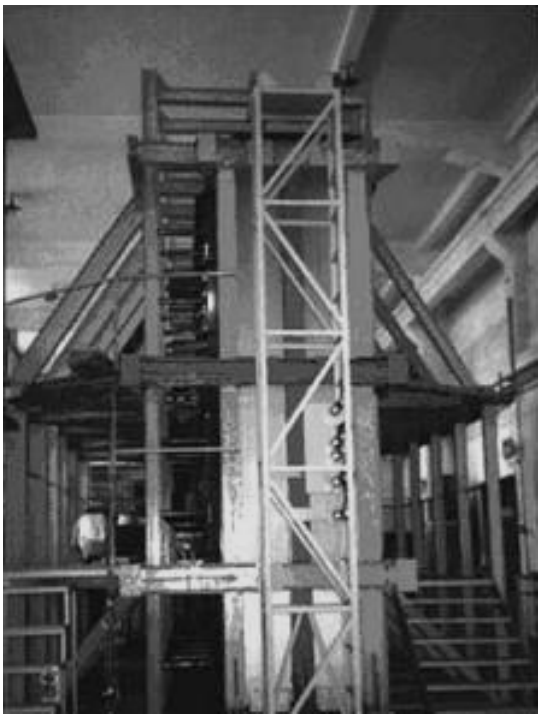

Figure 2.3 Photos of the Xiluodu 3-D geo-mechanical model test platform (Li et al., 2005).

Ma and Brady (1999) studied the dynamic performance of an underground excavation in jointed rock under repeated seismic loading. The results from field observations of dynamic behaviour of an underground excavation have been compared with numerical studies of the rock deformation history. They concluded that the field behaviour shows progressive accumulation of rock displacement and excavation deformation under successive episodes of dynamic loading. It is possible to reproduce the modes of rock response quite well using a distinct element model of the rock mass, but the way displacements develop is dependent on the joint model used in the analysis. It is suggested that, in rock masses subject to repeated dynamic loading, excavation design may need to take account of the prospect of repeated episodes of transient loading at the excavation site.

Ren et al. (2006) applied the physical simulation to analyze the failure mechanism of the wall rock around the goaf and the time effect characters of the wall rock's deformation and the ground's deformation and subsidence. They discovered the physical simulating result was more accurately close to in situ monitoring result than each of the numerical simulating results.

Genis and Aydan (2002) have used the dynamic shaking table tests as a tool in modeling of shallow opening. In model test, they used saw-cutting surface of Ryukyu limestone blocks. The geometry of the openings is rectangular (W/H=2/3) and square in cross-section since they are the optimum shapes in view of the existence discontinuity sets and gravitational loading. Four difference conditions were investigated by considering the orientation of bedding planes and discontinuity patterns (Figure 2.4). There was no unstable block around the opening during and

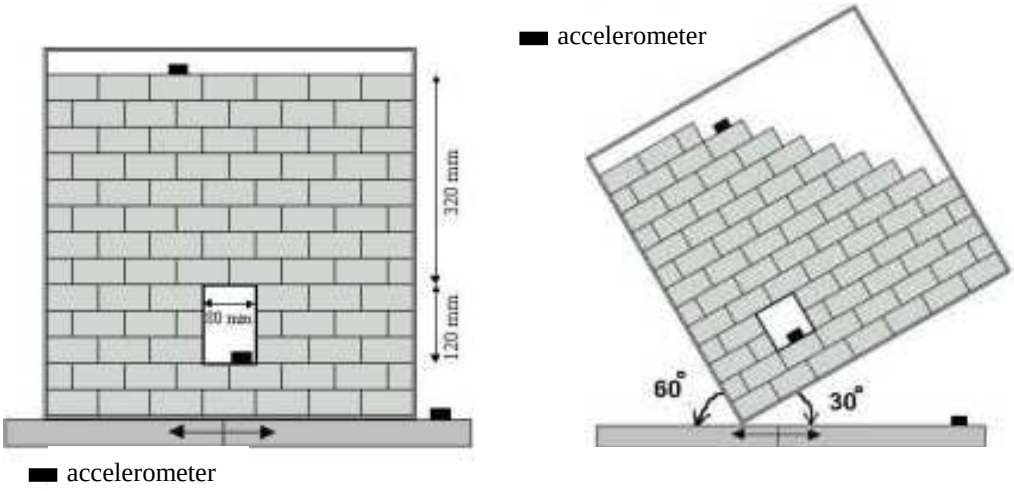

(a) Horizontal model (b) 30° Inclined model

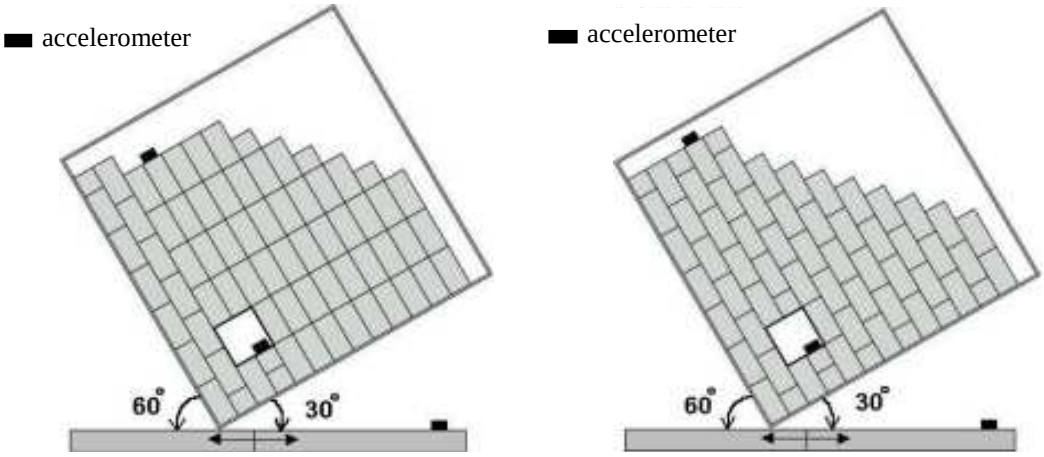

(c) 60° Inclined model (Continuous joint)

(d) 60° Inclined model (Intermittent joint)

Figure 2.4 The model tests of underground openings on the shaking table (Genis and Aydan, 2002).

after shaking (Figure 2.5). In all tests, a mass of rock blocks bounded by two bedding planes emanating from the corners of the opening and extending to ground surface slide into the opening as if a rigid block. Figure 2.6 shows the post-failure state of a model. They concluded that the stability of shallow opening are strictly depends upon the relations between the maximum acceleration, discontinuity orientation and the geometry of opening and overburden height. If the inclination of bedding planes become steeper and the overburden becomes smaller, a mass of rock mass day-lighting in the opening and extending to the ground surface slid into the opening. The amplitude of input acceleration wave to cause such a failure is consistent with the predictions by a method proposed by Aydan et al. (1994).

Jongpradist et al. (2009) studied the failure behavior of rock mass around gas storage cavern with physical model test. They designed the physical character of model test as a silo, 0.1 meter in diameter, 0.2 meter high, and the location of the cavern center is 0.5 m. under the ground surface (Figure 2.7). The rocks are simulated from mixture of plaster, sand and water. The test arrangement is shown in Figure 2.8. They concluded that the lateral earth pressure coefficient at rest, Ko has strong influence on the position of the initiation point as obtained by numerical analyses.

2.5 Numerical models

The numerical analyses, primarily with distinct element methods, have been employed to simulate the stability conditions of underground openings. Discrete element method (DEM) is a common tool for the numerical approach to study the effect of dynamic loading on geologic structures. Some researchers used DEM for simulating fracture rock masses (e.g. Souley and Homand, 1996; Gong et al., 2006;

Figure 2.5 Horizontal bedded model after test (Genis and Aydan, 2002).

Figure 2.6 A post-test view of the model with bedding planes inclined at an angle of 60° and non-persistent joint (Genis and Aydan, 2002).

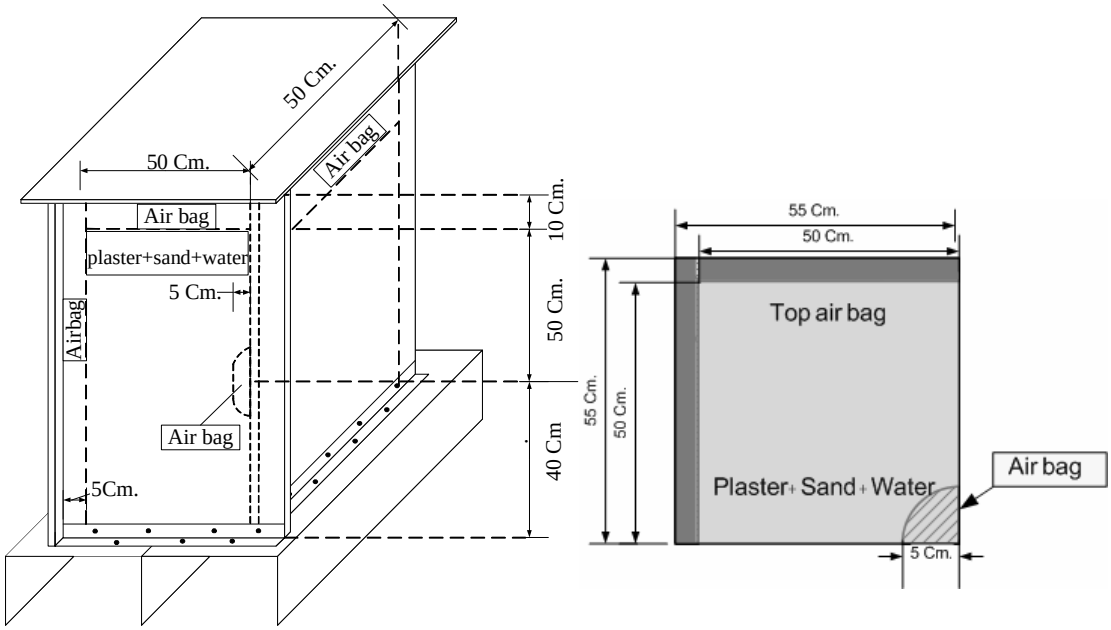

a.) Perspective view b.) Top view

Figure 2.7 The dimension of physical model test by Jongpradist et al. (2009)**.**

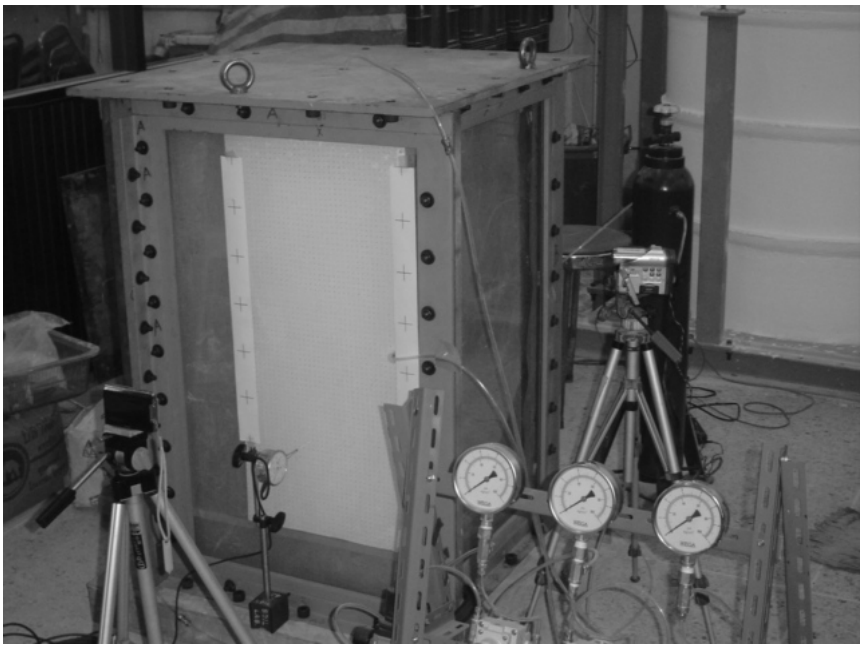

Figure 2.8 Physical model testing set up (Jongpradist et al., 2009).

Jiang et al., 2009). Souley and Homand (1996) used universal distinct element code (UDEC) to studied the mechanical behaviour of rock joints. UDEC is a discontinuous code to simulate fractured rock masses. In UDEC, a rock mass is treated as an assemblage of discrete blocks separated by discontinuities, namely rock joints (Gong et al., 2005). Jiang et al. (2009) developed an expanded distinct element method (EDEM) for simulating the crack generation and propagation due to the shear and tension failures in the matrix rock blocks. Hu and Zhao (2005) simulated the whole deformation and failure process of surrounding rock masses of the underground cavern project of Heihe River Reservoir in Xi'an city by used the 2D elastoplastic finite element method (FEM). Fakhimi et al. (2002) simulated the failure around a circular opening in rock. They concluded that the results of a numerical simulation by particle flow code (PFC^{2D}) of a model tunnel were in very good agreement with the experimental test. Cai et al. (2007) used the fast lagrangian analysis of continua / particle flow code (FLAC/PFC) coupled approach to simulate the acoustic emission (AE) activities at other AE sensor locations and the results compare well with the field AE monitoring data.

CHAPTER III

TEST PLATFORM

3.1 Introduction

A test platform (Pangpetch & Fuenkajorn, 2007) has been modified for use in the simulation of failure of scaled-down shallow openings under real gravitational force. This chapter describes the modifications of the test platform, calculation of the horizontal pseudo-static accelerations, and calculation of lateral stress.

3.2 Design requirements and components

The test platform developed by Pangpetch & Fuenkajorn (2007) is used in this study. The functional requirements for the test platform are (1) to test shallow opening models with a maximum depth of 1.0 m and width of 1.2 m, (2) to induce failure of shallow opening model using real gravitational force, (3) to allow continuous monitoring of the failure process during testing, and (4) to allow incorporating the effect of earthquake on the stability condition.

To meet these requirements the test platform comprises two main components: a 2.2×2.2 m test frame supported by a movable stand. The frame is made of four 5 cm wide C-shaped steel bars at each side linked with a steel plate at each corner (Figures 3.1 through 3.3). A custom-made 2×2 m clear acrylic sheet with 10 mm thick is placed in the front of the frame, while an aluminum plate with the same size is in the back. The spacing between the acrylic sheet and the steel plate is 5 cm. It also allows visual inspection and monitoring of roof rocks movement or failure during the test.

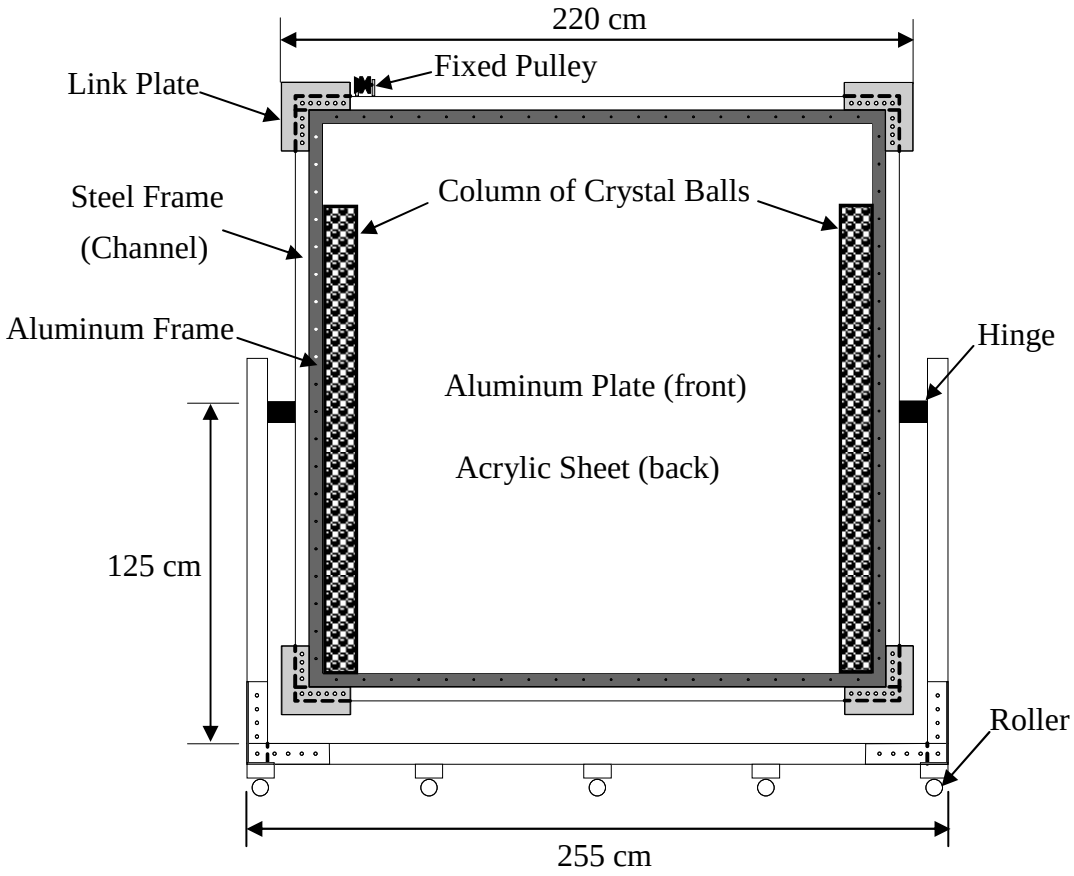

Figure 3.1 Front view schematic drawing of test platform for physical model (Pangpetch & Fuenkajorn, 2007).

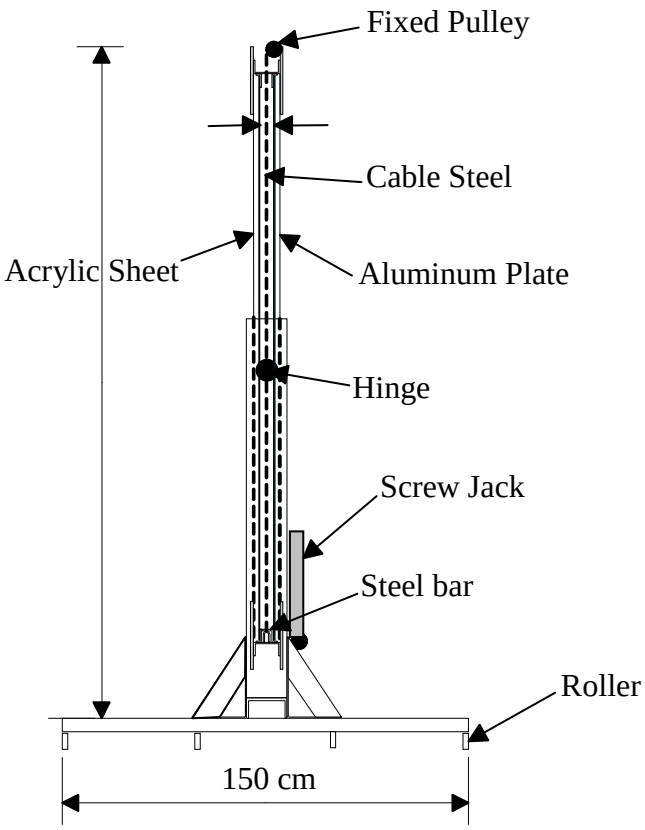

Figure 3.2 Schematic drawing of test platform for physical model (Pangpetch & Fuenkajorn, 2007).

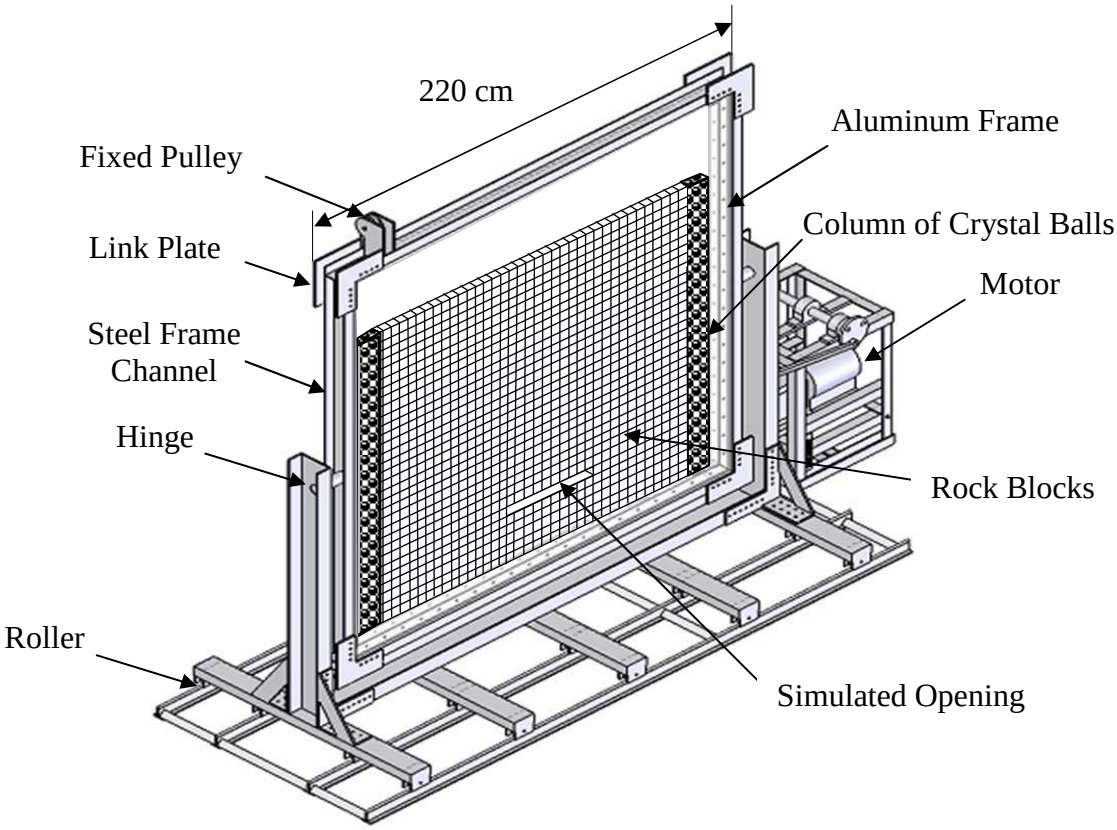

Figure 3.3 Test platform used to simulate shallow openings in rock mass (modified from Pangpetch & Fuenkajorn, 2007).

The test frame can accommodate 4 cm thick rock blocks arranged to a maximum depth and width of 1.2 m to simulate a two-dimensional section of shallow openings in a jointed rock mass. A lateral lithostatic pressure is applied on both sides of the model using a column of crystal balls. A minimum clearance of 0.5 cm is maintained between the front acrylic sheet and rock blocks and between the rear aluminum plate and the rock to ensure that no friction is induced at these interfaces. Figure 3.4 shows the test platform with block samples loaded inside the test frame.

Steel grooved rollers mounted underneath the stand are used for testing under dynamic loading. The rollers will be placed on a set of steel rails equipped with a high torque motor and piston to induce a cyclic motion of the entire test platform. The lateral static acceleration can be created and controlled by adjusting the frequencies and amplitudes of the piston and speed of the motor.

Figure 3.5 shows the crank arm components used to generate the horizontal acceleration to the test frame. The acceleration at point B, represented by a, can be calculated using a set of equations given by Riley & Sturges (1993).

$$a = R\omega_{OA}^2 \cos\theta + y\omega_{AB}^2 \cos\phi - y\alpha_{AB} \sin\phi \tag{3.1}$$

where R = radius of wheel, y = length of crack arm, ω_{OA} and ω_{AB} = angular velocity of OA and AB, θ = angle between AO and OB, α_{AB} = relationship between the acceleration of points A and B, and T = duration of flywheel rotation. The angle ϕ can be obtained from:

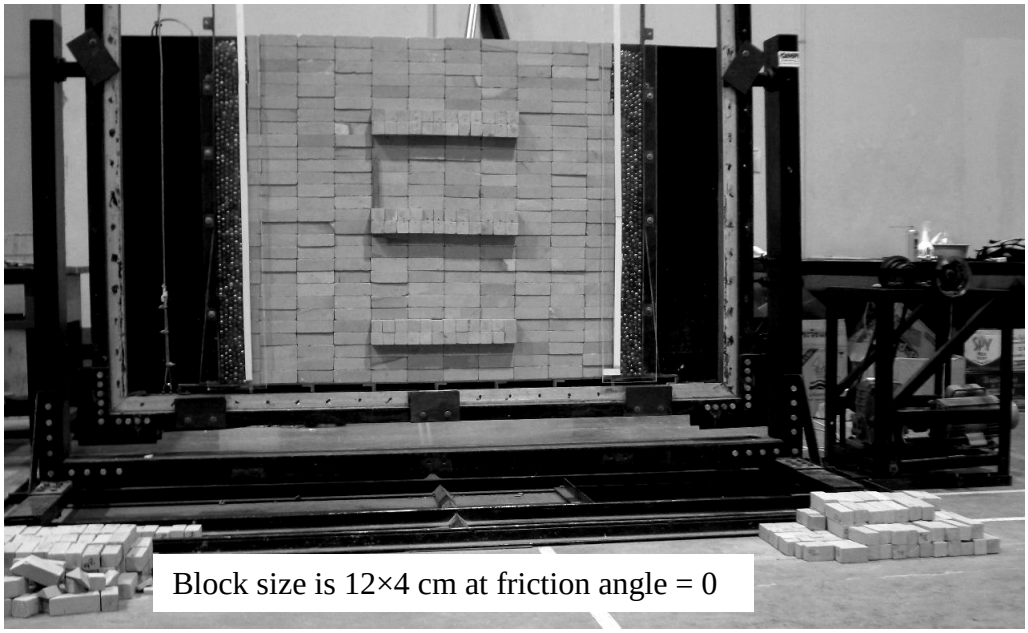

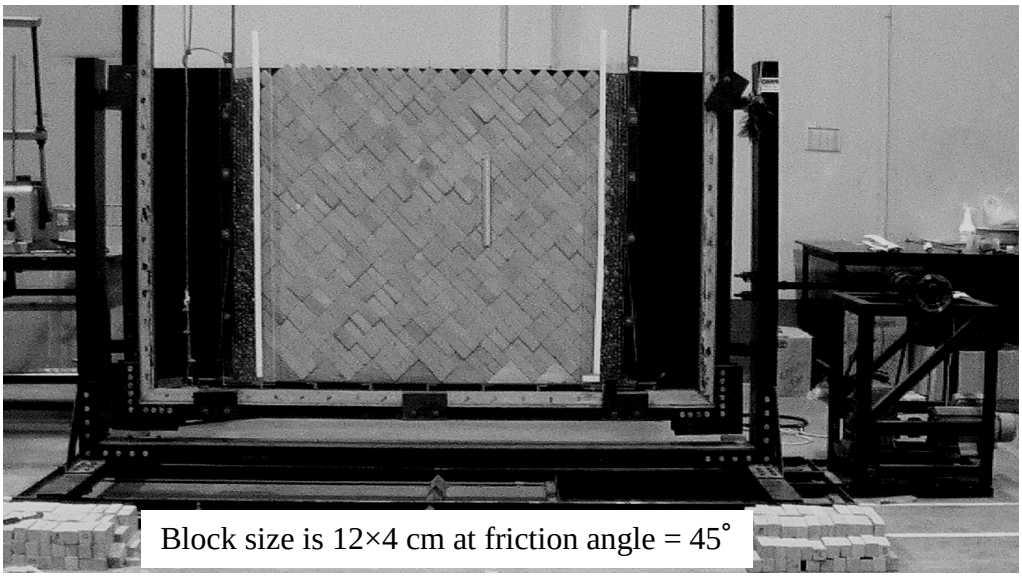

Figure 3.4 Test platform with rock block samples placed inside the test frame.

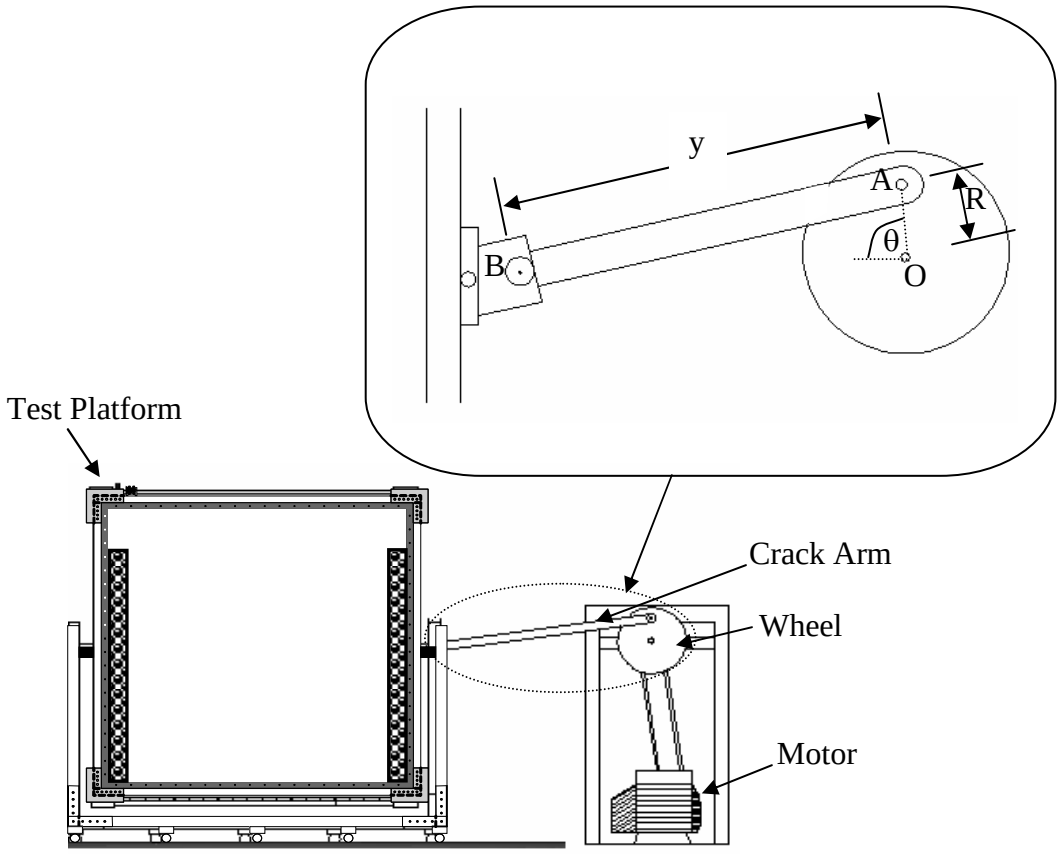

Figure 3.5 Crank arm and flywheel used to induce dynamic loading to the test platform (Pangpetch & Fuenkajorn, 2007).

$$\phi = \sin^{-1}\left[\frac{R\sin\theta}{y}\right] \tag{3.2}$$

The angular velocity of OA and AB can be calculated by:

$$\omega_{OA} = \frac{2\pi}{T}; \quad \omega_{AB} = \frac{R\omega_{OA}\cos\theta}{y\cos\phi} \tag{3.3}$$

The relationship between point A and B, and α_{AB}, is calculated by:

$$\alpha_{AB} = \frac{R\omega_{OA}^2\sin\theta - y\omega_{AB}^2\sin\phi}{y\cos\phi} \tag{3.4}$$

The actual rotational duration (T) is monitored for each model hence changes the speed of the test platform and the flywheel rotation.

3.3 Calculation of lateral stresses

A lateral lithostatic pressure is applied on both sides of the model using a column of crystal balls with a diameter of 16 mm packed in the gap between the model and the test frame. Bulk density of the pack of crystal balls is measured as 2.3 g/cc, which is comparable to the density of the intact block of Phu Phan sandstone. Elevated vertical and lateral stresses can be applied in the test frame to simulate the rock mass behavior under a great depth. They are not applied here because this study involves opening behavior at shallow depths as affected by joint system. Figure 3.6 shows the key variables defined in the physical test models. The model height, H, determines the applied maximum lithostatic pressure at the bottom of the model which is calculated as 28.0 kPa. The opening depth,

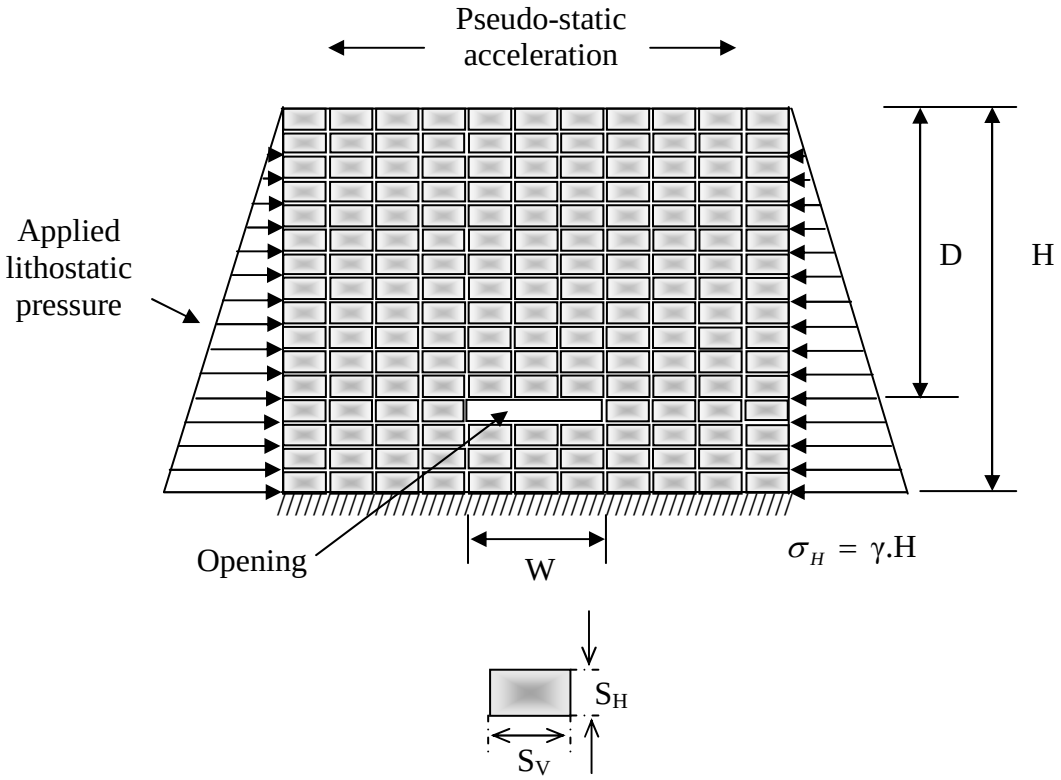

Figure 3.6 Variables used in physical model simulations and analysis. Joint inclination can be set at any angle by tilting the rock blocks in the model.

D, is measured from the opening roof to the top of the model. The maximum unsupported span, W, corresponds to the maximum number of rock blocks removed before failure occurs. Spacings for the vertical and horizontal joint sets are defined as S_V and S_H for joint angles of 0° and 90°. For an inclined joint angle the apparent spacings projected on the vertical and horizontal planes are calculated. The effect of opening height is not studied here. It is always set equal to the block height which is the spacing of the horizontal joints, S_H, for each test model. The simulated joint sets have their strike parallel to the opening axis, and hence represent a worst case scenario of the opening stability.

Video camera continuously records the roof rocks movement before failure. The video playbacks are also very useful to identify the location where the failure was initiated, and how it progressed.

CHAPTER IV

MODEL SIMULATIONS

4.1 Introduction

This chapter describes the method and results of the shallow opening model simulations. The simulations are made under static and dynamic conditions. The opening depths vary from 24 to 96 cm.

4.2 Rock models

Phu Phan sandstone from Nakhon Ratchasima province has been selected for use as rock models primarily because it has highly uniform texture, density and strength. It is classified as fine-grained quartz sandstone with 72% Quartz (0.2-0.8 mm), 20% feldspar (0.1-0.8 mm), 3% mica (0.1-0.3 mm), 3% rock fragments (0.5-2mm), and 2% others (0.5-1 mm). The average density is 2.27 g/cc. To form opening models with two mutually perpendicular joint sets, cubical (4x4x4 cm) and rectangular (4×4×8 cm and 4×4×12 cm) shaped sandstone blocks have been prepared. The cubical blocks are used to simulate joint sets with equal spacing, while the rectangular blocks simulate joint sets with different spacings. Quality control has been carried out to ensure that the geometry of each block meets the specifications. A total of nearly 1000 blocks of Phu Phan sandstone has been prepared (Figure 4.1). The basic friction angle is about 26 degrees and cohesion is 0.053 kPa (Pangpetch and Fuenkajorn, 2007). The cohesion is extremely low which agrees with the results obtained by Kemthong (2006). He reports that the basic friction angle for smooth

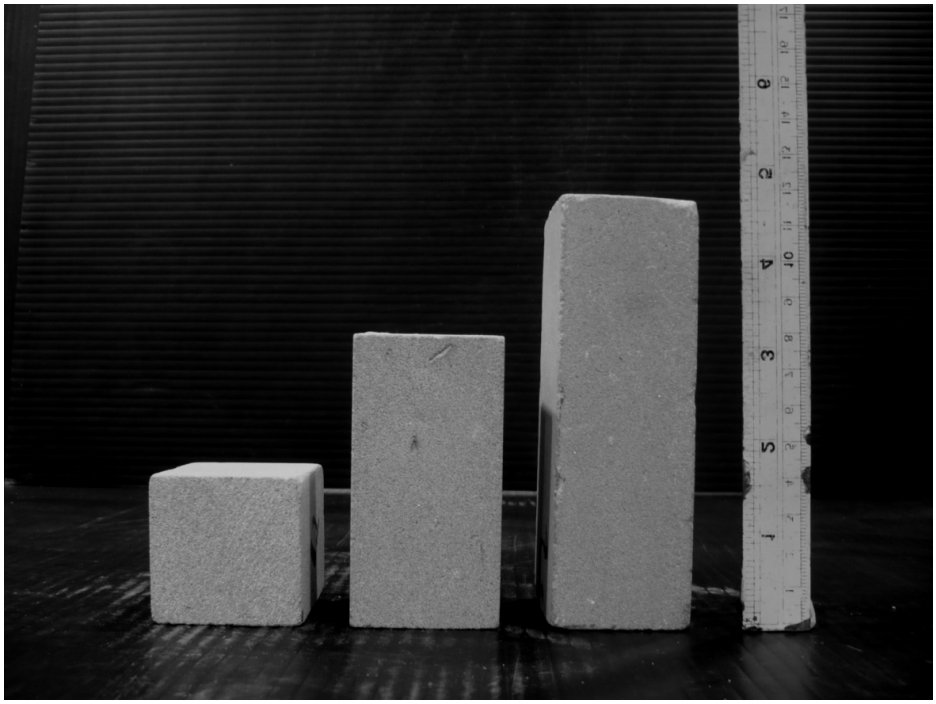

Figure 4.1 Nearly 1000 blocks of Phu Phan sandstone prepared for testing and block size are 4×4, 4×8 and 4×12 cm.

(saw-cut) surfaces of Phu Phan sandstone is averaged as 32 degrees with virtually zero cohesion. The discrepancy of the friction angles is probably due to the intrinsic variability of the rock and the difference in the ranges of normal loads used in the tests. The uniaxial compressive strength of the tested sandstone is 72.4 ± 8.5 MPa and elastic modulus equals to 18.4 ± 1.1 GPa (Kemthong, 2006).

4.3 Test Models under Static Condition

The simulations involve two-dimensional of shallow opening formed by cubical (4×4×4 cm) and rectangular (4×4×8 cm and 4×4×12 cm) blocks of sandstone, under various maximum unsupported span with the maximum opening depth of 1.2 m. For the block length from 4 cm to 12 cm tested here using the rock mass model width of 1.2 m is sufficiently large to minimize the edge effect on the results, as suggested by Zhu and Zhao (2004) that a physical model width should be 10 times greater than the block size. Deformation and failure of the sandstone blocks are not considered in this study (assumed as rigid blocks) because the rock strength and stiffness are very high as compared to the maximum applied lithostatic stresses at 1.2 m depth.

Over fifty test models have been simulated under static condition with vertical to horizontal joint spacing ratios (S_V:S_H ratios) from 1:3, 1:2, 1:1, 2:1 to 3:1. The opening depths vary from 16 to 100 cm. The test parameters and results are described in Appendix A. Each set of opening geometries is formed by sandstone blocks with the same dimension. The joint angles of 0 and 90° are fixed by steel base underneath rock blocks. For the inclined joint angle of 45°, triangle timbers are placed on the steel base to obtain the desired inclination of joint angle (Figures 4.2 and 4.3). Rock block samples are arranged with a maximum height up to 1.2 m. Video records are

taken for a post-test analysis. After all blocks are arranged to the maximum height and width in the test frame, a rectangular opening is created by carefully removing a rock block at a pre-defined depth. The blocks adjacent to the opening on both sides are then removed one-by-one until movement or failure of the roof rocks is visually observed. The opening width immediately before the failure occurs is taken as the maximum unsupported span. The test is repeated at least 3 times under the same condition to ensure the repeatability of the results.

Table 4.1 summarizes the ranges of test parameters and results under static conditions. The observed maximum unsupported spans (W) and their corresponding depths (D) are normalized by spacings of the vertical and horizontal joints (S_V and S_H), respectively. Figure 4.4 gives examples of the test models for various opening depths and joint spacings. Roof collapse occurs when the opening width exceeds its maximum unsupported span. Figures 4.5 and 4.6 plots the normalized maximum span (W/S_V) as a function of normalized depth (D/S_H) for various joints spacings. The results indicate that the maximum span increases with depth which can be best represented by a logarithmic equation. As the depth increases, the maximum span approaches an ultimate value for each joint spacing ratio (S_V/S_H). The maximum span also increases with decreasing S_V:S_H ratio, suggesting that it is more sensitive to the horizontal joint spacing than to the vertical one. This means that the maximum spans are larger for a smaller joint spacing ratio (smaller S_V or larger S_H). This probably holds true only for the range of the spacing ratios used here. For the condition where S_V=S_H, an inclination of the two joint sets to 45° results in an about 20% decrease in the maximum span. The

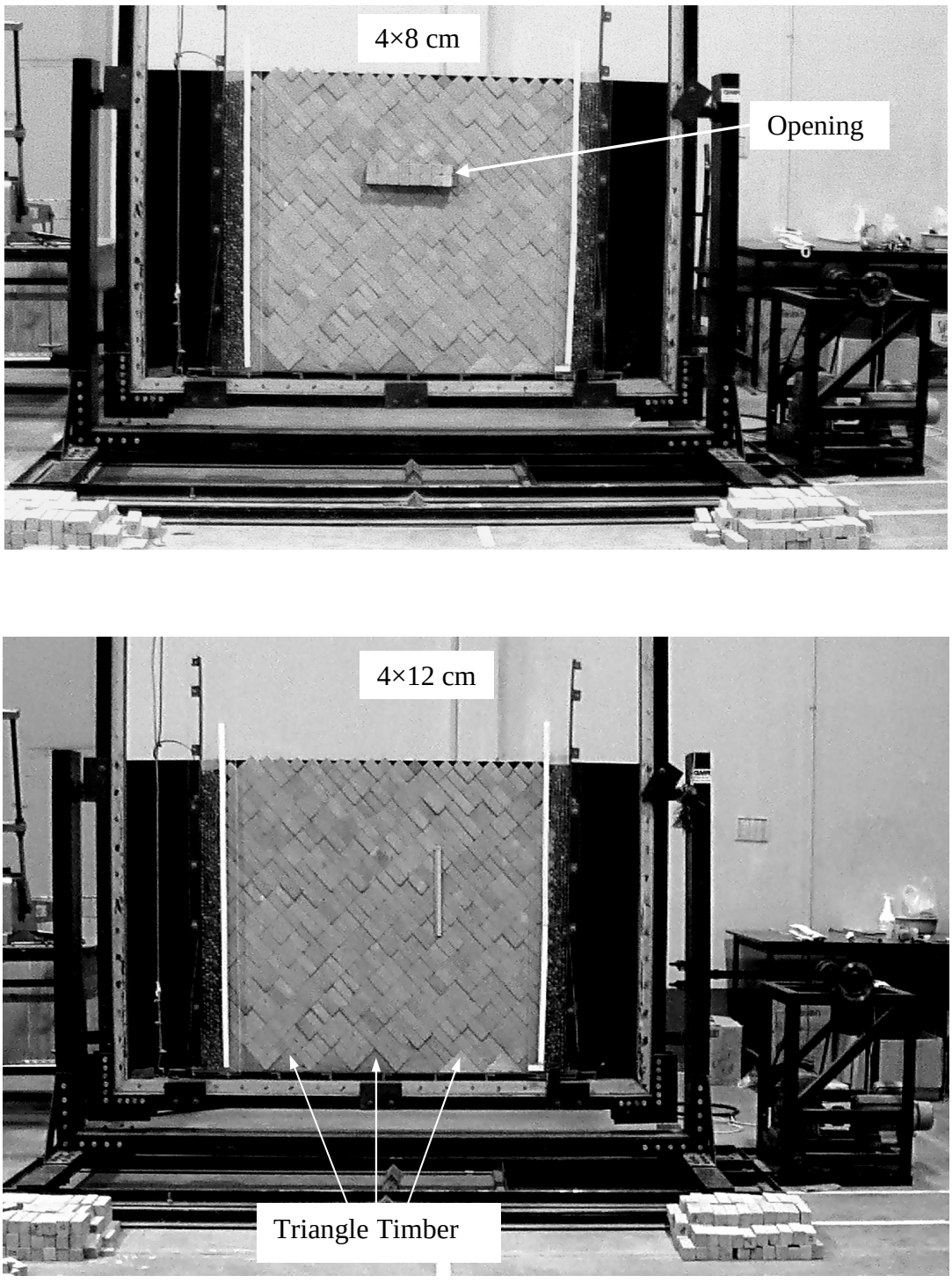

Figure 4.2 Rock samples for 4×8 and 4×12 cm blocks at joint angle of 45° load inside the test frame and the joint angle are controlled by triangle timbers.

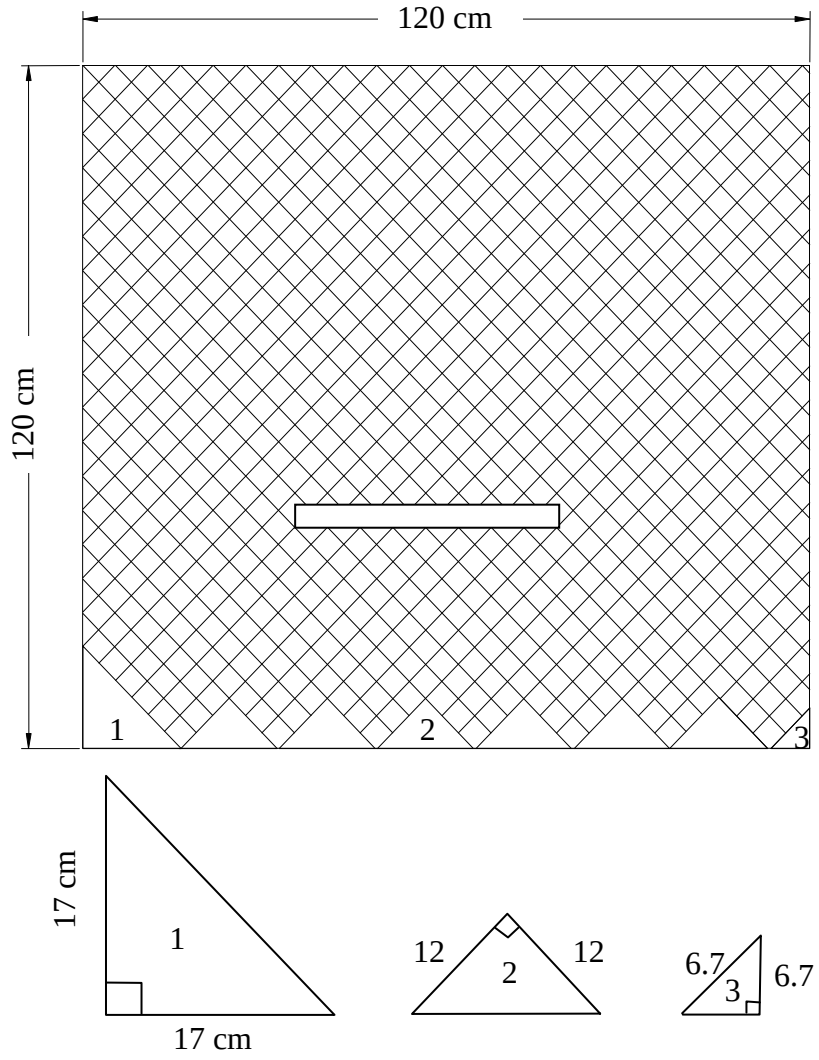

Figure 4.3 The inclined joint angles are obtained by placing triangle timbers at the bottom of the rock blocks.

Table 4.1 Ranges of test parameters and results under static condition.

Spacing Ratio (S_V/S_H)	Block Arrange-ment	S_V	S_H	No. of Tests	Depth, D (cm)	D/S_H	Maximum Span, W (cm)	W/S_V
1:1		2.88	2.88	8	24-92	4.2-16.3	16-40	2.8-7.2
		4	4	21	16-96	4-24	12-28	3-7
1:2 or 2:1		2.88	5.66	8	24-80	4.2-14.1	12-32	2.1-5.6
1:2		8	4	12	24-96	3-12	12-28	2-7
1:3 or 3:1		2.88	8.48	6	28-88	5.1-15.5	12-32	2.1-5.6
1:3		12	4	8	24-84	2-7	12-24	3-6
2:1		4	8	8	20-92	5-23	8-40	1-5
3:1		4	12	8	36-100	9-25	12-48	1-4

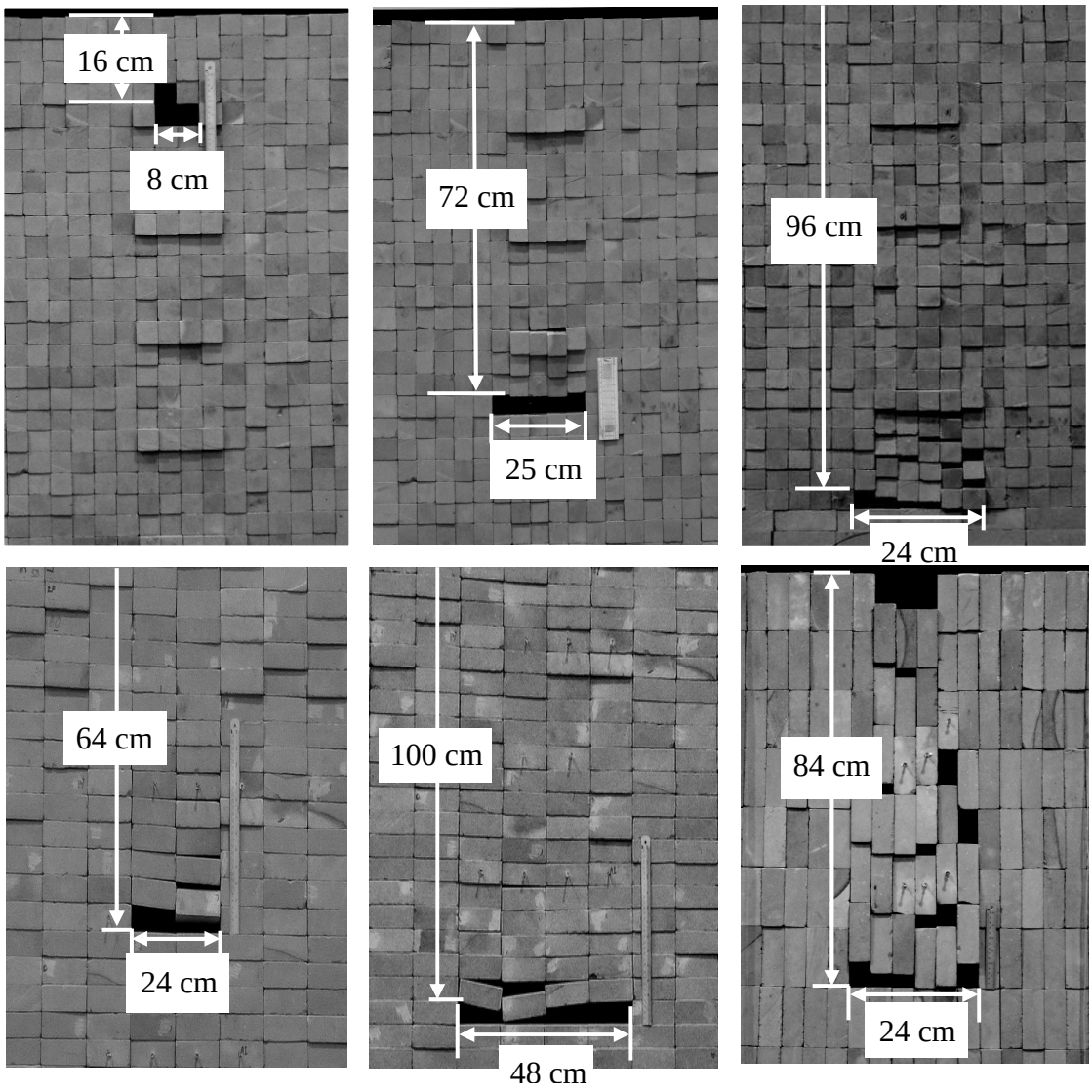

Figure 4.4 Examples of physical models showing roof failure after opening widths exceed their maximum unsupported spans. Top: openings in rock mass model formed by 4×4 blocks. Bottom: openings in rock mass model formed by 4×12 blocks.

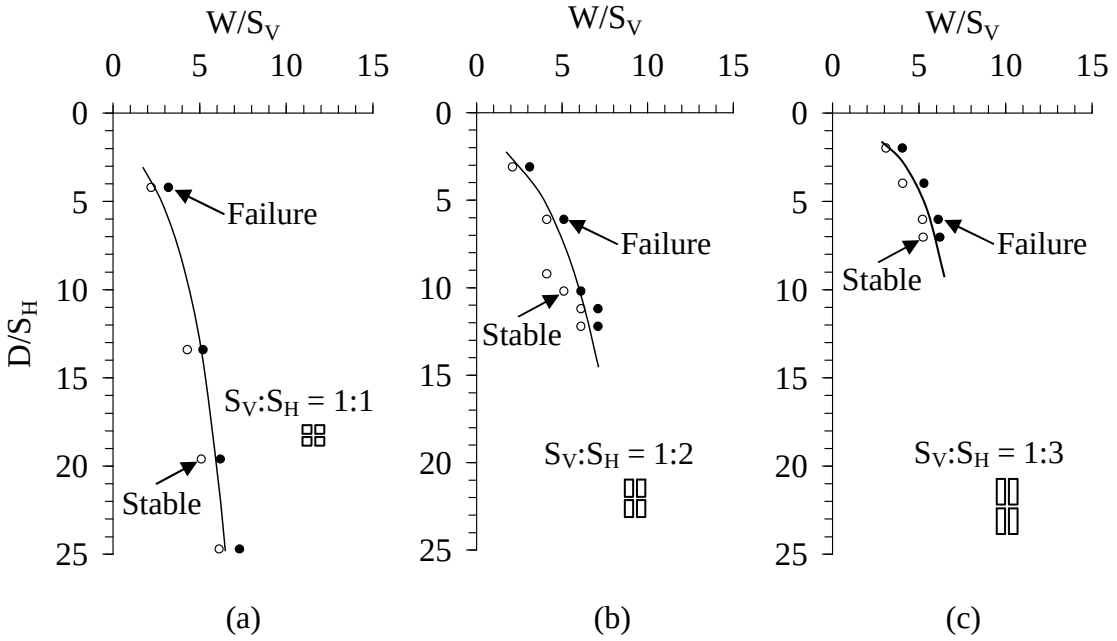

Figure 4.5 Normalized maximum span (W/S_V) as a function of normalized depth (D/S_H) for joint spacing ratios of 1:1 (a), 1:2 (b), and 1:3 (c) under static condition.

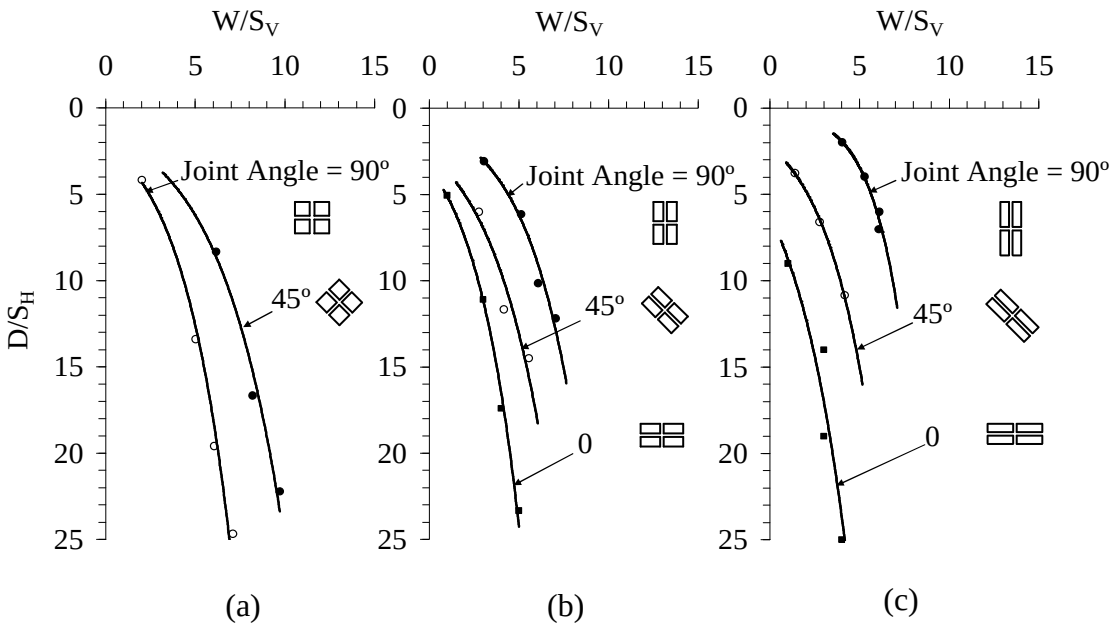

Figure 4.6 Normalized maximum span (W/S_V) as a function of normalized depth (D/S_H) for various joint spacing ratios and joint orientations. The empirical relations of the results are given in Table 4.2.

empirical relations between the normalized maximum span (W/S_V) and the normalized depth (D/S_H) can be expressed as:

$$W/S_V = A \cdot \ln(D/S_H) - B \quad (1)$$

The constants A and B can be determined as a function of the joint spacing ratio (S_V/S_H) as follows:

$$A = \alpha_A \cdot (S_V/S_H) + \beta_A \quad (2)$$

$$B = \alpha_B \cdot (S_V/S_H) + \beta_B \quad (3)$$

where α_A, β_A, α_B, and β_B are empirical constants. Table 4.2 summarizes the numerical values for A, α_A, β_A, B, α_B, and β_B calculated for some applicable joint spacing ratios. The empirical relations above can probably represent a lower bound of the maximum unsupported span for actual shallow openings under similar joint conditions and field stresses.

4.4 Maximum spans estimated from Q and RMR systems

The maximum unsupported span predicted by the empirical equation derived from the test models is compared with those estimated from the RMR and Q systems of rock mass classification (Hoek and Brown, 1980). The comparisons are made for an assumed mine opening at depths (D) ranging from 25, 50, 75 to 100 m. The empirical equation derived for the test results of 4×4 cm blocks is used in the comparison. The joint spacings are assumed as 10, 30 and 50 cm. The rating parameters used in the RMR and Q classification systems are determined or projected

Table 4.2 Empirical relations obtained from regression analysis on the test results under static condition. $W/S_V = A \cdot \ln(D/S_H) - B$, where; $A = \alpha_A \cdot (S_V/S_H) + \beta_A$; $B = \alpha_B \cdot (S_V/S_H) + \beta_B$.

Spacing Ratio (S_V/S_H)	Block Arrangement	A	α_A	β_A	B	α_B	β_B
1:1		2.76	-0.28	2.60	1.99	1.28	-1.02
1:2		2.76			0.02		
1:3		1.71			-2.89		
2:1		2.56			3.16		
3:1		1.31			1.35		

from the relevant conditions used in the test models. The rock mass is completely dry, with three sets of slick, planar and open joints (two sets parallel to the opening axis, one set normal to the opening axis). The joint orientations represent a very unfavorable stability condition. The joints are continuous, having 100% persistence with no alteration. The joint spacings defined above are used to approximate the corresponding RQD's for this example. The intact rock compressive strength of 62.0 MPa is used, representing the actual strength of Phu Phan sandstone.

Table 4.3 compares the maximum spans estimated from RMR and Q systems with those predicted from the physical models using empirical equation from Table 4.2. The physical model predicts the span narrower than the RMR and Q systems do, particularly at shallow depths. This is probably due to the high magnitudes of RQD's estimated from the joint spacings, leading to a high value for RMR and Q, and subsequently makes the calculated maximum span larger. The discrepancies become smaller as the depth increases. At 100 m depth the maximum span from the three methods are comparable.

Under these assumed conditions, the maximum spans determined from the RMR and Q systems are chiefly governed by the joint spacing, and are independent of the opening depth. This is because the RMR system does not consider the effect of depth or in-situ stress in the calculation. For the Q system the effect of in-situ stresses is represented by the stress reduction factor (SRF). Here the SRF is set equal to 1.0 because the openings are at relatively shallow depths. The maximum spans predicted by the physical model can however increase with the opening depth and joint spacing, which are probably similar to the actual opening behavior.

Table 4.3 Predictions of maximum unsupported spans (W) using empirical equations and RMR and Q rock mass classification systems.

Depth (m)	Assumed S_V and S_H (m)	RQD	Q	RMR	W from Q system* (m)	W from RMR system** (m)	W from test model*** (m)
25	0.1	74	0.41	34	5.5	4.5	1.3
	0.3	96	0.53	41	6.1	6.2	3.0
	0.5	98	0.55	51	6.2	9.0	4.4
50	0.1	74	0.41	34	5.5	4.5	1.4
	0.3	96	0.53	41	6.1	6.2	3.5
	0.5	98	0.55	51	6.2	9.0	5.2
75	0.1	74	0.41	34	5.5	4.5	1.5
	0.3	96	0.53	41	6.1	6.2	3.8
	0.5	98	0.55	51	6.2	9.0	5.7
100	0.1	74	0.41	34	5.5	4.5	1.6
	0.3	96	0.53	41	6.1	6.2	4.0
	0.5	98	0.55	51	6.2	9.0	6.0

* For Q system of rock mass classification:

$$W = 2 \cdot ESR \cdot Q^{0.4}$$

ESR = 3.0 (for temporary mine openings), RQD = 100 exp $(-0.1/S_V)(1+0.1/S_V)$, where $S_V = S_H$

$$Q = \left(\frac{RQD}{J_n}\right) \times \left(\frac{J_r}{J_a}\right) \times \left(\frac{J_w}{SRF}\right)$$

J_n = 9.0 (for 3 joint sets), J_r = 0.5 (for slick and planar joints), J_a = 1.0 (for no alteration of joints), J_w = 1.0 (for dry condition), SRF = 5.0 (for loose rock with open discontinuities)

** For RMR system of rock mass classification:
UCS = 62.0 MPa, Open and continuous joints, Correction factor = -12 (for joints with very unfavorable orientation)

*** For test model (using 4×4 cm blocks):

$$W = S_V \cdot [2.32 \cdot \ln(D/S_H) - 0.26]$$

4.5 Test models under dynamic condition

The effects of the pseudo-static accelerations of 0.132 g and 0.225 g on the maximum unsupported span have been experimentally assessed. Only the horizontal acceleration is simulated here because it has more impact on the geological structures than does the vertical acceleration (Kramer, 1996). The test procedure is similar to that under static condition. After removing a rock block at a pre-defined depth a pseudo static acceleration is applied for one minute. If no displacement of the rock blocks is observed, a block adjacent to the opening on each side is then removed, and the acceleration is re-applied. The process is repeated until any visible movement or failure of roof rock is obtained. The opening width immediately before the failure occurs is taken as the maximum unsupported span under the given acceleration. Over one hundred models have been simulated under static condition with S_V:S_H ratios from 1:3, 1:2, 1:1, 2:1 to 3:1. The opening depths vary from 24 to 96 cm. The test parameters and results are described in Appendix B.

Table 4.4 summarizes the ranges of the test parameters and the results under dynamic loads. Figure 4.7 plot the normalized maximum span as a function of normalized depth for testing under pseudo-static accelerations of 0.132 g and 0.225 g for joint spacing ratios are 1:1, 1:2, and 1:3. The summations of the normalized maximum span and depth relationship for testing under pseudo-static accelerations are shown in Figures 4.8 and 4.9. Similar to the test results under static condition, the maximum span increases with depth which can be best represented by a logarithmic equation for each joint spacing ratio. Numerical values for the empirical constants are listed in Table 4.5. As the depth increases, the maximum span approaches an ultimate value. The higher the acceleration applied to the test models, the smaller the

maximum span obtained. The acceleration of 0.225 g can reduce the maximum span by up to 50%, particularly when the S_V:S_H ratio is greater than 2:1.

As the depth increases the maximum spans under dynamic loads are close to those tested under static condition, suggesting that the impact of dynamic loading decreases with depth. At shallow depth, a pseudo-static force generated by the cyclic motion of the test frame may be high enough to effectively reduce the normal stress at the rock block contacts. This subsequently reduces their shearing resistance, resulting in a relative movement between the rock blocks immediately above the opening. As the depth increases, the same magnitude of the pseudo-static force may not be high enough to overcome the applied lateral lithostatic stress, and hence have smaller effect on the shearing resistance at the block contacts.

Table 4.4 Results of physical models tested under dynamic loads.

Spacing Ratio (S_V/S_H)	Block Arrange-ment	No. of Tests	D (cm)	D/S_H	W (cm)	W/S_V	Frequency (Hz)	a (g)	Modified Mercalli Intensity*
1:1		8	40-92	8-24	8-24	2-6	1.833	0.225	VII
		8	40-92	7-16	16-32	3-6	1.429	0.132	VI
1:2 or 2:1		6	32-84	6-15	8-24	1-4	1.833	0.225	VII
1:2		9	24-96	3-12	8-24	2-6	1.429	0.132	VI
		8	24-96	3-12	8-20	2-5	1.833	0.225	VII
1:3 or 3:1		9	40-88	7-16	12-28	2-5	1.429	0.132	VI
		9	40-88	7-16	8-24	1-3.5	1.833	0.225	VII
1:3		12	24-96	2-8	12-24	3-6	1.429	0.132	VI
		8	24-96	2-8	8-24	2-6	1.833	0.225	VII
2:1		8	24-96	6-24	8-24	1-3	1.833	0.225	VII
3:1		8	36-100	9-25	12-36	1-3	1.429	0.132	VI

* Modified Mercalli Intensity from Richter (1958) and Wald et al. (1999) as:

VI = Felt by all; many frightened. Some heavy furniture moved; a few instances of fallen plaster. Damage slight.

VII = Damage negligible in building of good design and construction; slight to moderate in well-built ordinary structures; considerable damage in poorly built or badly designed structures; some chimneys broken.

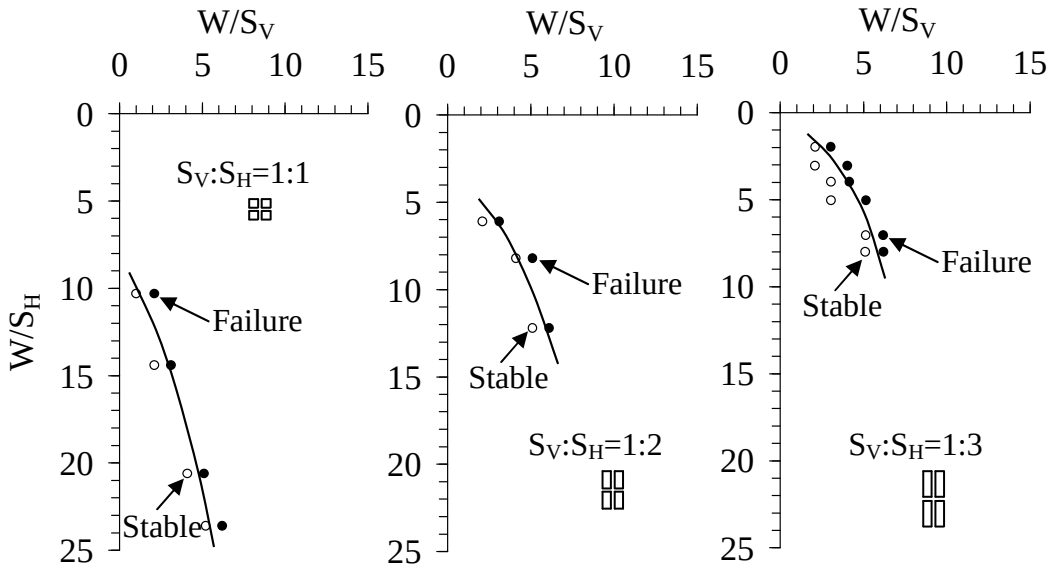

(a)

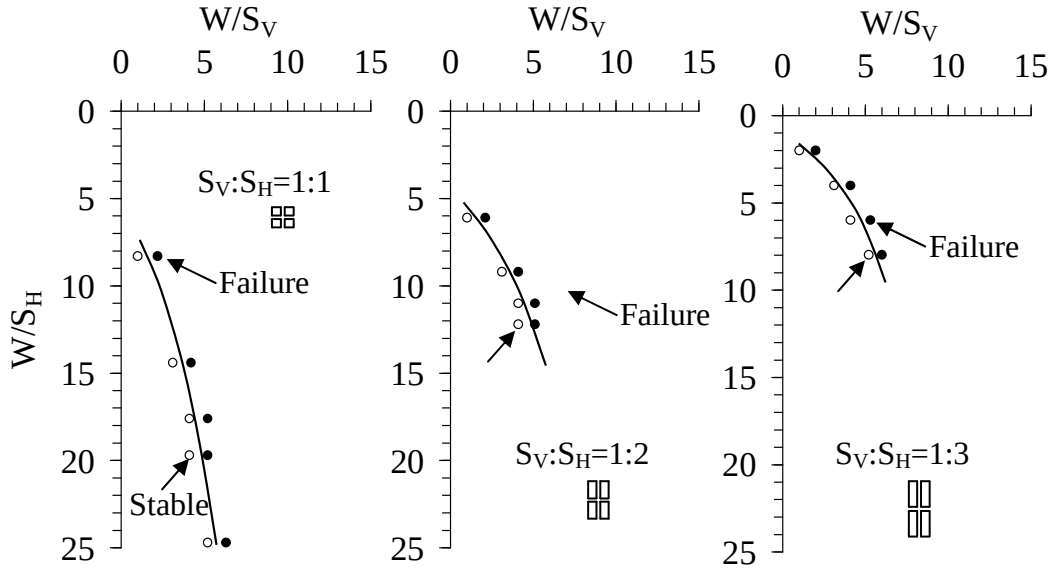

(b)

Figure 4.7 Normalized maximum span (W/S_V) as a function of normalized depth (D/S_H) for joint spacing ratios of 1:1, 1:2, and 1:3 under acceleration of 0.132 g (a) and 0.225 g (b).

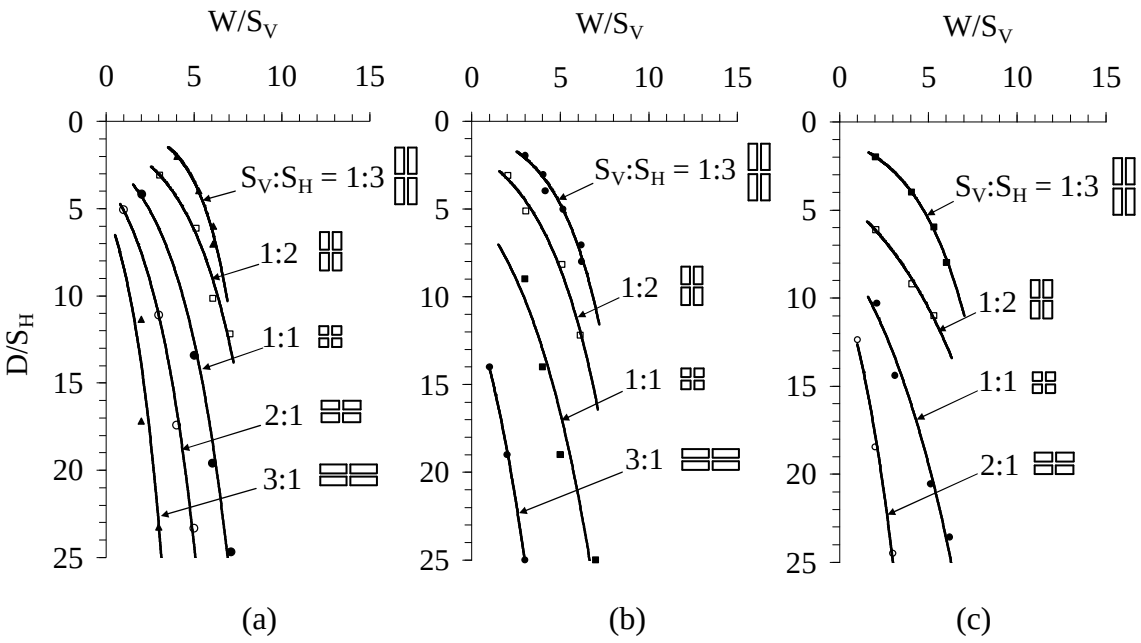

Figure 4.8 Normalized maximum span as a function of normalized depth under pseudo-static accelerations of 0.132 g (b) and 0.225 g (c) compared with the results under static condition (a) for vertical and horizontal joint sets with various spacing ratios.

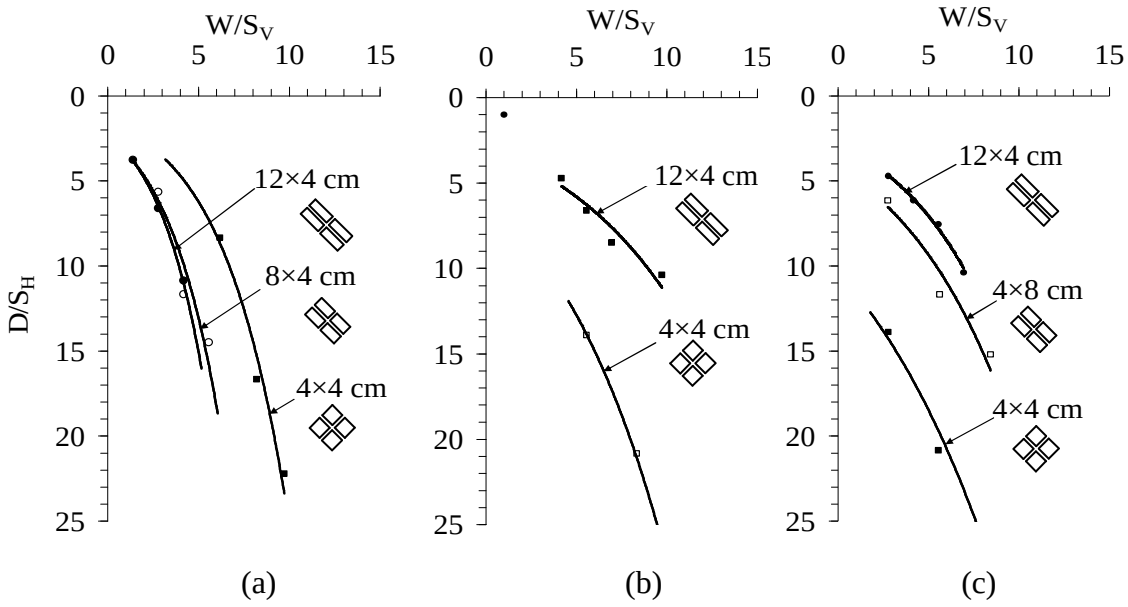

Figure 4.9 Normalized maximum span as a function of normalized depth under pseudo-static accelerations of 0.132 g (b) and 0.225 g (c) compared with the results under static condition (a) for 45º-inclined joint sets.

Table 4.5 Empirical relations obtained from regression analysis on the test results under dynamics load at a = 0.132 g and 0.225 g. $W/S_V = A \cdot \ln(D/S_H) - B$, where; $A = \alpha_A \cdot (S_V/S_H) + \beta_A$; $B = \alpha_B \cdot (S_V/S_H) + \beta_B$.

a (g)	**Spacing Ratio (S_V/S_H)**	**Block Arrangement**	**A**	**α_A**	**β_A**	**B**	**α_B**	**β_B**
0.132	1:1		3.74	0.24	2.88	5.54	2.95	-0.06
	1:2		3.11			1.65		
	1:3		2.38			-1.28		
	3:1		3.45			8.11		
0.225	1:1		4.93	-0.66	4.69	9.65	2.00	4.06
	1:2		5.49			7.95		
	1:3		2.92			-0.02		
	2:1		2.90			6.34		

CHAPTER V

DISCRETE ELEMENT ANALYSES

5.1 Introduction

This chapter describes the method and results of discrete element simulation for the shallow opening under static and dynamic conditions. The results are compared with those of the test model observations to reveal the predictability of the numerical simulation and the performance of the physical modeling.

5.2 Discrete element analysis

Discrete element analyses are performed using UDEC code (Itasca, 2004) to describe the stability conditions of the openings in the physical models. In the distinct element method, a rock mass is represented as an assembly of discrete blocks. The dynamic behavior is represented numerically by a timestepping algorithm in which the size of the timestep is limited by the assumption that velocities and accelerations are constant within the timestep. The calculations performed in the distinct element method alternate between application of a force-displacement law at all contacts and Newton's second law at all blocks.

Newton's second law of motion can be written in the form (Itasca, 2004):

$$\frac{du}{dt} = \frac{F}{m} \tag{5.1}$$

where u = velocity; t = time; and m = mass.

With velocities stored at the half-timestep point, it is possible to express displacement as

$$u^{(t+\Delta t)} = u^{(t)} + u^{(t+\Delta t/2)}\Delta t \tag{5.2}$$

The constitutive relations for deformable blocks are used in an incremental form. The actual form of the equations is:

$$\Delta\sigma_{ij}^{e} = \lambda\Delta\in_{\upsilon}\delta_{ij} + 2\mu\Delta\in_{ij} \tag{5.3}$$

where λ, μ are the Lame constants; $\Delta\sigma_{ij}^{e}$ are the elastic increments of the stress tensor; $\Delta\in_{ij}$ are the incremental strains; $\Delta\in_{\upsilon} = \Delta\in_{11} + \Delta\in_{22}$ is the increment of volumetric strain; and δ_{ij} is the Kronecker delta function.

The force-displacement models used in UDEC to represent axial and shear behavior are continuous, nonlinear algorithms written in terms of stiffness (axial or shear), the ultimate load capacity and a yield function. The force-displacement relation that describes the axial response is given by the following equation.

$$\Delta F_a = K_a|\Delta u_a|\, f(Fa) \tag{5.4}$$

where ΔF_a is an incremental change in axial force; Δu_a is an incremental change in axial displacement; K_a is the axial stiffness; and $f(F_a)$ is a function describing the path by which the axial force, F_a approaches the ultimate (or bounding) axial force $F_{a,b}^{max}$.

The function

$$f(\mathrm{Fa}) = [|\, F_{a,b}^{max} - \mathrm{Fa}|\, \frac{(F_{a,b}^{max} - F_a)}{[F_{a,b}^{max}]^2}]^{e_a} \tag{5.5}$$

is used to represent the axial yield curve. From Eq. (5.4), the axial force "seeks" the bounding force in an asymptomatic manner. The axial stiffness exponent, e_a, controls the rate at which the bounding force is reached. If $e_a = 0$, then the axial stiffness remains constant.

Apply dynamic loading and boundary conditions, the base of the model is considered to be flexible. The closed-form solution for crack slip as a function of time, as derived by Day (1985) is given by:

$$\delta_{u(x,t)} = \frac{2m_o\beta^2}{\pi\rho\alpha^2} R_e\left[\frac{p\eta_\alpha\eta_\beta}{R_{(p)}}\right]\left(\tau + \frac{2r}{\alpha}\right)^{-1/2} \tau^{-1/2} H_{(\tau)} \tag{5.6}$$

where

$$R_{(p)} = (1 - 2\beta^2 p^2)^2 + 4\beta^4\eta_\alpha\eta_\beta p^2 + 2\beta\eta_\beta\gamma$$

$$p = \frac{1}{r^2}\left[\left(\tau + \frac{r}{\alpha}\right)x + i\left(\tau + \frac{2r}{\alpha}\right)^{1/2} \tau^{1/2} h\right]$$

and : $r = (x^2+h^2)^{1/2}$, distance from the point source to the point on the crack where the slip is monitored; $H(\tau)$=step function; $\tau = t-(r/\alpha)$; m_o=source strength; α= velocity of pressure wave; β= velocity of shear wave; ρ= density; $\eta_\alpha=(\alpha^{-2}-p^2)^{1/2}$, Re $\eta_\alpha \geq 0$; $\eta_\beta=(\alpha^{-2}-p^2)^{1/2}$, Re $\eta_\beta \geq 0$; γ= dimensionless bonding parameter.

The solution for the displacement due to a center of dilation in an infinite medium (Achenbach, 1975) is described by:

$$u_i = \frac{1}{4\pi C_p^2} \frac{\partial}{\partial x_i} \left[\frac{1}{r} \int (t - \frac{r}{C_p}) \right] \tag{5.7}$$

where $r^2=x^2+y^2+z^2$; C_p=P-wave velocity; and f(t)=source time history.

Over 200 discrete element models are constructed to represent various opening depths and joint spacing ratios. The joint friction angle and cohesion used in the simulations are 26° and 0.053 kPa. UDEC simulation results are shown in Appendix C. Table 5.1 summarizes the simulation parameters. Joint angles are 0 and 90º, depth varies from 12 to 76 cm, and spans vary from 8 to 24 cm. After several trials (by varying opening widths) the maximum unsupported span can be determined for each opening depth and joint spacing ratio. Figures 5.1 and 5.2 shows examples of rock blocks failure of shallow opening for joint spacing ratios of 1:1 and 1:3 with physical model tests under static condition.

The maximum spans are plotted as a function of depth. The UDEC results are compared with those observed from the physical models under static loading for joint spacing ratio of 1:3 to 3:1 in Figure 5.3. UDEC simulation gives smaller maximum span than do the test model for static acceleration of 0.225 g as shown in Figure 5.4.

The UDEC simulations show the increasing trends of the maximum span with depth, which are similar to those observed from the test models. For all cases the predicted maximum spans slightly under-estimate the test results. The largest discrepancies are less than 20%. This is probably because the block models in the discrete element analyses are perfectly shaped with identical joint properties while in the test models the block shapes are not perfect and the frictional strength is unlikely to be identical for all contacts (joint surfaces). As a result the rock blocks constructed

in the UDEC models can slide more easily than those tested in the physical models, and hence yield a slightly narrower maximum unsupported span.

Table 5.1 Summary of UDEC simulations for shallow opening. The sandstone blocks have ψ_b=26º, c=53 Pa, and γ_r=2.38 kN/m^3, under 14000 cycles.

Testing Condition	Joint Spacing Ratios	Depth (cm)	Maximum Span (cm)	No. of Simula-tions	Static Accelera-tions (g)	Times of failure ($\times 10^{-1}$sec)
Static	1:3	24-72	8-20	5	-	2.09-2.11
	1:2	16-96	8-24	11	-	2.01-2.02
	1:1	8-72	4-20	17	-	1.54-1.77
	2:1	12-56	8-16	11	-	1.78-1.95
	3:1	32-76	12-36	17	-	1.91-2.54
Dynamic	1:3	32-76	8-20	11	0.132	2.12-2.21
				11	0.225	2.01-2.22
	1:2	48-96	8-16	7	0.132	1.54-1.77
				7	0.225	1.78-1.95
	1:1	36-72	8-16	7	0.132	1.94-2.62
				7	0.225	2.19-2.32
	2:1	20-56	8-16	10	0.132	2.01-2.02
				10	0.225	1.34-1.76
	3:1	24-96	8-20	7	0.132	1.58-2.05
				7	0.225	1.91-2.54

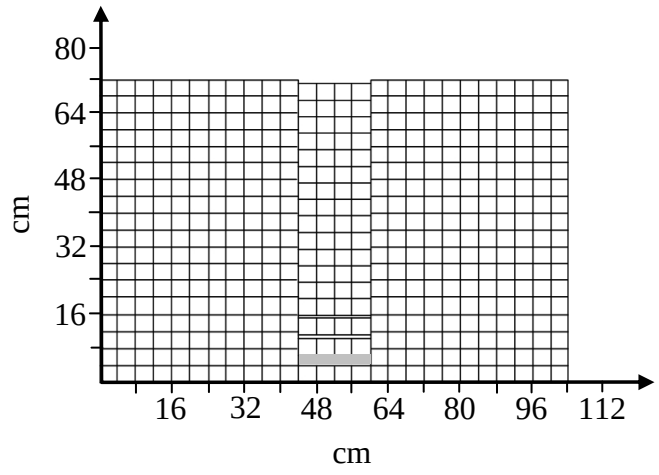

(a)

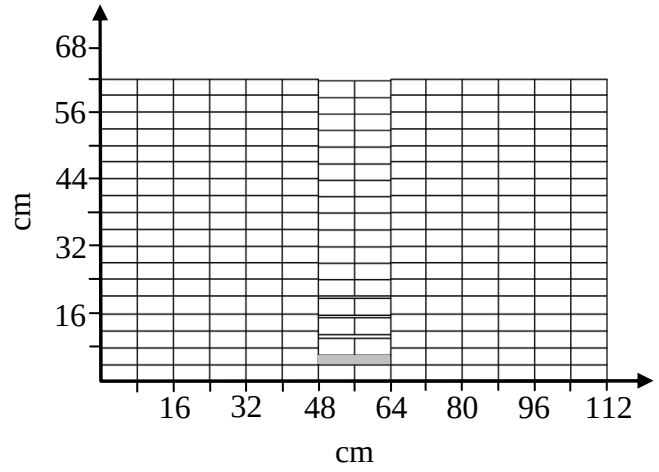

(b)

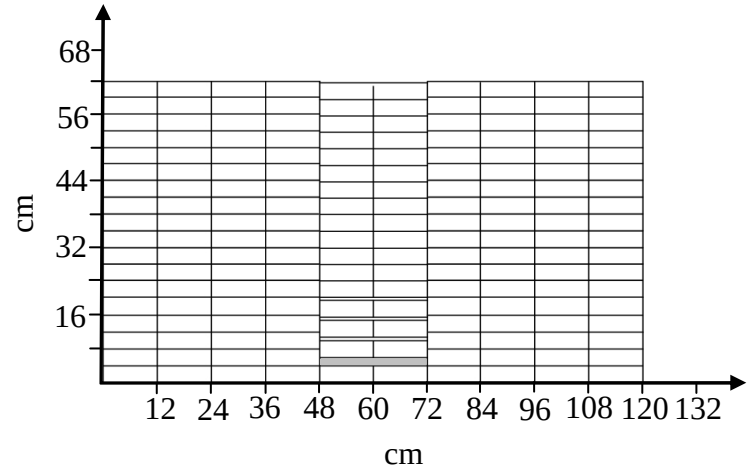

(c)

Figure 5.1 UDEC simulation results for joint spacing ratios of 1:1 (a), 2:1 (b) and 3:1 (c) under static condition.

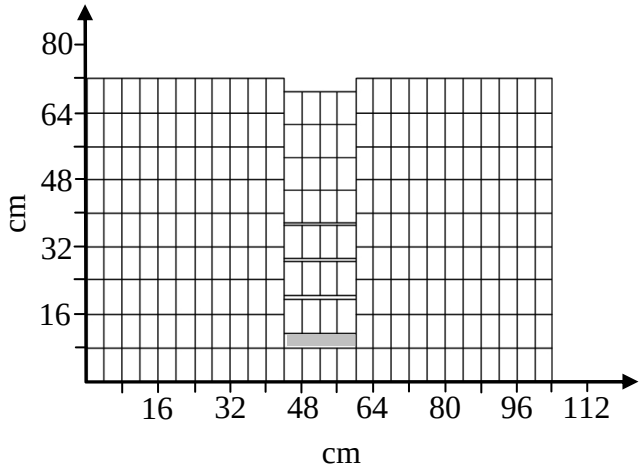

(a)

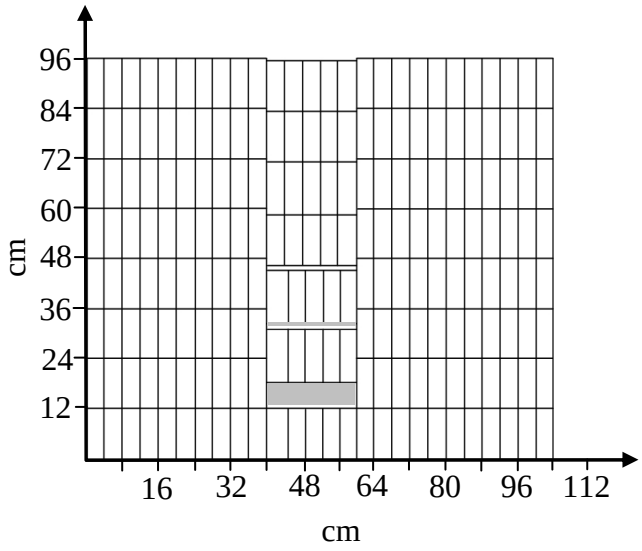

(b)

Figure 5.2 UDEC simulation results for joint spacing ratios of 1:2 (a) and 1:3 (b) under static condition.

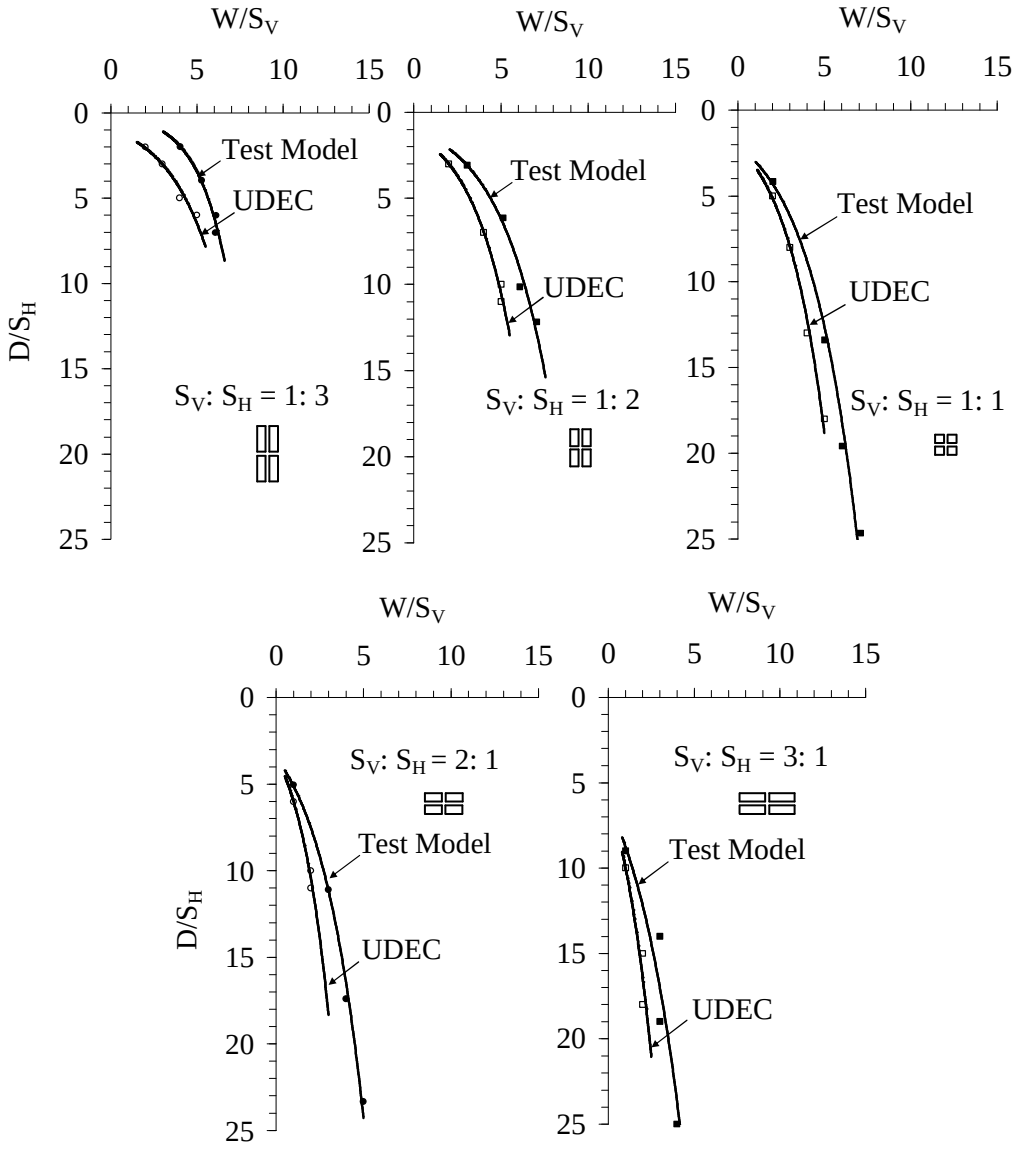

Figure 5.3 Comparisons of UDEC simulations with test models for various spacing ratios.

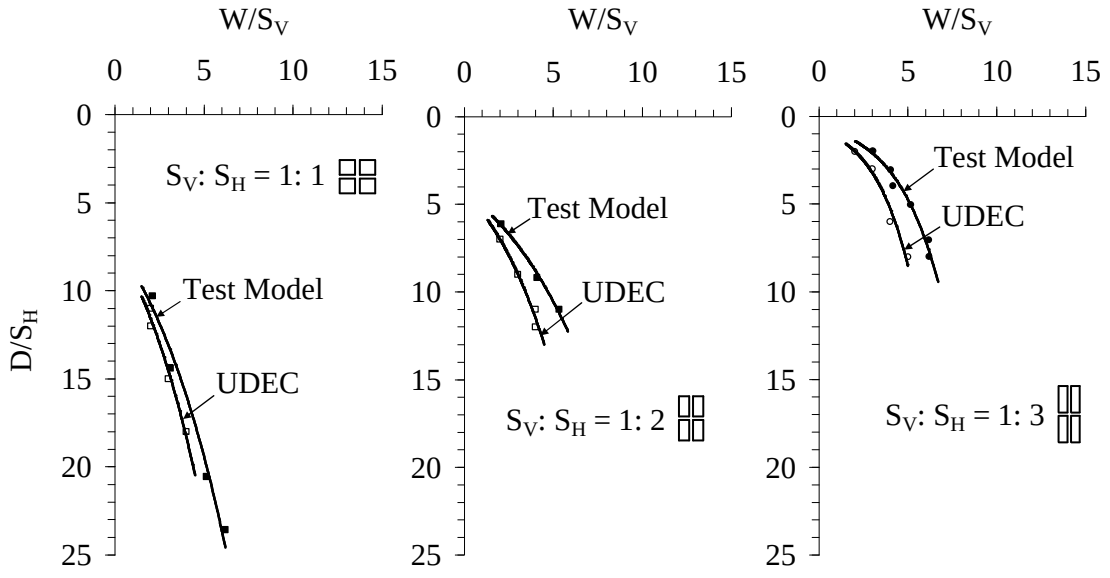

Figure 5.4 Comparisons of UDEC simulations with test models under pseudo-static acceleration of 0.225 g.

CHAPTER VI

DISCUSSIONS, CONCLUSIONS, AND RECOMMENDATIONS FOR FUTURE STUDIES

6.1 Discussions

The maximum spans predicted by the physical model increase with the opening depth and joint spacing. This is also supported by the UDEC simulation results. Despite the discrepancies and the limitation of the proposed empirical equations, as a minimum, the physical model predictions can give a lower bound for the maximum unsupported span for shallow openings in rock mass, under similar rock strengths and joint conditions as tested here. The physical model results yield empirical relations between the maximum unsupported span and depth for shallow openings. The physical model test results clearly indicate that the maximum unsupported span of shallow openings is controlled by the spacing and orientation of joints, S_V:S_H ratio, and depth. The smaller the S_V:S_H ratio, the larger the maximum span. The tested maximum span increases with depth and approaches an ultimate value for each joint spacing ratio, which conforms to the simulation results from discrete element analyses. It is believed that such similar behavior occurs in actual in-situ conditions, which however can not be described by the RMR and Q systems of rock mass classification. The effect of the pseudo-static accelerations tends to be more pronounced under a larger S_V:S_H ratio. The dynamic impact however gradually reduces with depth, as evidenced by the fact that the observed maximum spans under

both pseudo-static accelerations are close to those tested under static condition when the normalized depth, D/S_H, approaches 25.

6.2 Conclusions

A test platform is used in the simulations of scaled-down shallow opening models comprising sets of cubical and rectangular sandstone blocks. True gravitational force is used to initiate the failure. Observations of the failure behavior during video playback reveal that for roof rocks movement the failure is felled into opening. Physical model simulations have been performed to determine the effects of depth, joint spacing and orientation on the maximum unsupported span of shallow underground openings under static and dynamic loads. Cubical and rectangular blocks of Phu Phan sandstone are arranged in vertical and horizontal test frame to simulate a two-dimensional representation of single rectangular openings in rock mass with two mutually perpendicular joint sets. Under the same depth and joint spacing ratio, inclination of the joint angles from 0° to 45° can reduce the maximum span by up to 20%. The horizontal pseudo-static accelerations of 0.132 g and 0.225 g can significantly reduce the maximum unsupported span for shallow openings. Up to 50% reduction of the maximum opening span resulted for the acceleration of 0.225 g. The test results under both static and dynamic loading compare reasonably well with those calculated from discrete element analyses using the UDEC code.

6.3 Recommendations for future studies

The physical models tested here have a narrow range of the size and shape of the rock blocks used to simulate the joint spacing in the test frame. Since the models are simulated under very simplified conditions of joints and stress states with a

narrow range of test parameters, care should be taken in extrapolating these relations to actual in-situ openings under greater depths or under complex joint conditions and stress states. Additional test results obtained from opening models with larger blocks, probably up to 16×16 cm, and with smaller blocks, 2×2 cm, would provide a clearer indication of the effect of joint spacing on shallow opening stability. More testing is required to assess the effects of surface roughness, joint orientations, number of joint sets, effect of lateral load, and static acceleration. Studying the impact of joint roughness determined from the physical test models is also desirable. It would reveal the adequacy or inadequacy of the deterministic methods and the sensitivity of the induced acceleration to the joint roughness. This may be experimentally assessed by using cast cement blocks with various degrees of pre-defined roughness on the surfaces. The impact of joint infilling such as sand clay and silt should be simulated.

REFERENCES

Achenbach, L. D. (1975). **Wave Propagation in Elastic Solids**. New York: Nort-Holland.

Adhikary, D. P. and Dyskin, A. V. (1997). Modelling the deformation of underground excavation in layered rock masses. In **International Journal of Rock Mechanics and Mining Sciences**. 34(3): 714-719.

Arias, A. (1970). A measure of earthquake intensity. In R.J. Hansen (Editor). **Seismic Design for Nuclear Power Plants**. MIT Press: Cambridge. Massachusetts. pp. 438-483.

Aydan, O., Shimizu, Y. and Karaca, M. (1994). The dynamic and static stability of shallow underground openings in jointed rock masses. **The 3rd International Symposium on Mine Planning and Equipment Selection**. Istanbul, pp. 851-858.

Bakhtar, K. (1997). Studies under physical modeling at 1-g. **International Journal of Rock Mechanics and Mining Sciences**. 34(3-4): 536.

Bakhtar, K., Jones, A. H. and Cameron, R. (1986). Use of rock simulators for rock mechanics studies. In **Proceedings of the 27th US Symposium on Rock Mechanics**. Society of Mining Engineers of AIME (pp 219-223). New York.

Baraza, J., Ercilla, G. and Lee, J. (1992). Geotechnical properties and preliminary assessment of sediment stability on the continental slope of the Northwestern Alboran Sea. **Geo-Marine Letters**, 12: 150-156.

Barton, N. and Hansteen, H. (1979). Very large span openings at shallow depth: deformation magnitudes from jointed models and finite element analysis. In **Proceedings of the 4th Excavation and Tunnelling Conference** (Vol. 2, pp 1331-1353). Atlanta.

Barton, N. R., Lien, R. and Lunde, J. (1974). Engineering classification of rock masses for the design of tunnel support. **Rock Mechanics**. 6(4): 189-239.

Barton, N. (2002). Some new Q-value correlations to assist in site characterization and tunnel design. **International Journal of Rock Mechanics and Mining Sciences and Geomechanics**. 39(2): 185-216.

Bhasin, R. and Hoeg, K. (1998). Numerical modeling of block size effects and influence of joint properties in multiply jointed rock. **Tunnelling and Underground Space Technology**. 13(2): 181-188.

Bieniawski, Z. T. (1974). Geomechanics classification of rock masses and its application in tunnelling. In **Proceedings of the 3rd International Congress on Rock Mechanics** (pp 27-32). Denver.

Bieniawski, Z. T. (1976). Rock mass classification in rock engineering. In **Proceedings of the Exploration for rock engineering** (Vol. 1, pp 97-106). Cape Town: Balkema.

Bieniawski, Z. T. (1989). **Engineering rock mass classifications**. New York: Wiley and Sons.

Bieniawski, Z. T., (1973). Engineering classification of jointed rock masses. **Trans South African Insternational Civil Engineerings**. 15(12): 335-344.

Blume, J. A. (1970). An engineering intensity scale for earthquakes and other ground motion. **Bulletin of the Seismological Society of America**. 60(1): 217-229.

Brune, J. N. and Anooshehpoor, A. (1991). Foam rubber modeling of the Lotung Large-Scale Seismic Experiment. **EERI: Earthquake Spectra**. 7: 165-178.

Cai, M., Kaiser, P. K., Morioka, H., Minami, M., Maejima, T., Tasaka, Y. and Kurose, H. (2007). FLAC/PFC coupled numerical simulation of AE in large-scale underground excavations. **International Journal of Rock Mechanics and Mining Sciences**. 44: 550-564.

Chengzhi, Q., Canshou, C., Qihu, Q. and Jian, L. (2008). **Dynamic Instability of Tunnel in blocky rock mass**. Transactions of Tianjin University. 4(6): 457-463.

Console, R. Murru, M. and Catalli, F. (2006). Physical and stochastic models of earthquake clustering. **Istituto Nazionale di Geofisicae Vulcanologia**. Via di Vigna Murata 605, Italy. Tectonophysics. 417: 141-153.

Daisuke, M., Hiroshi, C., Kaoru, K. and Kazunobu, M. (2003). Underground large cavern with shallow overburden considered earthquake protection against disasters. In **Proceedings of the Symposium on Underground Space** (Vol. 8, pp 267-272). Japan.

Davenport, P. N. (2003). Instrumental measures of earthquake intensity in New Zealand. In **2003 Pacific Conference on Earthquake Engineering**. Institute of Geological and Nuclear Sciences, Lower Hutt. New Zealand. Paper number 071.

Deere, D. U., Hendron, A. J., Patton, F. D. and Cording, E. J. (1967). Design of surface and near surface construction in rock. In **Proceedings of the 8th United State Symposium Rock Mechanics** (pp 237-302). New York.

Earthquake Engineering Research Institute EERI. (1990). Loma Prieta Earthquake Reconnaissance Report. **Earthquake Spectra**, EERI, Supplement to Vol. 6.

Fakhimi, A., Carvalho, F., Ishida, T. and Labuz, J. F. (2002). Simulation of failure around a circular opening in rock. **International Journal of Rock Mechanics and Mining Sciences**. 39(4): 507-515.

Gendzwill, D. (2008). **Glossary of Seismic Techniques and Terminology**. [On-line]. Available: http://www.usask.ca/geology/labs/seismo/glossary.html

Genis, M. and Aydan, O. (2002). Evaluation of dynamic response and stability of shallow underground openings in discontinuous rock masses using model tests. İn **Proceeding. of 2002 ISRM Regional Symposium (3rd Korea-Japan Joint Symposium) on Rock Engineering Problems and Approaches in Underground Construction** (Vol. 2, pp 787-794.). Seoul.

Gong, Q. M., Jiao, Y. Y. and Zhao, J. (2006). Numerical modelling of the effects of joint spacing on rock fragmentation by TBM cutters. **Tunnelling and Underground Space Technology**. 21: 46-55.

Gong, Q. M., Zhao, J. and Jiao, Y. Y., (2005). Numerical modeling of the effects of joint orientation on rock fragmentation by TBM cutters. **Tunnelling Underground Space Technology**. 20(2): 183-191.

Grimstad, E. and Barton, N. (1993). Updating the Q-System for NMT. In **Proceedings of the International Symposium on Sprayed Concrete-Modern use of Wet Mix Sprayed Concrete for Underground Support** (pp 46-66). Oslo: Norwegian Concrete Assn. Fagernes.

Guler, G., Kuijpers, J. S., Wojno, L., Milev, A. and Haile, A. (2001). Determine the effect of repeated dynamic loading on the performance of tunnel support systems. **Safety in Mines Research Advisory Committee**. Mining Technology, Division of CSIR.

Hashash, Y. M. A., Hook, J. J., Schmidt, B. and Yao, J. I. C. (2001). Seismic design and analysis of underground structures. **Tunnelling and Underground Space Technology**. 16: 247-293.

Hashimoto, C. and Matsu'ura, M. (2000). **3-D physical modelling of stress accumulation and release processes at transcurrent plate boundarie**. Pure Applied Geophysics, in press.

Hatzor, Y. H., Arzi, A. A., Zaslavskyc, Y. and Shapira, A. (2004). Dynamic stability analysis of jointed rock slopes using the DDA method: King Herod's Palace, Masada, Israel. **International Journal of Rock Mechanics and Mining Sciences**, 4: 813-832.

Hoek, E. and Brown, E. T. (1980). **Underground excavations in rock**. Institute of Mining and Metallurgy: London. England.

Hoek, E., Kaiser, P. K. and Bawden, W. F. (2000). **Support of underground excavations in hard rock**. Great Britain: Taylor and Francies. 300 pp.

Hu, X. S. and Zhao, F. S. (2005). Simulation of deformation and failure of surrounding rock masses of underground cavern in low ground stress regions with finite element method. **Chinese Journal of Rock Mechanics and Engineering**. Academia Sinica. 24(10): 1708-1714.

Itasca Consulting Group, Inc. (2004). **UDEC 4.0 GUI A Graphical User Interface for UDEC**, Minneapolis, Minnesota.

Jiang, Y., Li, B. and Yamashita, Y. (2009). Simulation of cracking near a large underground cavern in a discontinuous rock mass using the expanded distinct element method. **International Journal of Rock Mechanics and Mining Sciences**. 46(1): 97-106.

Jin, X. G. and Zhang, Y. X. (2008). **Earthquake response properties of the support structure of large cross section tunnel**. **Journal of Chongqing Jianzhu University**, China. 30(1): 44-48**.**

Jongpradist, P., Kongkitkul, W. and Tunsskul, J. (2009). Investigation of failure behavior of rock mass around gas storage cavern with physical model test. **In Proceeding of second Thailand Symposium of rock mechanics** (pp 257-269). March 12-13, 2009, Nakhon Ratchasima: Suranaree University of Technology.

Karim, K. R. and Yamazaki, F. (2002). Correlation of JMA instrumental seismic intensity with strong motion parameters. **Earthquake Engineering and Structural Dynamics**. 31: 1191-1212.

Kemthong, R. (2006). **Determination of rock joint shear strength based on rock physical properties**. Mining Engineering Thesis. Suranaree University of Technology. Nakhon Ratchasima.

Kim, E. J., Bielak, J. and Ghattas, O. (2003). Large-scale northridge earthquake simulation using octree-based multiresolution mesh method. **16th ASCE Engineering Mechanics Conference**. University of Washington: Seattle.

Kramer, S. L, (1996). Geotechnical earthquake engineering. New Jersey: Prentice Hall. Lama, R.D. and Vutukuri, V.S. (1978). **Handbook on Mechanical Properties of Rocks**. Vol. 4. Trans Tech Publication.

Lama, R. D. and Vutukuri, V. S. (1978). **Handbook on Mechanical Properties of Rocks**. Vol. 4. Trans Tech Publication.Lauffer, H. (1958). Gebirgsklassifizierung fur den Stollenbau. Geologie and Bauwesen. 24(1): 46-51.

Li, Z., Liu, H., Dai, R. and Su, X. (2005). Application of numerical analysis principles and key technology for high fidelity simulation to 3-D physical model tests for underground caverns. **Tunnelling and Underground Space Technology**. 20: 390-399.

Liu, T., Shen, M., Tao, B., He, Z. and Yuan, Y. (2006). Model test and 3d numerical simulation study on excavation of double-arch tunnel. **Yanshilixue Yu Gongcheng Xuebao/Chinese Journal of Rock Mechanics and Engineering**. Academia Sinica. 25(9): 1802-1808.

Ma, M. and Brady, B. H. (1999). Analysis of the dynamic performance of an underground excavation in jointed rock under repeated seismic loading. **Geotechnical and Geological Engineering**. 17(1): 1-20.

Madariaga, R., Olsen, K. and Archuleta, R. (1998). Modeling dynamic rupture in a 3D earthquake fault model. **Bulletin of the Seismological Society of America**. Seismological Society of America. 88(5): 1182-1197.

Matsu'ura, M., Mora, P., Donnellan, A. and Yin, X. C. (2002). Earthquake Processes: Physical Modelling. **Numerical Simulation and Data Analysis**. Pure and Applied Geophysics. Birkha user Verlag, Basel. 159: 2169-2171.

Maugeri, M., Musumeci, G., Novita, D. and Taylor, C. A. (2000). Shaking table test of failure of a shallow foundation subjected to an eccentric load. **Soil dynamics and Earthquake Engineering**. 20: 435-444.

Medvedev, Y. (1953). **Generalization of a theorem of F.Reisz. Uspehi Math. Nauk**., 8: 18-115.

Milne D., Hadjigeorgiou J. and Pakalnis R. (1998). Rock mass characterization for underground hard rock mines. **Tunnelling and Underground Space Technology**. 13(4): 383-391.

Ohtani, K., Ogawa, N., Katayama, T. and Shibata, H. (2003). **Project on 3-D Full-Scale Earthquake Testing Facility-The Third Report**, 34UJNR.

Owen, G. N. and Scholl, R. E. (1981). **Earthquake Engineering of Large Underground Structures**. San Francisco; URS/Blume (John A.) and Associates.

Pakbaz, M. C. and Yareevand, A. (2005). 2-D analysis of circular tunnel against earthquake loading. **Tunnelling and Underground Space Technology**. 20(5): 411-417.

Palmstrom, A. (1982). The volumetric joint count-a useful and simple measure of the degree of rock jointing. In **Proceedings of the 4th congress International Assigns Engineering Geology** (Vol. 5, pp 221-228). Delhi.

Pangpetch, P. and Fuenkajorn, K. (2007). Simulation of rock slope failure using physical model. In **Proceedings of the First Thailand Symposium on Rock Mechanics. Suranaree University of Technology** (pp 227-243). Nakhon Ratchasima.

Ren, W. Z., Wang, Y. G., Bai, S. W. and Ge, X. R. (2006). Research on deformation and subsidence characters of ground and wall rock due to underground mining by model testing. In **Proceedings of the 6th International Conference on Physical Modelling in Geotechnics** (Vol. 2, pp 1527-1533). Taylor and Francis/ Balkema.

Richter, C. (1958**)**. **Elementary Seismology**. W.H. Freeman and Co., San Francisco. pp 165-187.

Riley, W. F. and Sturges, L. D. (1993). **Engineering Mechanics: Dynamics**. Second Edition, New York.

Riley, F. J., Brabhaharan, P. and Stewart, D. L. (2006). Seismic Performance of the Terrace Tunnel Approach Walls, Wellington. **Opus International Consultants**, Wellington, New Zealand.

Siad, L. (2003). Seismic stability analysis of fracture rock slopes by yield design theory. **Soil and Earthquake Engineering**. 23: 203-212.

Silva, P. G., Goy, J. L., Zazo, C., Bardaji, T., Lario, J., Somoza, L., Luque, L. and Gonzalez-Hernandez, F.M. (2006). Neotectonic fault mapping at the Gibraltar Strait Tunnel area, Bolonia Bay (South Spain). **Engineering Geology**. 84: 31-47.

Souley, M. and Homand, F. (1996). Stability of jointed rock masses evaluated by UDEC with an extended saeb-amadei constitutive law. **International Journal of Rock Mechanics and Mining Sciences**. 33(3): 233-244.

Sterpi, D. and Cividini, A. (2004). A physical and numerical investigation on the stability of shallow tunnels in strain softening media. **Rock Mechanics and Rock Engineering**. 37(4): 277-298.

Stimpson, B. (1979). Simple physical modelling technique for the demonstration of interaction between underground openings. **International Journal of Rock Mechanics and Mining Sciences and Geomechanics Abstracts**. 16(3): 217-219.

Stiros, S. C. and Kontogianni, V. A. (2009). Coulomb stress changes: From earthquakes to underground excavation failures. **International Journal of Rock Mechanics and Mining Sciences**. 46(1): 182-187.

Terzaghi, K. (1946). Rock defects and loads on tunnel supports. In **Rock Tunneling with Steel Supports**. Youngstown, OH: Commercial Shearing and Stamping Company. 1: 17-99.

The U. S. Department of Homeland Security, FEMA (2005). **Federal Guidelines for Dam Safety**. Earthquake Analyses and Design of Dams. May 2005

Toyra, J. (2004). Stability of shallow seated constructions in hard rock-A Pilot Study. **Department of Civil and Environmental Engineering**. Division of Rock Mechanics. Lulea University of Technology. pp. 35-40.

Trifunac, M. D. and Brady, A. G. (1975). On the correlation of seismic intensity scales with the peaks of recorded strong ground motion. **Bulletin of the Seismological Society of America**. 65(1): 139-162.

Wald, D. A., Quitoriano, V., Heaton, T. H. and Kanamori, H. (1999). Relationships between peak ground acceleration, peak ground velocity, and modified Mercalli intensity in California. **Earthquake Spectra**. 15: 557-564.

Wang, W. H., Li, X. B., Zuo, Y. J., Zhou, Z. L. and Zhang, Y. P. (2006). 3DEC modeling on effect of joints and interlayer on wave propagation. **Transactions of Nonferrous Metals Society of China**. 16(3): 728-734.

Wickham, G. E., Tiedemann, H. R. and Skinner, E. H. (1972). Support determination based on geologic predictions. In **Proceedings of the North American Rapid Excavation Tunneling Conference**. Chicago.

Zhu, H., Zhang, F., Drumm, E. C., Chin, C. T. and Zhang, D. (2006). 2D model tests and numerical simulation in shallow tunneling considering existing building load. Underground Construction and Ground Movement (GPS 155). In **Proceedings of the Sessions of GeoShanghai 2006** (pp 304-311).

Zhu, W. and Zhao, J. (2004). Stability analysis and modelling of underground excavations in fractured rocks. **Elsevier Geo-Engineering Book Series Volume 1**. In Hudson (Editor). J. A. Netherlands: Elsevier.

APPENDIX A

RESULTS OF SHALLOW OPENING UNDER STATIC CONDITION

Table A-1 Test parameters and results for 4×4 cm block sizes or joint spacing ratio equal to 1:1 under static condition.

Model	Depth, D (cm)	D/S_H	Maximum span, W (cm)	W/S_V	Results
H5C1	16	4	4	1	Stable
H5C2	16	4	8	2	Stable
H5C3	16	4	12	3	Failure
Hr3C1	52	13	4	1	Stable
Hr3C2	52	13	8	2	Stable
Hr3C3	52	13	12	3	Stable
Hr3C4	52	13	16	4	Stable
Hr3C5	52	13	20	5	Failure
H2C1	76	19	4	1	Stable
H2C2	76	19	8	2	Stable
H2C3	76	19	12	3	Stable
H2C4	76	19	16	4	Stable
H2C5	76	19	20	5	Stable
H2C6	76	19	24	6	Failure
H1C1	96	24	4	1	Stable
H1C2	96	24	8	2	Stable
H1C3	96	24	12	3	Stable
H1C4	96	24	16	4	Stable
H1C5	96	24	20	5	Stable
H1C6	96	24	24	6	Stable
H1C7	96	24	28	7	Failure

Table A-2 Test parameters and results for 4×8 cm block sizes or joint spacing ratio equal to 1:2 under static condition.

Model	Depth, D (cm)	D/S_H	Maximum span, W (cm)	W/S_V	Results
R8V-D1-C2	24	3	8	2	Stable
R8V-D1-C3	24	3	12	3	Failure
R8V-D2-C4	48	6	16	4	Stable
R8V-D2-C5	48	6	20	5	Failure
R8V-D3-C4a	72	9	16	4	Stable
R8V-D3-C5a	72	9	20	5	Failure
R8V-D3-C5b	80	10	20	5	Stable
R8V-D3-C6b	80	10	24	6	Failure
R8V-D4-C6a	88	11	24	6	Stable
R8V-D4-C7a	88	11	28	7	Failure
R8V-D4-C6b	96	12	24	6	Stable
R8V-D4-C7b	96	12	28	7	Failure

Table A-3 Test parameters and results for 4×8 cm block sizes or joint spacing ratio equal to 2:1 under static condition.

Model	Depth, D (cm)	D/S_H	Maximum span, W (cm)	W/S_V	Results
R8H-D1-C1a	16	4	8	1	Stable
R8H-D1-C1b	20	5	8	1	Failure
R8H-D2-C2a	36	9	16	3	Stable
R8H-D2-C2b	44	11	16	2	Stable
R8H-D2-C3b	44	11	24	3	Failure
R8H-D3-C3a	64	16	24	3	Stable
R8H-D3-C3b	72	18	24	3	Stable
R8H-D3-C4b	72	18	32	4	Failure
R8H-D3-C4a	84	21	32	4	Stable
R8H-D3-C4b	92	23	32	4	Stable
R8H-D3-C4b	92	23	40	5	Failure

Table A-4 Test parameters and results for 4×12 cm block sizes or joint spacing ratio equal to 1:3 under static condition.

Model	Depth, D (cm)	D/S_H	Maximum span, W (cm)	W/S_V	Results
R12V-D1-C3	24	2	12	3	Stable
R12V-D1-C4	24	2	16	4	Failure
R12V-D2-C4	48	4	16	4	Stable
R12V-D2-C5	48	4	20	5	Failure
R12V-D3a-C5	72	6	20	5	Stable
R12V-D3a-C6	72	6	24	6	Failure
R12V-D3b-C5	84	7	20	5	Stable
R12V-D3b-C6	84	7	24	6	Failure

Table A-5 Test parameters and results for 4×12 cm block sizes or joint spacing ratio equal to 3:1 under static condition.

Model	Depth, D (cm)	D/S_H	Maximum span, W (cm)	W/S_V	Results
R12H-D1-C1a	24	6	12	1	Failure
R12H-D1-C1b	24	6	12	1	Failure
R12H-D2-C1	48	12	12	1	Stable
R12H-D2-C2	48	12	24	2	Failure
R12H-D3-C1	68	17	12	1	Stable
R12H-D3-C2	68	17	24	2	Failure
R12H-D3-C2	92	23	24	2	Stable
R12H-D3-C3	92	23	36	3	Failure

Table A-6 Test parameters and results for joint spacing ratio equal to 1:1, 1:2, 2:1, 1:3, and 3:1 under static condition at joint angle = 45°.

Model	Depth, D (cm)	D/S_H	Maximum span, W (cm)	W/S_V	Results
R4-45-D1-C3	24	8.3	12.2	4.2	Stable
R4-45-D1-C4	24	8.3	17.8	6.2	Failure
R4-45-D2-C5	48	16.7	20.4	7.1	Stable
R4-45-D2-C6	48	16.7	23.6	8.2	Failure
R4-45-D3-C6	64	22.2	24.2	8.4	Stable
R4-45-D3-C7	64	22.2	28.0	9.7	Failure
R4-45-D4-C7	92	31.9	28.1	9.8	Stable
R4-45-D4-C8	92	31.9	32.0	11.1	Failure
R8-45-D1-C1	32	5.7	4.0	1.39	Stable
R8-45-D1-C2	32	5.7	8.0	2.78	Failure
R8-45-D2-C2	66	11.7	8.0	2.78	Stable
R8-45-D2-C3	66	11.7	12.0	4.17	Failure
R8-45-D3-C3	82	14.5	12.0	4.17	Stable
R8-45-D3-C4	82	14.5	16.0	5.56	Failure
R12-45-D1a-C1	28	3.3	4.0	1.39	Stable
R12-45-D1b-C1	32	3.8	4.0	1.39	Failure
R12-45-D2a-C2	48	5.6	8.0	2.78	Stable
R12-45-D2b-C2	56	6.6	8.0	2.78	Failure
R12-45-D3-C2	92	10.8	8.0	2.78	Stable
R12-45-D3-C3	92	10.8	12.0	4.17	Failure

APPENDIX B

RESULTS OF SHALLOW OPENING UNDER DYNAMIC CONDITION

Table B-1 Test parameters and results for joint spacing ratio equal to 1:1 under horizontal pseudo-static acceleration of 0.132 g and 0.225 g.

Model	Depth, D (cm)	D/S_H	Maximum span, W (cm)	W/S_V	a (g)	Results
Hr4C1d	33.3	8.3	4.1	1.0	0.132	Stable
Hr4C2d	33.3	8.3	8.6	2.2	0.132	Failure
Hs2C4d	70.2	17.6	16.4	4.1	0.132	Stable
Hs2C5d	70.2	17.6	20.7	5.2	0.132	Failure
Ht3C3d	57.6	14.4	12.3	3.1	0.132	Stable
Ht3C4d	57.6	14.4	16.7	4.2	0.132	Failure
Ht2C4d	78.6	19.7	16.5	4.1	0.132	Stable
Ht2C5d	78.6	19.7	20.9	5.2	0.132	Failure
Ht1C5d	98.7	24.7	20.6	5.2	0.132	Stable
Ht1C6d	98.7	24.7	25.0	6.3	0.132	Failure
Ha1C4d	82.2	20.6	16.5	4.1	0.225	Stable
Ha1C5d	82.2	20.6	20.5	5.1	0.225	Failure
Hb1C1d	41.2	10.3	4.1	1.0	0.225	Stable
Hb1C2d	41.2	10.3	8.4	2.1	0.225	Failure
Hb2C2d	57.6	14.4	8.5	2.1	0.225	Stable
Hb2C3d	57.6	14.4	12.5	3.1	0.225	Failure
Hb5C5d	94.3	23.6	20.6	5.2	0.225	Stable
Hb5C6d	94.3	23.6	24.8	6.2	0.225	Failure

Table B-2 Test parameters and results for joint spacing ratio equal to 1:2 under horizontal pseudo-static acceleration of 0.132 g and 0.225 g.

Model	Depth, D (cm)	D/S_H	Maximum span, W (cm)	W/S_V	a (g)	Results
R8V-D1-C2d	24.8	3.1	8.2	2.1	0.132	Failure
R8V-D1-C3d	24.8	3.1	12.3	3.1	0.132	Failure
R8V-D2-C3d	41.0	5.1	12.2	3.1	0.132	Failure
R8V-D2-C3d	49.1	6.1	8.3	2.1	0.132	Stable
R8V-D2-C4d	49.1	6.1	12.2	3.1	0.132	Failure
R8V-D3-C4d	65.4	8.2	16.4	4.1	0.132	Stable
R8V-D3-C5d	65.4	8.2	20.4	5.1	0.132	Failure
R8V-D4-C6d	97.6	12.2	20.4	5.1	0.132	Stable
R8V-D4-C6d	97.6	12.2	24.5	6.1	0.132	Failure
R8V-D1-C2d	24.5	3.1	8.2	2.1	0.225	Failure
R8V-D2-C1d	49.0	6.1	4.1	1.0	0.225	Stable
R8V-D2-C2d	49.0	6.1	8.2	2.1	0.225	Failure
R8V-D3-C3d	73.5	9.2	12.3	3.1	0.225	Stable
R8V-D3-C4d	73.5	9.2	16.3	4.1	0.225	Failure
R8V-D3-C4d	88.0	11.0	16.4	4.1	0.225	Stable
R8V-D3-C5d	88.0	11.0	20.4	5.1	0.225	Failure
R8V-D4-C4d	97.5	12.2	16.4	4.1	0.225	Stable
R8V-D4-C5d	97.5	12.2	20.4	5.1	0.225	Failure

Table B-3 Test parameters and results for joint spacing ratio equal to 2:1 under horizontal pseudo-static acceleration of 0.132 g and 0.225 g.

Model	Depth, D (cm)	D/S_H	Maximum span, W (cm)	W/S_V	a (g)	Results
R8H-D1a-C1d	20	5	8	1	0.225	Stable
R8H-D1b-C1d	24	6	8	1	0.225	Failure
R8H-D2-C1d	48	12	8	1	0.225	Stable
R8H-D2-C1d	48	12	8	1	0.225	Failure
R8H-D3a-C2d	56	14	16	2	0.225	Stable
R8H-D3b-C2d	72	18	16	2	0.225	Failure
R8H-D4-C2d	96	24	16	2	0.225	Stable
R8H-D4-C3d	96	24	24	3	0.225	Failure

Table B-4 Test parameters and results for joint spacing ratio equal to 1:3 under horizontal pseudo-static acceleration of 0.132 g and 0.225 g.

Model	Depth, D (cm)	D/S_H	Maximum span, W (cm)	W/S_V	a (g)	Results
R12V-D1a-C2d	23.60	1.97	8.40	2.10	0.132	Stable
R12V-D1a-C3d	23.60	1.97	12.10	3.03	0.132	Failure
R12V-D1b-C2d	36.60	3.05	8.30	2.08	0.132	Stable
R12V-D1b-C3d	36.60	3.05	16.10	4.03	0.132	Failure
R12V-D2a-C3d	47.60	3.97	12.20	3.05	0.132	Stable
R12V-D2a-C4d	47.60	3.97	16.60	4.15	0.132	Failure
R12V-D2b-C3d	60.30	5.03	12.20	3.05	0.132	Stable
R12V-D2b-C4d	60.30	5.03	20.60	5.15	0.132	Failure
R12V-D3b-C5d	84.50	7.04	20.50	5.13	0.132	Stable
R12V-D3b-C6d	84.50	7.04	24.70	6.18	0.132	Failure
R12V-D4-C5d	95.90	7.99	20.40	5.10	0.132	Stable
R12V-D4-C6d	95.90	7.99	24.80	6.20	0.132	Failure
R12V-D1-C1d	23.90	1.99	4.0	1.0	0.225	Stable
R12V-D1-C2d	23.90	1.99	8.1	2.0	0.225	Failure
R12V-D2-C3d	48.00	4.00	12.3	3.1	0.225	Stable
R12V-D2-C4d	48.00	4.00	16.2	4.1	0.225	Failure
R12V-D3-C4d	71.70	5.98	16.4	4.1	0.225	Stable
R12V-D3-C5d	71.70	5.98	21.3	5.3	0.225	Failure
R12V-D4-C5d	95.80	7.98	20.9	5.2	0.225	Stable
R12V-D4-C6d	95.80	7.98	24.1	6.0	0.225	Failure

Table B-5 Test parameters and results for joint spacing ratio equal to 3:1 under horizontal pseudo-static acceleration of 0.132 g and 0.225 g.

Model	Depth, D (cm)	D/S_H	Maximum span, W (cm)	W/S_V	a (g)	Results
R12H-D1b-C1d	36	9	12	1	0.132	Stable
R12H-D2-C1d	56	14	12	1	0.132	Stable
R12H-D2-C2d	56	14	24	2	0.132	Failure
R12H-D3-C3d	76	19	12	1	0.132	Stable
R12H-D3-C3d	76	19	24	2	0.132	Failure
R12H-D4-C4d	100	25	24	2	0.132	Stable
R12H-D4-C4d	100	25	36	3	0.132	Failure

Table B-6 Test parameters and results for joint spacing ratio equal to 1:1, 1:2, 2:1, 1:3, and 3:1 under horizontal pseudo-static acceleration of 0.132 g at joint angle = 45°.

Model	Depth, D (cm)	D/S_H	Maximum span, W (cm)	W/S_V	a (g)	Results
R4-45-D1-C3d	40.0	7.1	12.2	2.2	0.132	Stable
R4-45-D1-C4d	40.0	7.1	16.0	2.8	0.132	Failure
R4-45-D2-C5d	60.0	10.6	20.3	3.6	0.132	Stable
R4-45-D2-C6d	60.0	10.6	24.0	4.2	0.132	Failure
R4-45-D3-C6d	76.0	13.4	24.2	4.3	0.132	Stable
R4-45-D3-C7d	76.0	13.4	28.0	4.9	0.132	Failure
R4-45-D4-C7d	92.0	16.3	28.0	4.9	0.132	Stable
R4-45-D4-C8d	92.0	16.3	32.0	5.7	0.132	Failure
R12-45-D1-C2d	40.0	7.1	8.1	1.4	0.132	Stable
R12-45-D1-C3d	40.0	7.1	12.0	2.1	0.132	Failure
R12-45-D2-C3d	56.0	9.9	12.2	2.2	0.132	Stable
R12-45-D2-C4d	56.0	9.9	16.3	2.9	0.132	Failure
R12-45-D3-C4d	72.0	12.7	16.4	2.9	0.132	Stable
R12-45-D3-C5d	72.0	12.7	20.2	3.6	0.132	Failure
R12-45-D4-C6d	88.0	15.6	24.2	3.6	0.132	Stable
R12-45-D4-C7d	88.0	15.6	28.0	4.9	0.132	Failure

Table B-7 Test parameters and results for joint spacing ratio equal to 1:1, 1:2, 2:1, 1:3, and 3:1 under horizontal pseudo-static acceleration of 0.225 g at joint angle = 45°.

Model	Depth, D (cm)	D/S_H	Maximum span, W (cm)	W/S_V	a (g)	Results
R4-45-D1a-C1d	36.0	6.6	4.0	0.7	0.225	Stable
R4-45-D1b-C2d	40.0	7.1	8.0	1.4	0.225	Failure
R4-45-D2-C3d	60.0	10.6	12.0	2.1	0.225	Stable
R4-45-D2-C4d	60.0	10.6	16.0	2.8	0.225	Failure
R4-45-D3-C5d	76.0	13.4	20.0	3.3	0.225	Stable
R4-45-D3-C6d	76.0	13.4	24.0	4.2	0.225	Failure
R4-45-D4-C6d	92.0	16.3	24.0	4.2	0.225	Stable
R4-45-D4-C7d	92.0	16.3	28.0	4.9	0.225	Failure
R8-45-D1a-C2d	28.5	5.0	6.7	1.2	0.225	Stable
R8-45-D1b-C2d	34.3	6.2	6.8	1.2	0.225	Failure
R8-45-D2-C2d	66.0	11.7	6.8	1.2	0.225	Stable
R8-45-D2-C4d	66.0	11.7	16.2	2.9	0.225	Failure
R8-45-D3-C5d	82.0	14.5	20.1	3.6	0.225	Stable
R8-45-D3-C6d	82.0	14.5	24.3	4.3	0.225	Failure
R12-45-D1-C2d	40.0	7.1	8.0	1.4	0.225	Stable
R12-45-D1-C3d	40.0	7.1	12.0	2.1	0.225	Failure
R12-45-D2-C3d	52.0	9.2	12.0	2.1	0.225	Stable
R12-45-D2-C4d	52.0	9.2	16.0	2.8	0.225	Failure
R12-45-D3-C4d	64.0	11.3	16.0	2.8	0.225	Failure
R12-45-D3-C5d	64.0	11.3	20.0	3.5	0.225	Failure
R12-45-D4-C4d	88.0	15.6	16.0	2.8	0.225	Stable
R12-45-D4-C5d	88.0	15.6	20.0	3.5	0.225	Failure
R12-45-D4-C6d	88.0	15.6	24.0	4.2	0.225	Failure

APPENDIX C

SIMULATION RESULTS OF SHALLOW OPENING

USING UDEC CODE

Table C-1. UDEC simulation results for shallow opening of sandstone blocks under static condition at ψ_b=26º, c=53 Pa, and γ_r=2.38 kN/m^3.

Model of Simulation	Joint Spacing Ratios	Depth (cm)	Maximum Span (cm)	No. of Cycle	Times of Simulation ($\times 10^{-1}$sec)	Stability
R4-D1-C1d	1:1	8	4	12000	1.52	Stable
R4-D2-C1d	1:1	12	4	12000	1.52	Stable
R4-D3-C1d	1:1	16	4	12000	1.54	Stable
R4-D3-C2d	1:1	16	8	12000	1.53	Failure
R4-D4-C1d	1:1	20	4	12000	1.57	Stable
R4-D4-C2d	1:1	20	8	12000	1.58	Failure
R4-D5-C2d	1:1	24	8	12000	1.53	Stable
R4-D5-C3d	1:1	24	12	12000	1.57	Failure
R4-D6-C2d	1:1	28	8	12000	1.56	Stable
R4-D6-C3d	1:1	28	12	12000	1.59	Failure
R4-D7-C2d	1:1	32	8	12000	1.58	Stable
R4-D7-C3d	1:1	32	12	12000	1.58	Failure
R4-D8-C2d	1:1	36	8	12000	1.53	Stable
R4-D8-C3d	1:1	36	12	12000	1.57	Failure
R4-D9-C2d	1:1	40	8	12000	1.56	Stable
R4-D9-C3d	1:1	40	12	12000	1.59	Failure
R4-D9-C2d	1:1	44	8	12000	1.57	Stable
R4-D9-C3d	1:1	44	12	12000	1.58	Failure
R4-D9-C3d	1:1	48	12	12000	1.58	Stable
R4-D9-C4d	1:1	48	16	12000	1.57	Failure
R4-D9-C3d	1:1	52	12	12000	1.56	Stable
R4-D9-C4d	1:1	52	16	12000	1.63	Failure
R4-D9-C3d	1:1	56	12	12000	1.65	Stable
R4-D9-C4d	1:1	56	16	12000	1.71	Failure
R4-D9-C3d	1:1	60	12	12000	1.79	Stable
R4-D9-C4d	1:1	60	16	12000	1.75	Failure
R4-D9-C3d	1:1	64	12	12000	1.74	Stable
R4-D9-C4d	1:1	64	16	12000	1.78	Failure
R4-D9-C4d	1:1	68	16	12000	1.78	Stable
R4-D9-C5d	1:1	68	20	12000	1.77	Failure
R4-D9-C4d	1:1	72	16	12000	1.75	Stable
R4-D9-C5d	1:1	72	20	12000	1.77	Failure
R8V-D1-C1d	1:2	16	4	14000	1.72	Stable
R8V-D1-C2d	1:2	16	8	14000	1.72	Failure
R8V-D2-C1d	1:2	24	4	14000	1.78	Stable
R8V-D2-C2d	1:2	24	8	14000	1.78	Failure
R8V-D3-C2d	1:2	32	8	14000	1.84	Stable

Table C-1. UDEC simulation results for shallow opening of sandstone blocks under static condition at ψ_b=26º, c=53 Pa, and γ_r=2.38 kN/m^3. (cont.)

Model of Simulation	Joint Spacing Ratios	Depth (cm)	Maximum Span (cm)	No. of Cycle	Times of Simulation ($\times 10^{-1}$sec)	Stability
R8V-D3-C3d	1:2	32	12	14000	1.84	Failure
R8V-D4-C2d	1:2	40	8	14000	2.03	Stable
R8V-D4-C3d	1:2	40	12	14000	2.01	Failure
R8V-D5-C3d	1:2	48	12	14000	2.01	Stable
R8V-D5-C4d	1:2	48	16	14000	2.01	Failure
R8V-D6-C3d	1:2	56	12	14000	2.00	Stable
R8V-D6-C4d	1:2	56	16	14000	2.01	Failure
R8V-D7-C3d	1:2	64	12	14000	2.00	Stable
R8V-D7-C4d	1:2	64	16	14000	2.03	Failure
R8V-D8-C3d	1:2	72	12	14000	2.01	Stable
R8V-D8-C4d	1:2	72	16	14000	2.01	Failure
R8V-D9-C4d	1:2	80	16	14000	2.01	Stable
R8V-D9-C5d	1:2	80	20	14000	2.00	Failure
R8V-D10-C4d	1:2	88	16	14000	2.01	Stable
R8V-D10-C5d	1:2	88	20	14000	2.00	Failure
R8V-D10-C5d	1:2	96	20	14000	2.03	Stable
R8V-D10-C6d	1:2	96	24	14000	2.02	Failure
R8H-D1-C1d	2:1	12	8	13000	1.74	Stable
R8H-D2-C2d	2:1	16	8	13000	1.75	Stable
R8H-D3-C3d	2:1	20	8	13000	1.78	Stable
R8H-D4-C4d	2:1	24	8	13000	1.75	Failure
R8H-D5-C5d	2:1	28	8	13000	1.73	Failure
R8H-D6-C6d	2:1	32	8	13000	1.75	Stable
R8H-D6-C6d	2:1	32	16	13000	1.78	Failure
R8H-D7-C7d	2:1	36	8	13000	1.75	Stable
R8H-D7-C7d	2:1	36	16	13000	1.73	Failure
R8H -D7-C8d	2:1	40	8	13000	1.75	Stable
R8H -D7-C8d	2:1	40	16	13000	1.73	Failure
R8H -D8-C8d	2:1	44	8	13000	1.78	Stable
R8H -D8-C8d	2:1	44	16	13000	1.75	Failure
R8H -D9-C9d	2:1	48	8	13000	1.75	Stable
R8H -D9-C9d	2:1	48	16	13000	1.78	Failure
R8H -D10-C10d	2:1	52	8	13000	1.75	Stable
R8H -D10-C10d	2:1	52	16	13000	1.74	Failure
R8H -D11-C11d	2:1	56	8	13000	1.78	Stable
R8H -D11-C11d	2:1	56	16	13000	1.75	Failure

Table C-1. UDEC simulation results for shallow opening of sandstone blocks under static condition at ψ_b=26º, c=53 Pa, and γ_r=2.38 kN/m^3. (cont.)

No. of simulation	Joint Spacing Ratios	Depth (cm)	Maximum Span (cm)	No. of Cycle	Times of Simulation ($\times 10^{-1}$sec)	Stability
R12V-D1-C1d	1:3	24	4	14000	2.10	Stable
R12V-D1-C2d	1:3	24	8	14000	2.08	Failure
R12V-D2-C2d	1:3	36	8	14000	2.07	Stable
R12V-D2-C3d	1:3	36	12	14000	2.09	Failure
R12V-D3-C2d	1:3	48	8	14000	2.07	Stable
R12V-D3-C3d	1:3	48	12	14000	2.08	Failure
R12V-D4-C3d	1:3	60	12	14000	2.07	Stable
R12V-D4-C4d	1:3	60	16	14000	2.09	Failure
R12V-D5-C4d	1:3	72	16	14000	2.08	Stable
R12V-D5-C5d	1:3	72	20	14000	2.09	Failure
R12H-D1-C1d	3:1	32	12	12000	1.86	Stable
R12H-D2-C1d	3:1	36	12	12000	1.87	Stable
R12H-D3-C1d	3:1	40	12	12000	1.86	Failure
R12H-D4-C1d	3:1	44	12	12000	1.85	Failure
R12H-D5-C1d	3:1	48	12	12000	1.86	Failure
R12H-D6-C1d	3:1	52	12	12000	1.85	Stable
R12H-D6-C2d	3:1	52	24	12000	1.84	Failure
R12H-D7-C1d	3:1	56	12	12000	1.86	Stable
R12H-D7-C2d	3:1	56	24	12000	1.84	Failure
R12H-D8-C1d	3:1	60	12	12000	1.86	Stable
R12H-D8-C2d	3:1	60	24	12000	1.85	Failure
R12H-D9-C1d	3:1	64	12	12000	1.86	Stable
R12H-D9-C2d	3:1	64	24	12000	1.85	Failure
R12H-D10-C1d	3:1	68	12	12000	1.84	Stable
R12H-D10-C2d	3:1	68	24	12000	1.86	Failure
R12H-D11-C1d	3:1	72	12	12000	1.84	Stable
R12H-D11-C2d	3:1	72	24	12000	1.86	Failure
R12H-D12-C2d	3:1	76	24	12000	1.85	Stable
R12H-D12-C3d	3:1	76	36	12000	1.86	Failure

Table C-2. UDEC simulation results for shallow opening of sandstone blocks under dynamic condition at ψ_b=26º, c=53 Pa, and γ_r=2.38 kN/m^3.

No. of simulation	Joint Spacing Ratios	Depth (cm)	Maximum Span (cm)	No. of Cycle	Static Accelera-tions (g)	Times of Simulation ($\times 10^{-1}$sec)	Stability
R4-D9-C1d	1:1	40	4	12000	0.132	1.59	Stable
R4-D9-C2d	1:1	40	8	12000	0.132	1.58	Failure
R4-D9-C1d	1:1	48	4	12000	0.132	1.58	Stable
R4-D9-C2d	1:1	48	8	12000	0.132	1.53	Failure
R4-D9-C3d	1:1	56	12	12000	0.132	1.57	Stable
R4-D9-C4d	1:1	56	16	12000	0.132	1.56	Failure
R4-D9-C3d	1:1	60	12	12000	0.132	1.59	Stable
R4-D9-C4d	1:1	60	16	12000	0.132	1.57	Failure
R4-D9-C4d	1:1	64	16	12000	0.132	1.58	Stable
R4-D9-C5d	1:1	64	20	12000	0.132	1.53	Failure
R4-D9-C5d	1:1	68	20	12000	0.132	1.57	Stable
R4-D9-C6d	1:1	68	24	12000	0.132	1.56	Failure
R4-D1-C1d	1:1	40	4	12000	0.225	1.57	Stable
R4-D1-C2d	1:1	40	8	12000	0.225	1.58	Failure
R4-D2-C1d	1:1	44	4	12000	0.225	1.53	Stable
R4-D2-C2d	1:1	44	8	12000	0.225	1.57	Failure
R4-D3-C1d	1:1	48	4	12000	0.225	1.56	Stable
R4-D3-C2d	1:1	48	8	12000	0.225	1.59	Failure
R4-D4-C1d	1:1	52	4	12000	0.225	1.58	Stable
R4-D4-C2d	1:1	52	8	12000	0.225	1.58	Failure
R4-D5-C2d	1:1	56	8	12000	0.225	1.53	Stable
R4-D5-C3d	1:1	56	12	12000	0.225	1.57	Failure
R4-D6-C2d	1:1	60	8	12000	0.225	1.56	Stable
R4-D6-C3d	1:1	60	12	12000	0.225	1.59	Failure
R4-D7-C2d	1:1	64	8	12000	0.225	1.57	Stable
R4-D7-C3d	1:1	64	12	12000	0.225	1.58	Failure
R4-D8-C2d	1:1	68	8	12000	0.225	1.58	Stable
R4-D8-C3d	1:1	68	12	12000	0.225	1.57	Failure
R4-D9-C3d	1:1	72	12	12000	0.225	1.56	Stable
R4-D9-C4d	1:1	72	16	12000	0.225	1.63	Failure
R8V-D1-C2d	1:2	24	8	14000	0.132	2.03	Stable
R8V-D2-C1d	1:2	48	4	14000	0.132	2.01	Stable
R8V-D2-C2d	1:2	48	8	14000	0.132	2.01	Failure
R8V-D3-C3d	1:2	72	12	14000	0.132	2.01	Stable
R8V-D3-C4d	1:2	72	16	14000	0.132	2.00	Failure
R8V-D3-C4d	1:2	88	16	14000	0.132	2.01	Stable
R8V-D3-C5d	1:2	88	20	14000	0.132	2.01	Failure
R8V-D4-C4d	1:2	96	16	14000	0.132	2.01	Stable

Table C-2. UDEC simulation results for shallow opening of sandstone blocks under dynamic condition at ψ_b=26º, c=53 Pa, and γ_r=2.38 kN/m^3. (cont.)

No. of simulation	Joint Spacing Ratios	Depth (cm)	Maximum Span (cm)	No. of Cycle	Static Accelera-tions (g)	Times of Simulation ($\times 10^{-1}$sec)	Stability
R8V-D4-C5d	1:2	96	20	14000	0.132	2.01	Failure
R8V-D1-C1d	1:2	24	4	14000	0.225	2.03	Stable
R8V-D2-C1d	1:2	48	4	14000	0.225	2.01	Stable
R8V-D2-C2d	1:2	48	8	14000	0.225	2.01	Failure
R8V-D3-C2d	1:2	72	8	14000	0.225	2.01	Stable
R8V-D3-C3d	1:2	72	12	14000	0.225	2.00	Failure
R8V-D3-C3d	1:2	88	12	14000	0.225	2.01	Stable
R8V-D3-C4d	1:2	88	16	14000	0.225	2.01	Failure
R8V-D4-C3d	1:2	96	12	14000	0.225	2.01	Stable
R8V-D4-C4d	1:2	96	16	14000	0.225	2.01	Failure
R8H-D1a-C1d	2:1	48	8	14000	0.132	2.01	Stable
R8H-D1b-C1d	2:1	56	8	14000	0.132	2.01	Failure
R8H-D2-C2d	2:1	64	16	14000	0.132	2.00	Failure
R8H-D3-C1d	2:1	72	8	14000	0.132	2.01	Stable
R8H-D3-C2d	2:1	72	16	14000	0.132	2.01	Failure
R8H-D4-C1d	2:1	80	8	14000	0.132	2.03	Stable
R8H-D4-C2d	2:1	80	16	14000	0.132	2.01	Failure
R8H-D5-C1d	2:1	88	8	14000	0.132	2.03	Stable
R8H-D5-C2d	2:1	88	16	14000	0.132	2.01	Failure
R8H-D1a-C1d	2:1	48	8	14000	0.225	2.01	Stable
R8H-D1b-C1d	2:1	56	8	14000	0.225	2.01	Failure
R8H-D2-C1d	2:1	64	8	14000	0.225	2.01	Stable
R8H-D2-C2d	2:1	64	16	14000	0.225	2.00	Failure
R8H-D3-C1d	2:1	72	8	14000	0.225	2.01	Stable
R8H-D3-C2d	2:1	72	16	14000	0.225	2.01	Failure
R8H-D4-C1d	2:1	80	8	14000	0.225	2.03	Stable
R8H-D4-C2d	2:1	80	16	14000	0.225	2.01	Failure
R8H-D5-C1d	2:1	88	8	14000	0.225	2.03	Stable
R8H-D5-C2d	2:1	88	16	14000	0.225	2.01	Failure
R8H-D6-C1d	2:1	96	8	14000	0.225	2.03	Stable
R8H-D6-C2d	2:1	96	16	14000	0.225	2.01	Failure
R12V-D1-C1d	1:3	24	4	12000	0.132	1.86	Stable
R12V-D1-C2d	1:3	24	8	12000	0.132	1.87	Failure
R12V-D2-C3d	1:3	48	12	12000	0.132	1.86	Stable
R12V-D2-C4d	1:3	48	16	12000	0.132	1.85	Failure

Table C-2. UDEC simulation results for shallow opening of sandstone blocks under dynamic condition at ψ_b=26º, c=53 Pa, and γ_r=2.38 kN/m^3. (cont.)

No. of simulation	Joint Spacing Ratios	Depth (cm)	Maximum Span (cm)	No. of Cycle	Static Accelera-tions (g)	Times of Simulation ($\times 10^{-1}$sec)	Stability
R12V-D3-C4d	1:3	56	12	12000	0.132	1.86	Stable
R12V-D3-C5d	1:3	56	16	12000	0.132	1.85	Failure
R12V-D4-C5d	1:3	72	16	12000	0.132	1.86	Stable
R12V-D4-C6d	1:3	72	20	12000	0.132	1.85	Failure
R12V-D5-C5d	1:3	96	20	12000	0.132	1.84	Stable
R12V-D5-C6d	1:3	96	24	12000	0.132	1.86	Failure
R12V-D1-C1d	1:3	24	4	12000	0.225	2.08	Stable
R12V-D1-C2d	1:3	24	8	12000	0.225	2.08	Failure
R12V-D1-C2d	1:3	36	8	12000	0.225	2.08	Stable
R12V-D1-C3d	1:3	36	12	12000	0.225	2.08	Failure
R12V-D2-C2d	1:3	48	8	12000	0.225	2.08	Stable
R12V-D2-C3d	1:3	48	12	12000	0.225	2.07	Failure
R12V-D2-C2d	1:3	60	8	12000	0.225	2.08	Stable
R12V-D2-C3d	1:3	60	12	12000	0.225	2.09	Failure
R12V-D3-C3d	1:3	72	12	12000	0.225	2.08	Stable
R12V-D3-C4d	1:3	72	16	12000	0.225	2.07	Failure
R12V-D3-C3d	1:3	84	12	12000	0.225	2.08	Stable
R12V-D3-C4d	1:3	84	16	12000	0.225	2.08	Failure
R12V-D4-C4d	1:3	96	16	12000	0.225	2.08	Stable
R12V-D4-C5d	1:3	96	20	12000	0.225	2.07	Failure
R12H-D1-C1d	3:1	36	12	12000	0.132	1.86	Stable
R12H-D2-C1d	3:1	48	12	12000	0.132	1.85	Failure
R12H-D3-C1d	3:1	56	12	12000	0.132	1.86	Stable
R12H-D3-C2d	3:1	56	24	12000	0.132	1.85	Failure
R12H-D4-C1d	3:1	72	12	12000	0.132	1.86	Stable
R12H-D4-C2d	3:1	72	24	12000	0.132	1.85	Failure
R12H-D5-C1d	3:1	96	12	12000	0.132	1.84	Stable
R12H-D5-C2d	3:1	96	24	12000	0.132	1.86	Failure
R12H-D1-C2d	3:1	36	12	12000	0.225	2.08	Stable
R12H-D2-C3d	3:1	48	12	12000	0.225	2.07	Failure
R12H-D3-C2d	3:1	56	12	12000	0.225	2.08	Failure
R12H-D4-C3d	3:1	60	12	12000	0.225	2.09	Failure
R12H-D6-C3d	3:1	64	12	12000	0.225	2.08	Failure
R12H-D7-C4d	3:1	72	12	12000	0.225	2.07	Failure
R12H-D8-C3d	3:1	84	12	12000	0.225	2.08	Stable
R12H-D8-C4d	3:1	84	24	12000	0.225	2.08	Failure
R12H-D9-C4d	3:1	96	12	12000	0.225	2.08	Stable
R12H-D9-C5d	3:1	96	24	12000	0.225	2.07	Failure

APPENDIX D

TECHNICAL PUBLICATIONS

LIST OF PUBLICATIONS

Sakulnitichai, C., Pangpetch, P. and Fuenkajorn, K., 2009. **Simulation of Shallow Opening in Jointed Rock Mass under Static and Dynamic Loading using Physical Model**. The 14th National Convention on Civil Engineering. Nakhon Ratchasima, Thailand. 13-15 May 2009.

Sakulnitichai, C., Pangpetch, P. and Fuenkajorn, K., 2009. **Physical model simulation of shallow openings in jointed rock mass under static and dynamic loads**. In Proceeding 2nd Thailand Symposium on Rock Mechanics. Chonburi, Thailand. 12 - 13 March 2009.

การประชุมวิชาการวิศวกรรมโยธาแห่งชาติครั้งที่ 14 มหาวิทยาลัยเทคโนโลยีสุรนารี 13-15 พฤษภาคม 2552

SIMULATION OF SHALLOW OPENINGS IN JOINTED ROCK MASS UNDER STATIC AND DYNAMIC LOADING USING PHYSICAL MODEL

C. Sakulnitichai[1]
P. Pangpetch[1]
K. Fuenkajorn[1]

[1]*Geomechanics Research Unit, Institute of Engineering, Suranaree University of Technology, Nakhon Ratchasima*

ABSTRACT : Physical model simulations have been performed to determine the effects of depth, joint spacing and orientation on the maximum unsupported span of shallow underground openings under static and dynamic loads. Cubical and rectangular blocks of Phu Phan sandstone are arranged in a vertical test frame to simulate a two-dimensional representation of single rectangular openings in rock mass with two mutually perpendicular joint sets. Results indicate that the normalized maximum span (W/S_V) rapidly increases with the normalized depth (D/S_H), and tends to approach a certain limit for each joint spacing ratio, S_V:S_H. The maximum span increases with decreasing S_V:S_H ratio. Under S_V=S_H condition, increasing the joint angles from 0° to 45° reduces the maximum span by about 20%. At shallow depths the acceleration of 0.225 g can reduce the maximum span by up to 50%. The impact of the dynamic loads however reduces as the depth increases. The test results under both static and dynamic loading compare reasonably well with those calculated from discrete element analyses using the UDEC code.

KEYWORDS : *opening, joint, friction, dynamic load, acceleration.*

1. INTRODUCTION

Physical test models or scaled-down models have been widely used in the laboratory to simulate the stability conditions of underground openings in rock masses [1]. They are commonly used to gain an understanding of the effects of unique rock characteristics, in-situ stress conditions or opening geometries [2]. The simulations usually simplify the actual conditions into two-dimensional problems. Recently some researchers have developed sophisticated devices to allow a three-dimensional simulation for tunnel stability in rock mass under high stresses (e.g., [3]). As a result failure conditions of the joints and intact rocks around the openings can be simulated simultaneously. Some devices can incorporate the effects of dynamic loading on the rock models. The modeling results are often compared with those from numerical simulations, usually by a discrete element analysis, either to verify the predictive capability of the computed results or to confirm the accuracy of the test models [4]. Most researchers above concentrate on studying the opening stability under site-specific conditions. Results obtained from the physical test models that can provide a more general solution of the opening stability in rock masses have been rare.

The objective of this research is to perform physical model tests to assess the effects of depth, joint spacing and orientation on the maximum unsupported span of shallow underground openings under static and dynamic loads. A vertical platform is used to test the rock mass model formed by cubical and rectangular blocks of Phu Phan sandstone. The models simulate two-dimensional sections of single rectangular openings in a rock mass with two mutually perpendicular joint sets. The vertical and horizontal joint spacings are varied from 4, 8 to 12 cm. The stability under horizontal pseudo-static accelerations of 0.132 g and 0.225 g is investigated. Empirical relations between the observed maximum span, opening depth and joint spacings are derived. They are used to predict the maximum span under shallow depths. The static and dynamic test results are compared with those simulated from discrete element analyses using UDEC code.

2. TEST PLATFORM

The test platform developed by Pangpetch and Fuenkajorn [5] is used in this study (Figure 1). It can accommodate 4 cm thick rock blocks arranged to a maximum depth and width of 1.2 m to simulate a two-dimensional section of shallow openings in a jointed rock mass. A lateral lithostatic pressure is applied on both sides of the model using a column of crystal balls with a diameter of 16 mm packed in the gap between the model and the test frame. Bulk density of the pack of crystal balls is measured as 2.3 g/cc, which is comparable to the density of the intact block of Phu Phan sandstone. Elevated vertical and lateral stresses can be applied in the test frame to simulate the rock mass behavior under a great depth. They are not applied here because this study involves opening behavior at shallow depths as affected by joint system. Steel grooved rollers mounted underneath the frame are used for testing under dynamic loads.

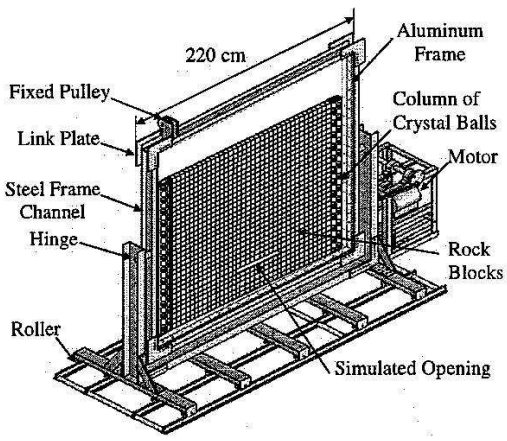

Figure 1 Test platform used to simulate shallow openings in rock mass.

The rollers are placed on a set of steel rails equipped with a high torque motor, gear system and crank arm to induce a cyclic motion to the entire test platform. The frequency and amplitude of the horizontal pseudo-static acceleration can be controlled by adjusting the rotational diameter of the flywheel and speed of the motor.

3. ROCK SAMPLE

Sandstone from the Phu Phan formation is used here as rock. It is classified as fine-grained quartz sandstone with highly uniform texture, density and strength. The rock forming minerals include 72% quartz (0.2-0.8 mm), 20% feldspar (0.1-0.8 mm), 3% mica (0.1-0.3 mm), 3% rock fragments (0.5-2mm), and 2% others (0.5-1 mm). The average density is 2.27 g/cc. To form rock mass models with two mutually perpendicular joint sets, cubical (4×4×4 cm) and rectangular (4×4×8 cm and 4×4×12 cm) sandstone blocks have been prepared using a saw-cutting machine. The cubical blocks are used to simulate joint sets with equal spacing, while the rectangular blocks simulate joint sets with different spacings. The friction angle and cohesion of the saw-cutting surfaces of the Phu Phan sandstone determined by tilt testing are 26° and 0.053 kPa [5]. The uniaxial compressive strength and elastic modulus of the sandstone determined from related research projects are 62.0 MPa and 10.3 GPa [5].

4. TEST MODELS UNDER STATIC CONDITION

Figure 2 shows the key variables defined in the physical test models. The model height, H, determines the applied maximum lithostatic pressure at the bottom of the model which is calculated as 28.0 kPa. The opening depth, D, is measured from the opening roof to the top of the model. The maximum unsupported span, W, corresponds to the maximum number of rock blocks removed before failure occurs. Spacings for the vertical and horizontal joint sets are defined as S_V and S_H for joint angles of 0° and 90°. For an inclined joint angle the apparent spacings projected on the vertical and horizontal planes are calculated. The effect of opening height is not studied here. It is always set equal to the block height which is the spacing of the horizontal joints, S_H, for each test model. The simulated joint sets have their strike parallel to the opening axis, and hence represent a worst case scenario of the opening stability.

For the block length from 4 cm to 12 cm tested here using the rock mass model width of 1.2 m is sufficiently large to minimize the edge effect on the results, as suggested by Zhu and Zhao [2] that a physical model width should be 10 times greater than the block size. Deformation and failure of the sandstone blocks are not considered in this study (assumed as rigid blocks) because the rock strength and stiffness are very high as compared to the maximum applied lithostatic stresses at 1.2 m depth.

Over fifty test models have been simulated under static condition with S_V:S_H ratios from 1:3, 1:2, 1:1, 2:1 to 3:1. The opening depths vary from 16 to 100 cm. Each set of opening geometries is formed by sandstone blocks with the same dimension. Video records are taken for a post-test analysis. After all blocks are arranged to the maximum height and width in the test frame, a rectangular opening is created by carefully removing a rock block at a pre-defined depth. The blocks adjacent to the opening on both sides are then removed one-by-one until movement or failure of the roof rocks is visually observed.

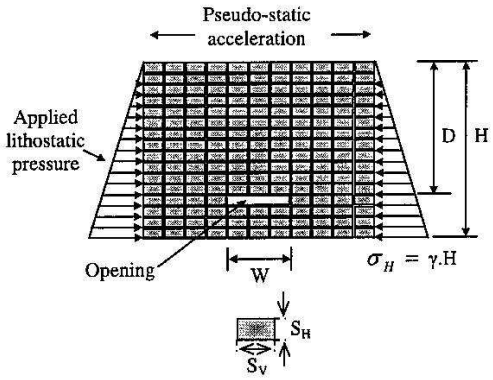

Figure 2 Variables used in physical model simulations and analysis. Joint inclination can be set at any angle by tilting the rock blocks in the model.

The opening width immediately before the failure occurs is taken as the maximum unsupported span. The test is repeated at least 3 times under the same condition to ensure the repeatability of the results.

Table 1 summarizes the ranges of test parameters and results under static conditions. The observed maximum unsupported spans (W) and their corresponding depths (D) are normalized by spacings of the vertical and horizontal joints (S_V and S_H), respectively. Figure 3 gives examples of the test models for various opening depths and joint spacings. Roof collapse occurs when the

Table 1 Ranges of test parameters and results under static condition

Spacing Ratio (S_V/S_H)	No. of Tests	Depth, D (cm)	D/S_H	Maximum Span, W (cm)	W/S_V
1:1	8	24-92	4.2-16.3	16-40	2.8-7.2
	21	16-96	4-24	12-28	3-7
1:2 or 2:1	8	24-80	4.2-14.1	12-32	2.1-5.6
1:2	12	24-96	3-12	12-28	2-7
1:3 or 3:1	6	28-88	5.1-15.5	12-32	2.1-5.6
1:3	8	24-84	2-7	12-24	3-6
2:1	8	20-92	5-23	8-40	1-5
3:1	8	36-100	9-25	12-48	1-4

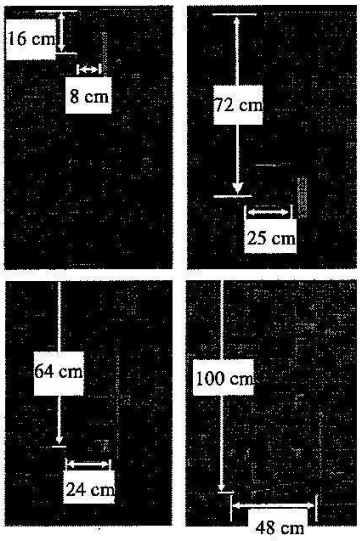

Figure 3 Examples of physical models showing roof failure after opening widths exceed their maximum unsupported spans. Top: openings in rock mass mo-del formed by 4×4 blocks. Bottom: openings in rock mass model formed by 4×12 blocks.

opening width exceeds its maximum unsupported span. Figure 4 plots the normalized maximum span (W/S_V) as a function of normalized depth (D/S_H) for various joints spacings. The results indicate that the maximum span increases with depth which can be best represented by a logarithmic equation. As the depth increases, the maximum span approaches an ultimate value for each joint spacing ratio (S_V/S_H). The maximum span also increases with decreasing S_V:S_H ratio, suggesting that it is more sensitive to the horizontal joint spacing than to the vertical one. This means that the maximum spans are larger for a smaller joint spacing ratio (smaller S_V or larger S_H). This probably holds true only for the range of the spacing ratios used here. For the condition where S_V=S_H, an inclination of the two joint sets to 45° results in an about 20% decrease in the maximum span.

The empirical relations between the normalized maximum span (W/S_V) and the normalized depth (D/S_H) can be expressed as:

$$W/S_V = A \cdot \ln(D/S_H) - B \qquad (1)$$

The constants A and B can be determined as a function of the joint spacing ratio (S_V/S_H) as follows:

$$A = \alpha_A \cdot (S_V/S_H) + \beta_A \qquad (2)$$

$$B = \alpha_B \cdot (S_V/S_H) + \beta_B \qquad (3)$$

where α_A, β_A, α_B, and β_B are empirical constants. Table 2 summarizes the numerical values for A, α_A, β_A, B, α_B, and β_B calculated for some applicable joint spacing ratios.

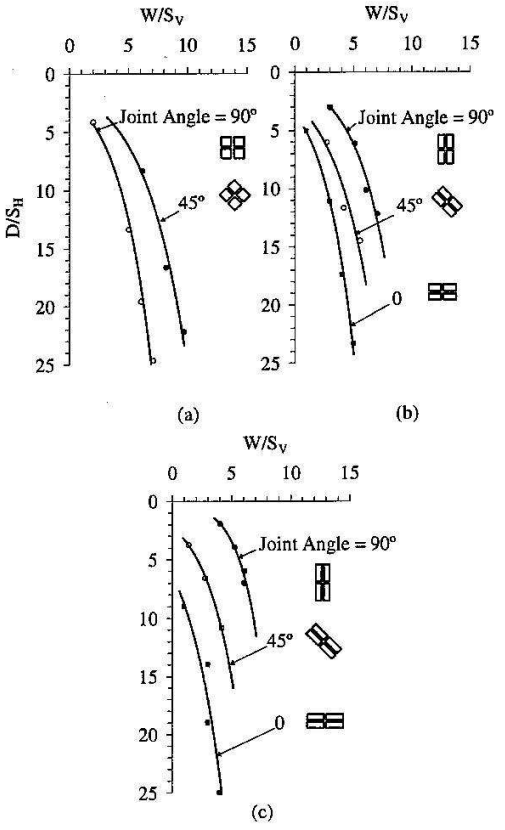

Figure 4 Normalized maximum span (W/S_V) as a function of normalized depth (D/S_H) for various joint spacing ratios and joint orientations.

The empirical relations above can probably represent a lower bound of the maximum unsupported span for

actual shallow openings under similar joint conditions and field stresses.

Table 2 Empirical relations obtained from regression analysis on the test results under static condition. $W/S_V = A \cdot \ln(D/S_H) - B$, where; $A = \alpha_A \cdot (S_V/S_H) + \beta_A$; $B = \alpha_B \cdot (S_V/S_H) + \beta_B$.

Spacing Ratio (S_V/S_H)	Block Arrange-ment	A	α_A	β_A	B	α_B	β_B
1:1		2.76			1.99		
1:2		2.76			0.02		
1:3		1.71	-0.28	2.60	-2.89	1.28	-1.02
2:1		2.56			3.16		
3:1		1.31			1.35		

5. TEST MODELS UNDER DYNAMIC LOADS

The effects of the pseudo-static accelerations of 0.132 g and 0.225 g on the maximum unsupported span have been experimentally assessed. Only the horizontal acceleration is simulated here because it has more impact on the geological structures than does the vertical acceleration [6]. The test procedure is similar to that under static condition.

Figure 5 plot the normalized maximum span as a function of normalized depth for testing under pseudo-static accelerations of 0.132 g and 0.225 g. Similar to the test results under static condition, the maximum span increases with depth which can be best represented by a logarithmic equation for each joint spacing ratio. As the depth increases, the maximum span approaches an ultimate value. The acceleration of 0.225 g can reduce the maximum span by up to 50%, particularly when the S_V:S_H ratio is greater than 2:1.

As the depth increases the maximum spans under dynamic loads are close to those tested under static condition, suggesting that the impact of dynamic loading decreases with depth. At shallow depth, a pseudo-static force generated by the cyclic motion of the test frame may be high enough to effectively reduce the normal stress at the rock block contacts.

This subsequently reduces their shearing resistance, resulting in a relative movement between the rock blocks immediately above the opening. As the depth increases, the same magnitude of the pseudo-static force may not be high enough to overcome the applied lateral lithostatic stress, and hence have smaller effect on the shearing resistance at the block contacts.

6. DISCRETE ELEMENT ANALYSES

Discrete element analyses are performed using UDEC code [7] to describe the stability conditions of the openings in the physical models. The discrete element models are constructed to represent various opening depths and joint spacing ratios. The joint friction angle and cohesion used in the simulations are 26° and 0.053 kPa. After several trials (by varying opening widths) the maximum unsupported span can be determined for each opening depth and joint spacing ratio.

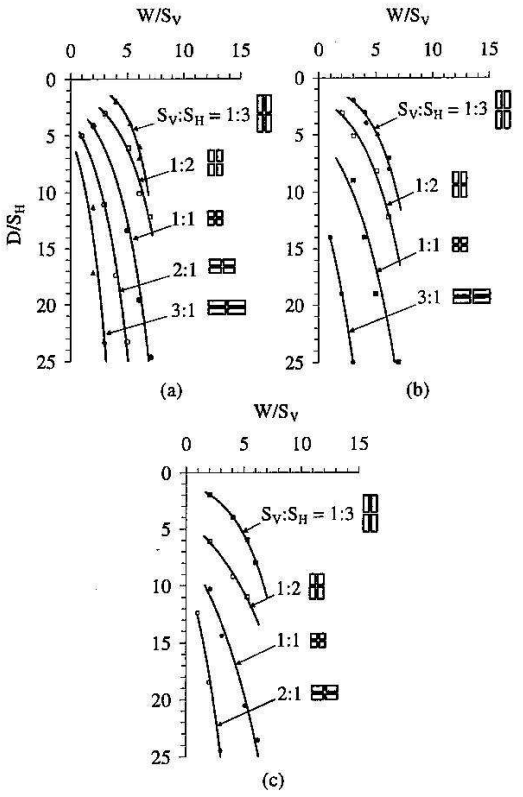

Figure 5 Normalized maximum span as a function of normalized depth under pseudo-static accelerations of 0.132 g (b) and 0.225 g (c) compared with the re-sults under static condition (a) for vertical and horizontal joint sets.

The UDEC results are compared with those observed from the physical models under static loading in Figure 6 and under dynamic loads in Figure 7 for various S_V:S_H ratios. The UDEC simulations show the increasing trends of the maximum span with depth which are similar to those observed from the test models. For all cases the predicted maximum spans slightly under-estimate the test results. The largest discrepancies are less than 20%. This is probably because the block models in the discrete element analyses are perfectly shaped with identical joint properties while in the test models the block shapes are not perfect and the frictional strength is unlikely to be identical for all contacts (joint surfaces). As a result the rock blocks constructed in the UDEC models can slide easier than those tested in the physical models, and hence yield a slightly narrower maximum unsupported span.

8. CONCLUSIONS

The physical model test results clearly indicate that the maximum unsupported span of shallow openings is controlled by the spacing and orientation of joints, S_V:S_H ratio, and depth. The smaller the S_V:S_H ratio, the larger the maximum span. Under the same depth and joint

spacing ratio, inclination of the joint angles from 0° to 45° can reduce the maximum span by up to 20%. The tested maximum span increases with depth and approaches an ultimate value for each joint spacing ratio, which conforms to the simulation results from discrete element analyses. The horizontal pseudo-static accelerations of 0.132 g and 0.225 g can significantly reduce the maximum unsupported span for shallow openings. Up to 50% reduction of the maximum opening span resulted for the acceleration of 0.225 g. The effect of the pseudo-static accelerations tends to be more pronounced under a larger S_V:S_H ratio. The dynamic impact however gradually reduces with depth, as evidenced by the fact that the observed maximum spans under both pseudo-static accelerations are close to those tested under static condition when the normalized depth, D/S_H, approaches 25.

The physical model results yield empirical relations between the maximum unsupported span and depth for shallow openings. Since the models are simulated under very simplified conditions of joints and stress states with a narrow range of test parameters, care should be taken in extrapolating these relations to actual in-situ openings under greater depths or under complex joint conditions and stress states.

9. ACKNOWLEDGEMENT

This research is funded by Suranaree University of Technology. Permission to publish this paper is gratefully acknowledged.

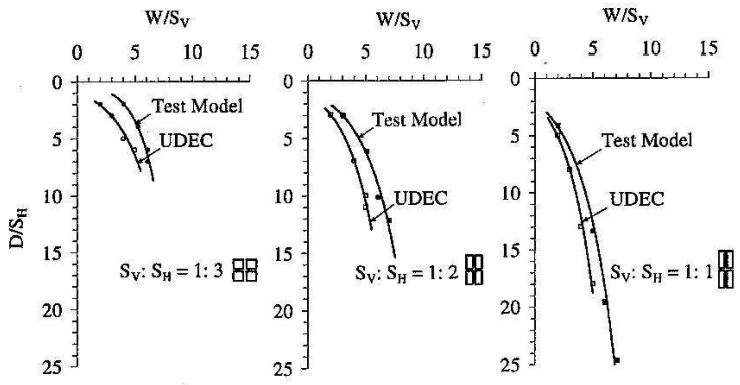

Figure 6 Comparisons of UDEC simulations with test models for various spacing ratios.

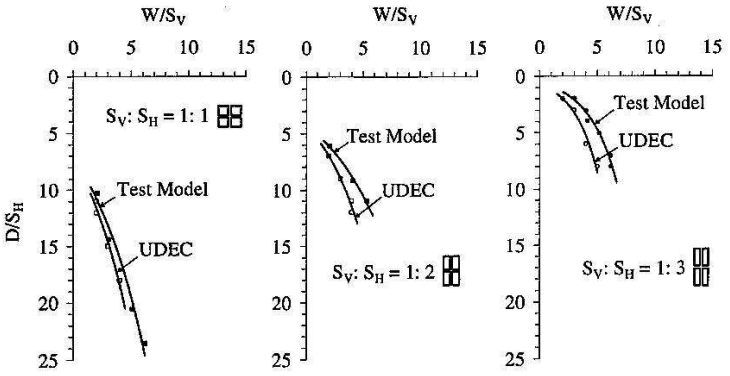

Figure 7 Comparisons of UDEC simulations with test models under pseudo-static acceleration of 0.225 g.

REFERENCES

[1] Lama, R.D. and Vutukuri, V.S. (1978). *Handbook on Mechanical Properties of Rocks*, Vol.4, Trans Tech Publication.

[2] Zhu, W. and Zhao, J. (2004). *Stability analysis and modelling of underground excavations in fractured rocks*, Elsevier Geo-Engineering Book Series Volume 1, Series Editor: Hudson, J.A. Netherlands: Elsevier.

[3] Sterpi, D. and Cividini, A. (2004). A physical and numerical investigation on the stability of shallow tunnels in strain softening media. *Rock Mechanics and Rock Engineering*, Vol.37, No.4, 277–298.

[4] Bhasin, R. and Hoeg, K. (1998). Numerical modeling of block size effects and influence of joint properties in multiply jointed rock. *Tunnelling and Underground Space Technolog*, Vol.13, No.2, 181-188.

[5] Pangpetch, P. and Fuenkajorn, K. (2007). Simulation of rock slope failure using physical model. *Proceedings of the First Thailand Symposium on Rock Mechanics*, Suranaree University of Technology, Nakhon Ratchasima, 227-243.

[6] Kramer, S.L. (1996). *Geotechnical earthquake engineering*, Prentice Hall, New Jersey.

[7] Itasca Consulting Group, Inc. (2004). *UDEC 4.0 GUI A Graphical User Interface for UDEC*, Minneapolis, Minnesota.

Rock Mechanics, Fuenkajorn & Phien-wej (eds) © 2009. ISBN 978 974 533 624 7

Physical model simulation of shallow openings in jointed rock mass under static and dynamic loads

C. Sakulnitichai, P. Pangpetch & K. Fuenkajorn
Geomechanics Research Unit, Suranaree University of Technology, Thailand

Keywords: Opening, joint, friction, dynamic load, acceleration

ABSTRACT: Physical model simulations have been performed to determine the effects of depth, joint spacing and orientation on the maximum unsupported span of shallow underground openings under static and dynamic loads. Cubical and rectangular blocks of Phu Phan sandstone are arranged in a vertical test frame to simulate a two-dimensional representation of single rectangular openings in rock mass with two mutually perpendicular joint sets. Results indicate that the normalized maximum span (W/S_V) rapidly increases with the normalized depth (D/S_H), and tends to approach a certain limit for each joint spacing ratio, S_V:S_H. The maximum span increases with decreasing S_V:S_H ratio. Under S_V=S_H condition, increasing the joint angles from 0° to 45° reduces the maximum span by about 20%. At shallow depths the acceleration of 0.225 g can reduce the maximum span by up to 50%. The impact of the dynamic loads however reduces as the depth increases. The test results under both static and dynamic loading compare reasonably well with those calculated from discrete element analyses using the UDEC code.

1 INTRODUCTION

Physical test models or scaled-down models have been widely used in the laboratory to simulate the stability conditions of underground openings in rock masses (Lama & Vutukuri, 1978; Stimpson, 1979; Bakhtar et al., 1986; Adhikary & Dyskin, 1997). They are commonly used to gain an understanding of the effects of unique rock characteristics, in-situ stress conditions or opening geometries (Zhu & Zhao, 2004). The simulations usually simplify the actual conditions into two-dimensional problems. Recently some researchers have developed sophisticated devices to allow a three-dimensional simulation for tunnel stability in rock mass under high stresses (e.g., Sterpi & Cividini, 2004; Li et al., 2005; Liu et al., 2006). As a result failure conditions of the joints and intact rocks around the openings can be simulated simultaneously. Some devices can incorporate the effects of dynamic loading on the rock models (Bakhtar, 1997; Ma & Brady, 1999). The modeling results are often compared with those from numerical simulations, usually by a discrete element analysis, either to verify the predictive capability of the computed results or to confirm the accuracy of the test models (Bhasin & Hoeg, 1998; Zhu et al., 2006). Most researchers (e.g. Zhu & Zhao, 2004; Li et al., 2005; Bakhtar, 1997; Liu et al., 2006) above concentrate on studying the opening stability

under site-specific conditions. Results obtained from the physical test models that can provide a more general solution of the opening stability in rock masses have been rare.

The objective of this research is to perform physical model tests to assess the effects of depth, joint spacing and orientation on the maximum unsupported span of shallow underground openings under static and dynamic loads. A vertical platform is used to test the rock mass model formed by cubical and rectangular blocks of Phu Phan sandstone. The models simulate two-dimensional sections of single rectangular openings in a rock mass with two mutually perpendicular joint sets. The vertical and horizontal joint spacings are varied from 4, 8 to 12 cm. The stability under horizontal pseudo-static accelerations of 0.132 g and 0.225 g is investigated. Empirical relations between the observed maximum span, opening depth and joint spacings are derived. They are used to predict the maximum span under shallow depths. The static and dynamic test results are compared with those simulated from discrete element analyses using UDEC code.

2 TEST PLATFORM

The test platform developed by Pangpetch & Fuenkajorn (2007) is used in this study (Figure 1). It can accommodate 4 cm thick rock blocks arranged to a maximum depth and width of 1.2 m to simulate a two-dimensional section of shallow openings in a jointed rock mass. A lateral lithostatic pressure is applied on both sides of the model using a column of crystal balls with a diameter of 16 mm packed in the gap between the model and the test frame. Bulk density of the pack of crystal balls is measured as 2.3 g/cc, which is comparable to the density of the intact block of Phu Phan sandstone. Elevated vertical and lateral stresses can be applied in the test frame to simulate the rock mass behavior under a great depth. They are not applied here because this study involves opening behavior at shallow depths as affected by joint system. Steel grooved rollers mounted underneath the frame are used for testing under dynamic loads. The rollers are placed on a set of steel rails equipped with a high torque motor, gear system and crank arm to induce a cyclic motion to the entire test platform. The frequency and amplitude of the horizontal pseudo-static acceleration can be controlled by adjusting the rotational diameter of the flywheel and speed of the motor.

3 ROCK SAMPLE

Sandstone from the Phu Phan formation is used here as rock. It is classified as fine-grained quartz sandstone with highly uniform texture, density and strength. The rock forming minerals include 72% quartz (0.2-0.8 mm), 20% feldspar (0.1-0.8 mm), 3% mica (0.1-0.3 mm), 3% rock fragments (0.5-2mm), and 2% others (0.5-1 mm). The average density is 2.27 g/cc. To form rock mass models with two mutually perpendicular joint sets, cubical (4×4×4 cm) and rectangular (4×4×8 cm and 4×4×12 cm) sandstone blocks have been prepared using a saw-cutting machine. The cubical blocks are used to simulate joint sets with equal spacing, while the rectangular blocks simulate joint sets with different spacings. The friction angle and cohesion of the saw-cutting surfaces of the Phu Phan sandstone determined by tilt testing are 26° and 0.053 kPa (Pangpetch & Fuenkajorn, 2007). The uniaxial compressive strength and elastic modulus of the sandstone determined from related research projects are 62.0 MPa and 10.3 GPa.

Rock Mechanics, Fuenkajorn & Phien-wej (eds) © 2009. ISBN 978 974 533 624 7

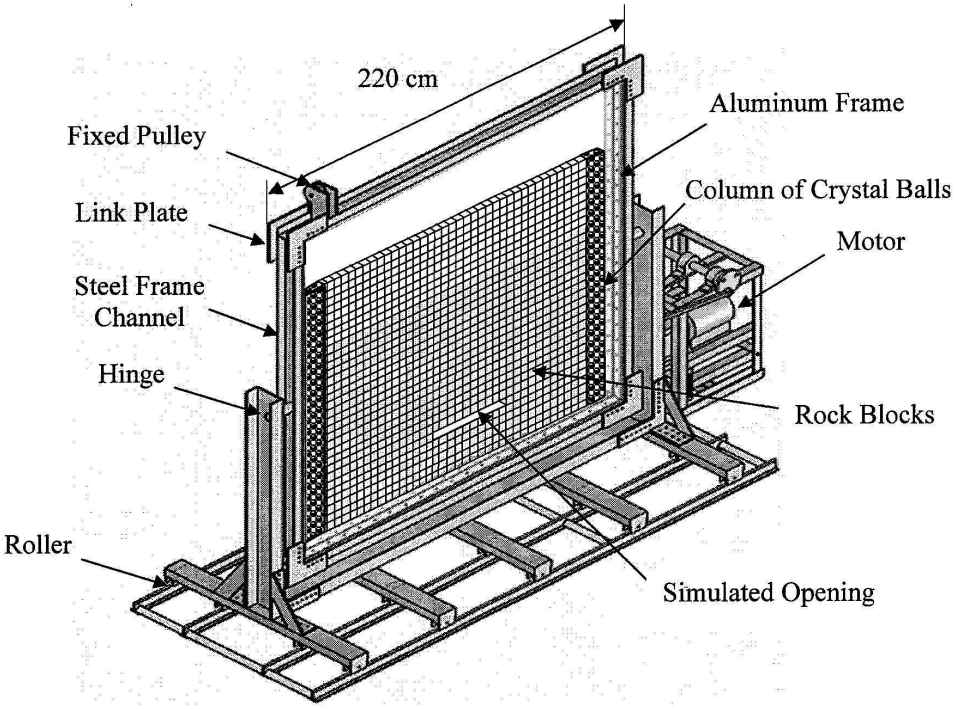

Figure 1. Test platform used to simulate shallow openings in rock mass.

4 TEST MODELS UNDER STATIC CONDITION

Figure 2 shows the key variables defined in the physical test models. The model height, H, determines the applied maximum lithostatic pressure at the bottom of the model which is calculated as 28.0 kPa. The opening depth, D, is measured from the opening roof to the top of the model. The maximum unsupported span, W, corresponds to the maximum number of rock blocks removed before failure occurs. Spacings for the vertical and horizontal joint sets are defined as S_V and S_H for joint angles of 0° and 90°. For an inclined joint angle the apparent spacings projected on the vertical and horizontal planes are calculated. The effect of opening height is not studied here. It is always set equal to the block height which is the spacing of the horizontal joints, S_H, for each test model. The simulated joint sets have their strike parallel to the opening axis, and hence represent a worst case scenario of the opening stability.

For the block length from 4 cm to 12 cm tested here using the rock mass model width of 1.2 m is sufficiently large to minimize the edge effect on the results, as suggested by Zhu & Zhao (2004) that a physical model width should be 10 times greater than the block size. Deformation and failure of the sandstone blocks are not considered in this study (assumed as rigid blocks) because the rock strength and stiffness are very high as compared to the maximum applied lithostatic stresses at 1.2 m depth.

Over fifty test models have been simulated under static condition with S_V:S_H ratios from 1:3, 1:2, 1:1, 2:1 to 3:1. The opening depths vary from 16 to 100 cm. Each set of opening geometries is formed by sandstone blocks with the same dimension. Video records are taken

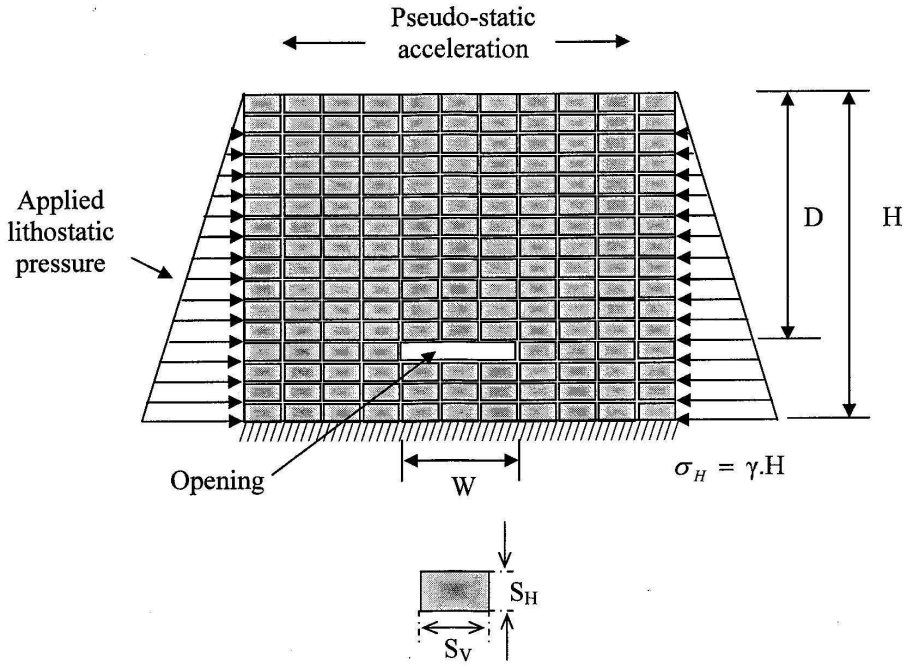

Figure 2. Variables used in physical model simulations and analysis. Joint inclination can be set at any angle by tilting the rock blocks in the model.

for a post-test analysis. After all blocks are arranged to the maximum height and width in the test frame, a rectangular opening is created by carefully removing a rock block at a pre-defined depth. The blocks adjacent to the opening on both sides are then removed one-by-one until movement or failure of the roof rocks is visually observed. The opening width immediately before the failure occurs is taken as the maximum unsupported span. The test is repeated at least 3 times under the same condition to ensure the repeatability of the results.

Table 1 summarizes the ranges of test parameters and results under static conditions. The observed maximum unsupported spans (W) and their corresponding depths (D) are normalized by spacings of the vertical and horizontal joints (S_V and S_H), respectively. Figure 3 gives examples of the test models for various opening depths and joint spacings. Roof collapse occurs when the opening width exceeds its maximum unsupported span. Figure 4 plots the normalized maximum span (W/S_V) as a function of normalized depth (D/S_H) for various joints spacings. The results indicate that the maximum span increases with depth which can be best represented by a logarithmic equation. As the depth increases, the maximum span approaches an ultimate value for each joint spacing ratio (S_V/S_H). The maximum span also increases with decreasing S_V:S_H ratio, suggesting that it is more sensitive to the horizontal joint spacing than to the vertical one. This means that the maximum spans are larger for a smaller joint spacing ratio (smaller S_V or larger S_H). This probably holds true only for the range of the spacing ratios used here. For the condition where S_V=S_H, an inclination of the two joint sets to 45° results in an about 20% decrease in the maximum span.

The empirical relations between the normalized maximum span (W/S_V) and the normalized depth (D/S_H) can be expressed as:

Rock Mechanics, Fuenkajorn & Phien-wej (eds) © 2009. ISBN 978 974 533 624 7

Table 1. Ranges of test parameters and results under static condition.

Spacing Ratio (S_V/S_H)	Block Arrangement	S_V	S_H	No. of Tests	Depth, D (cm)	D/S_H	Maximum Span, W (cm)	W/S_V
1:1		2.88	2.88	8	24-92	4.2-16.3	16-40	2.8-7.2
		4	4	21	16-96	4-24	12-28	3-7
1:2 or 2:1		2.88	5.66	8	24-80	4.2-14.1	12-32	2.1-5.6
1:2		8	4	12	24-96	3-12	12-28	2-7
1:3 or 3:1		2.88	8.48	6	28-88	5.1-15.5	12-32	2.1-5.6
1:3		12	4	8	24-84	2-7	12-24	3-6
2:1		4	8	8	20-92	5-23	8-40	1-5
3:1		4	12	8	36-100	9-25	12-48	1-4

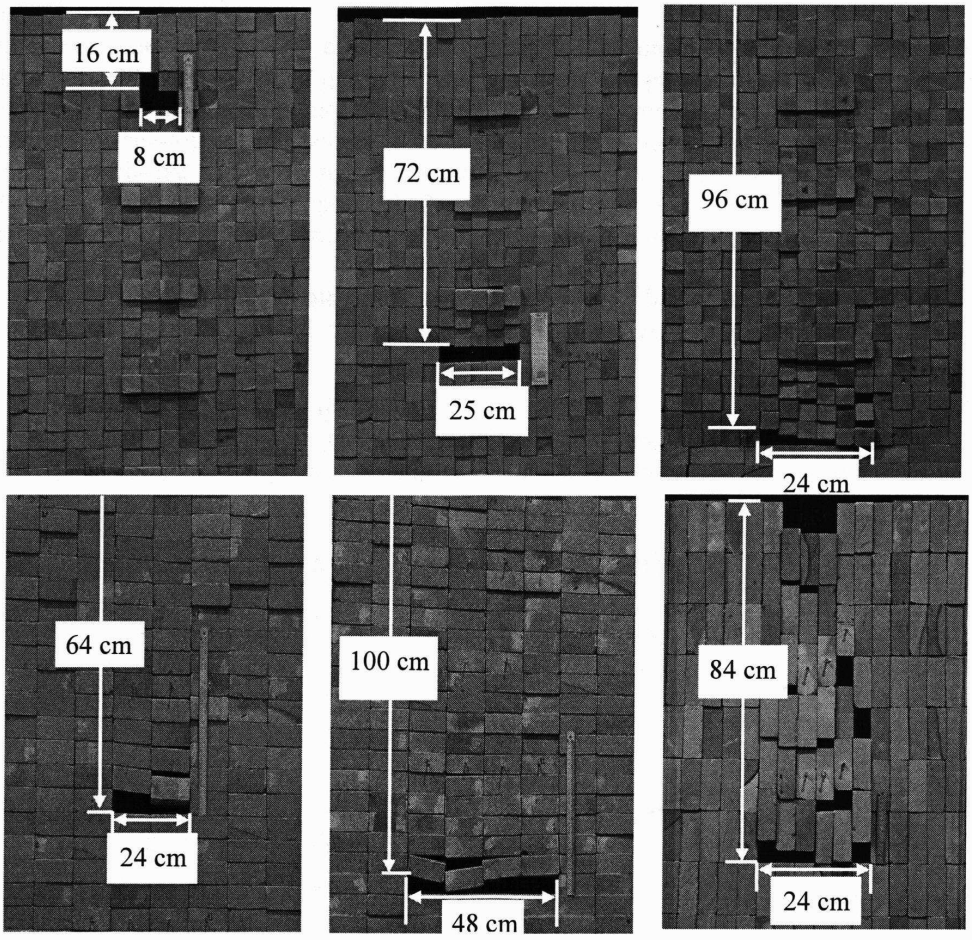

Figure 3. Examples of physical models showing roof failure after opening widths exceed their maximum unsupported spans. Top: openings in rock mass model formed by 4×4 blocks. Bottom: openings in rock mass model formed by 4×12 blocks.

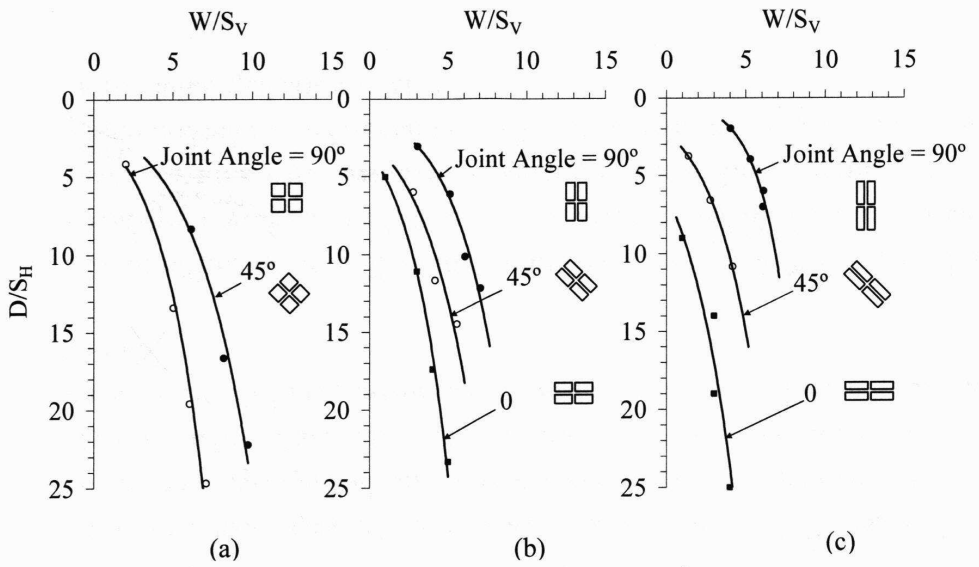

Figure 4. Normalized maximum span (W/S_V) as a function of normalized depth (D/S_H) for various joint spacing ratios and joint orientations. The empirical relations of the results are given in Table 2.

$$W/S_V = A \cdot \ln(D/S_H) - B \tag{1}$$

The constants A and B can be determined as a function of the joint spacing ratio (S_V/S_H) as follows:

$$A = \alpha_A \cdot (S_V/S_H) + \beta_A \tag{2}$$

$$B = \alpha_B \cdot (S_V/S_H) + \beta_B \tag{3}$$

where α_A, β_A, α_B, and β_B are empirical constants. Table 2 summarizes the numerical values for A, α_A, β_A, B, α_B, and β_B calculated for some applicable joint spacing ratios. The empirical relations above can probably represent a lower bound of the maximum unsupported span for actual shallow openings under similar joint conditions and field stresses.

5 TEST MODELS UNDER DYNAMIC LOADS

The effects of the pseudo-static accelerations of 0.132 g and 0.225 g on the maximum unsupported span have been experimentally assessed. Only the horizontal acceleration is simulated here because it has more impact on the geological structures than does the vertical acceleration (Kramer, 1996). The test procedure is similar to that under static condition. After removing a rock block at a pre-defined depth a pseudo static acceleration is applied for one minute. If no displacement of the rock blocks is observed, a block adjacent to the opening on each side is then removed, and the acceleration is re-applied. The process is repeated until any visible movement or failure of roof rock is obtained. The opening width immediately before the failure occurs is taken as the maximum unsupported span under the given acceleration.

Rock Mechanics, Fuenkajorn & Phien-wej (eds) © 2009. ISBN 978 974 533 624 7

Table 2. Empirical relations obtained from regression analysis on the test results under static condition. $W/S_V = A \cdot \ln (D/S_H) - B$, where; $A = \alpha_A \cdot (S_V/S_H) + \beta_A$; $B = \alpha_B \cdot (S_V/S_H) + \beta_B$.

Spacing Ratio (S_V/S_H)	Block Arrangement	A	α_A	β_A	B	α_B	β_B
1:1		2.76	-0.28	2.60	1.99	1.28	-1.02
1:2		2.76			0.02		
1:3		1.71			-2.89		
2:1		2.56			3.16		
3:1		1.31			1.35		

Table 3 summarizes the ranges of the test parameters and the results under dynamic loads. Figures 5 and 6 plot the normalized maximum span as a function of normalized depth for testing under pseudo-static accelerations of 0.132 g and 0.225 g. Similar to the test results under static condition, the maximum span increases with depth which can be best represented by a logarithmic equation for each joint spacing ratio. Numerical values for the empirical constants are listed in Table 4. As the depth increases, the maximum span approaches an ultimate value. The higher the acceleration applied to the test models, the smaller the maximum span obtained. The acceleration of 0.225 g can reduce the maximum span by up to 50%, particularly when the S_V:S_H ratio is greater than 2:1.

As the depth increases the maximum spans under dynamic loads are close to those tested under static condition, suggesting that the impact of dynamic loading decreases with depth. At shallow depth, a pseudo-static force generated by the cyclic motion of the test frame may be high enough to effectively reduce the normal stress at the rock block contacts. This subsequently reduces their shearing resistance, resulting in a relative movement between the rock blocks immediately above the opening. As the depth increases, the same magnitude of the pseudo-static force may not be high enough to overcome the applied lateral lithostatic stress, and hence have smaller effect on the shearing resistance at the block contacts.

6 DISCRETE ELEMENT ANALYSES

Discrete element analyses are performed using UDEC code (Itasca, 2004) to describe the stability conditions of the openings in the physical models. The discrete element models are constructed to represent various opening depths and joint spacing ratios. The joint friction angle and cohesion used in the simulations are 26° and 0.053 kPa. After several trials (by varying opening widths) the maximum unsupported span can be determined for each opening depth and joint spacing ratio.

The UDEC results are compared with those observed from the physical models under static loading in Figure 7 and under dynamic loads in Figure 8 for various S_V:S_H ratios. The UDEC simulations show the increasing trends of the maximum span with depth which are similar to those observed from the test models. For all cases the predicted maximum spans slightly under-estimate the test results. The largest discrepancies are less than 20%. This is probably because the block models in the discrete element analyses are perfectly shaped with identical joint properties while in the test models the block shapes are not perfect and the frictional

Table 3. Results of physical models tested under dynamic loads.

Spacing Ratio (S_V/S_H)	Block Arrangement	No. of Tests	D (cm)	D/S_H	W (cm)	W/S_V	Frequency (Hz)	a (g)	Modified Mercalli Intensity*
1:1		8	40-92	8-24	8-24	2-6	1.833	0.225	VII
		8	40-92	7-16	16-32	3-6	1.429	0.132	VI
1:2 or 2:1		6	32-84	6-15	8-24	1-4	1.833	0.225	VII
1:2		9	24-96	3-12	8-24	2-6	1.429	0.132	VI
		8	24-96	3-12	8-20	2-5	1.833	0.225	VII
1:3 or 3:1		9	40-88	7-16	12-28	2-5	1.429	0.132	VI
		9	40-88	7-16	8-24	1-3.5	1.833	0.225	VII
1:3		12	24-96	2-8	12-24	3-6	1.429	0.132	VI
		8	24-96	2-8	8-24	2-6	1.833	0.225	VII
2:1		8	24-96	6-24	8-24	1-3	1.833	0.225	VII
3:1		8	36-100	9-25	12-36	1-3	1.429	0.132	VI

* Modified Mercalli Intensity from Richter (1958) and Wald et al. (1999) as:
VI = Felt by all; many frightened. Some heavy furniture moved; a few instances of fallen plaster. Damage slight.
VII = Damage negligible in building of good design and construction; slight to moderate in well-built ordinary structures; considerable damage in poorly built or badly designed structures; some chimneys broken.

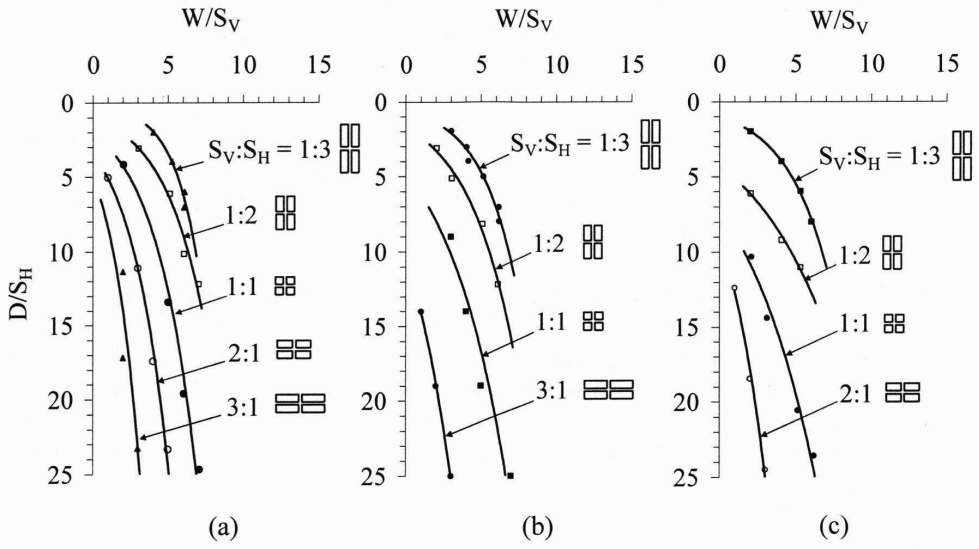

Figure 5. Normalized maximum span as a function of normalized depth under pseudo-static accelerations of 0.132 g (b) and 0.225 g (c) compared with the results under static condition (a) for vertical and horizontal joint sets with various spacing ratios.

Rock Mechanics, Fuenkajorn & Phien-wej (eds) © 2009. ISBN 978 974 533 624 7

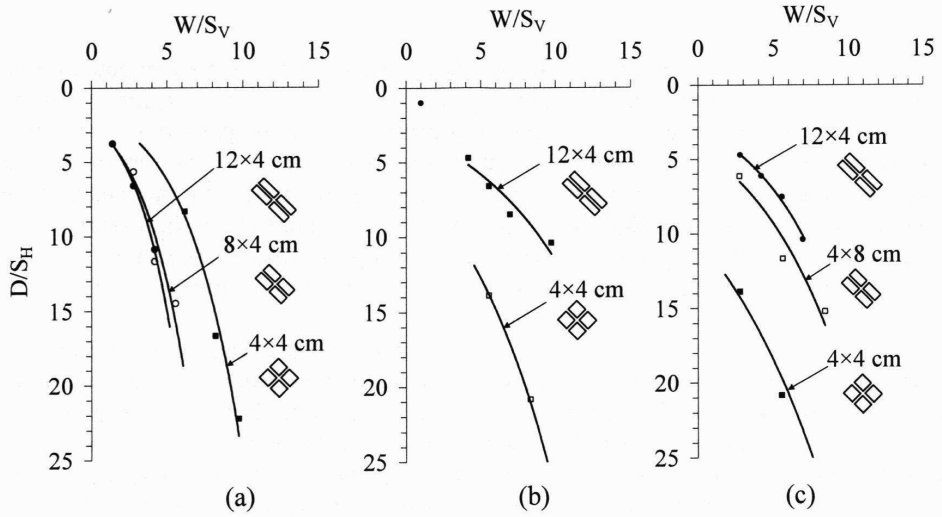

Figure 6. Normalized maximum span as a function of normalized depth under pseudo-static accelerations of 0.132 g (b) and 0.225 g (c) compared with the results under static condition (a) for 45°-inclined joint sets.

strength is unlikely to be identical for all contacts (joint surfaces). As a result the rock blocks constructed in the UDEC models can slide easier than those tested in the physical models, and hence yield a slightly narrower maximum unsupported span.

7 MAXIMUM SPANS ESTIMATED FROM Q AND RMR SYSTEMS

The maximum unsupported span predicted by the empirical equation derived from the test models is compared with those estimated from the RMR and Q systems of rock mass classification (Hoek & Brown, 1980). The comparisons are made for an assumed mine opening at depths (D) ranging from 25, 50, 75 to 100 m. The empirical equation derived for the test results of 4×4 cm blocks is used in the comparison. The joint spacings are assumed as 10, 30 and 50 cm.

Table 4. Empirical relations obtained from regression analysis on the test results under dynamics load at a = 0.132 g and 0.225 g. $W/S_V = A \cdot \ln(D/S_H) - B$, where; $A = \alpha_A \cdot (S_V/S_H) + \beta_A$; $B = \alpha_B \cdot (S_V/S_H) + \beta_B$.

a (g)	Spacing Ratio (S_V/S_H)	Block Arrangement	A	α_A	β_A	B	α_B	β_B
0.132	1:1		3.74	0.24	2.88	5.54	2.95	-0.06
	1:2		3.11			1.65		
	1:3		2.38			-1.28		
	3:1		3.45			8.11		
0.225	1:1		4.93	-0.66	4.69	9.65	2.00	4.06
	1:2		5.49			7.95		
	1:3		2.92			-0.02		
	2:1		2.90			6.34		

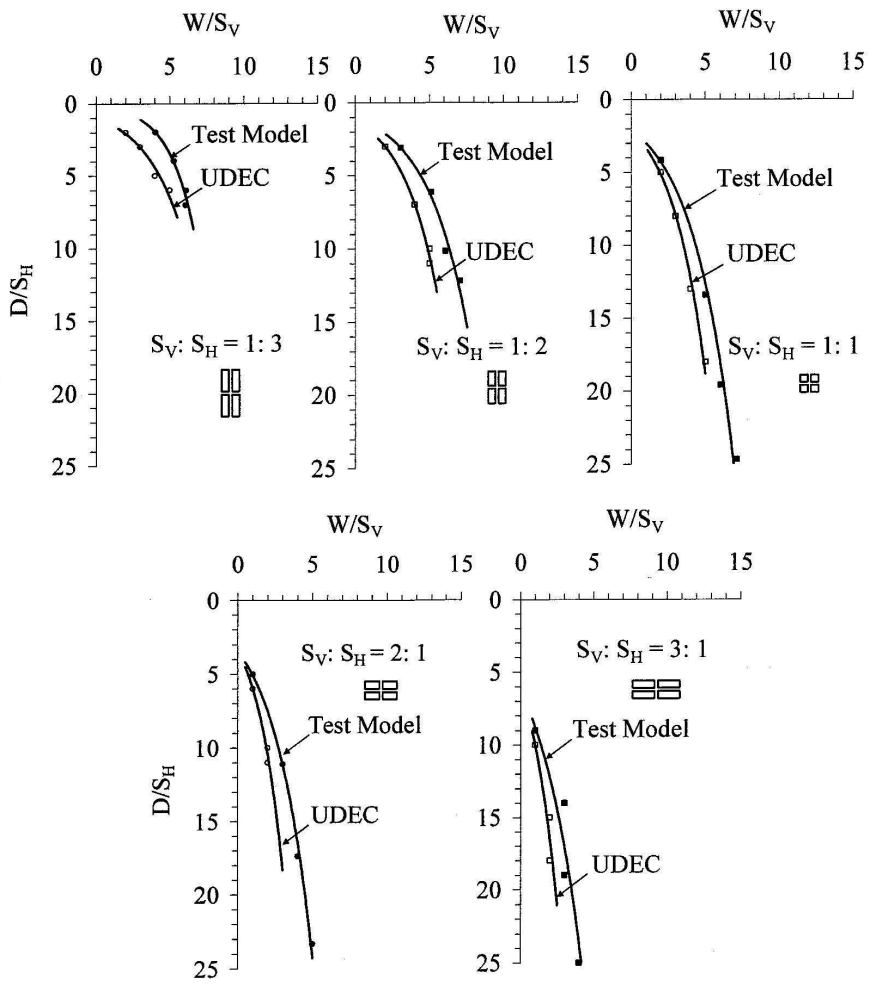

Figure 7. Comparisons of UDEC simulations with test models for various spacing ratios.

The rating parameters used in the RMR and Q classification systems are determined or projected from the relevant conditions used in the test models. The rock mass is completely dry, with three sets of slick, planar and open joints (two sets parallel to the opening axis, one set normal to the opening axis). The joint orientations represent a very unfavorable stability condition. The joints are continuous, having 100% persistence with no alteration. The joint spacings defined above are used to approximate the corresponding RQD's for this example. The intact rock compressive strength of 62.0 MPa is used, representing the actual strength of Phu Phan sandstone.

Table 5 compares the maximum spans estimated from RMR and Q systems with those predicted from the physical models using empirical equation from Table 2. The physical model predicts the span narrower than the RMR and Q systems do, particularly at shallow depths. This is probably due to the high magnitudes of RQD's estimated from the joint spacings, leading to a high value for RMR and Q, and subsequently makes the calculated maximum span larger. The discrepancies become smaller as the depth increases. At 100 m depth the maximum span from the three methods are comparable.

Rock Mechanics, Fuenkajorn & Phien-wej (eds) © 2009. ISBN 978 974 533 624 7

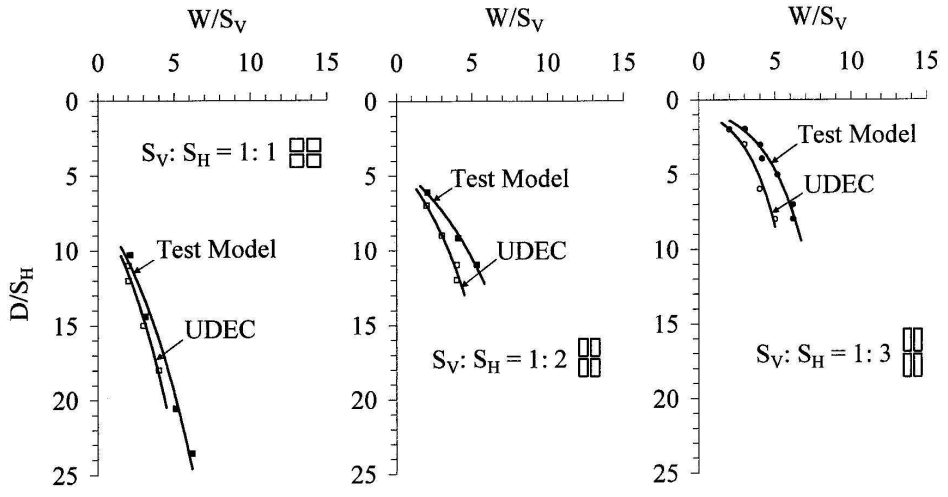

Figure 8. Comparisons of UDEC simulations with test models under pseudo-static acceleration of 0.225 g.

Under these assumed conditions, the maximum spans determined from the RMR and Q systems are chiefly governed by the joint spacing, and are independent of opening depth. This is because the RMR system does not consider the effect of depth or in-situ stress in the calculation. For the Q system the effect of in-situ stresses is represented by the stress reduction factor (SRF). Here the SRF is set equal to 1.0 because the openings are at relatively shallow depths. The maximum spans predicted by the physical model can however increase with the opening depth and joint spacing, which are probably similar to the actual opening behavior. This is also supported by the UDEC simulation results. Despite the discrepancies and the limitation of the proposed empirical equations, as a minimum, the physical model predictions can give a lower bound for the maximum unsupported span for shallow openings in rock mass, under similar rock strengths and joint conditions as tested here.

8 CONCLUSIONS

The physical model test results clearly indicate that the maximum unsupported span of shallow openings is controlled by the spacing and orientation of joints, S_V:S_H ratio, and depth. The smaller the S_V:S_H ratio, the larger the maximum span. Under the same depth and joint spacing ratio, inclination of the joint angles from 0° to 45° can reduce the maximum span by up to 20%. The tested maximum span increases with depth and approaches an ultimate value for each joint spacing ratio, which conforms to the simulation results from discrete element analyses. It is believed that such similar behavior occurs in actual in-situ conditions, which however can not be described by the RMR and Q systems of rock mass classification.

The horizontal pseudo-static accelerations of 0.132 g and 0.225 g can significantly reduce the maximum unsupported span for shallow openings. Up to 50% reduction of the maximum opening span resulted for the acceleration of 0.225 g. The effect of the pseudo-static accelerations tends to be more pronounced under a larger S_V:S_H ratio. The dynamic impact however gradually reduces with depth, as evidenced by the fact that the observed maximum spans under both pseudo-static accelerations are close to those tested under static condition when the normalized depth, D/S_H, approaches 25.

Table 5. Predictions of maximum unsupported spans using empirical equations and RMR and Q rock mass classification systems.

D (m)	Assumed S_V and S_H (m)	RQD	Q	RMR	W from Q system* (m)	W from RMR system** (m)	W from test model*** (m)
25	0.1	74	0.41	34	5.5	4.5	1.3
	0.3	96	0.53	41	6.1	6.2	3.0
	0.5	98	0.55	51	6.2	9.0	4.4
50	0.1	74	0.41	34	5.5	4.5	1.4
	0.3	96	0.53	41	6.1	6.2	3.5
	0.5	98	0.55	51	6.2	9.0	5.2
75	0.1	74	0.41	34	5.5	4.5	1.5
	0.3	96	0.53	41	6.1	6.2	3.8
	0.5	98	0.55	51	6.2	9.0	5.7
100	0.1	74	0.41	34	5.5	4.5	1.6
	0.3	96	0.53	41	6.1	6.2	4.0
	0.5	98	0.55	51	6.2	9.0	6.0

* For Q system of rock mass classification:

$$W = 2 \cdot ESR \cdot Q^{0.4}$$

ESR = 3.0 (for temporary mine openings), RQD = 100 exp $(-0.1/S_V)(1+0.1/S_V)$, where $S_V = S_H$

$$Q = \left(\frac{RQD}{J_n}\right) \times \left(\frac{J_r}{J_a}\right) \times \left(\frac{J_w}{SRF}\right)$$

J_n = 9.0 (for 3 joint sets), J_r = 0.5 (for slick and planar joints), J_a = 1.0 (for no alteration of joints), J_w = 1.0 (for dry condition), SRF = 5.0 (for loose rock with open discontinuities)

** For RMR system of rock mass classification:
UCS = 62.0 MPa, Open and continuous joints, Correction factor = -12 (for joints with very unfavorable orientation)

*** For physical model (from 4×4 cm blocks):

$$W = S_V \cdot [2.32 \cdot \ln(D/S_H) - 0.26]$$

The physical model results yield empirical relations between the maximum unsupported span and depth for shallow openings. Since the models are simulated under very simplified conditions of joints and stress states with a narrow range of test parameters, care should be taken in extrapolating these relations to actual in-situ openings under greater depths or under complex joint conditions and stress states.

ACKNOWLEDGEMENT

This research is funded by Suranaree University of Technology. Permission to publish this paper is gratefully acknowledged.

Rock Mechanics, Fuenkajorn & Phien-wej (eds) © 2009. ISBN 978 974 533 624 7

REFERENCES

Adhikary, D.P. & Dyskin, A.V., 1997. Modelling the deformation of underground excavation in layered rock masses. *International Journal of Rock Mechanics and Mining Sciences*. 34(3): 714-719.

Bakhtar, K. 1997. Studies under physical modeling at 1-g. *International Journal of Rock Mechanics and Mining Sciences*. 34(3-4): 536.

Bakhtar, K., Jones, A.H. & Cameron, R., 1986. Use of rock simulators for rock mechanics studies. In *Proceedings of the 27th US Symposium on Rock Mechanics*. Society of Mining Engineers of AIME. New York. pp. 219-223.

Bhasin, R. & Hoeg, K., 1998. Numerical modeling of block size effects and influence of joint properties in multiply jointed rock. *Tunnelling and Underground Space Technology*. 13(2): 181-188.

Hoek, E. & Brown, E.T., 1980. *Underground Excavations in Rock*. London: The Institution of Mining and Metallurgy.

Itasca Consulting Group, Inc., 2004. *UDEC 4.0 GUI A Graphical User Interface for UDEC*, Minneapolis, Minnesota.

Kramer, S.L, 1996. *Geotechnical earthquake engineering*. New Jersey: Prentice Hall.

Lama, R.D. & Vutukuri, V.S., 1978. *Handbook on Mechanical Properties of Rocks*, Vol. 4. Trans Tech Publication.

Li, Z., Liu, H., Dai, R. & Su, X., 2005. Application of numerical analysis principles and key technology for high fidelity simulation to 3-D physical model tests for underground caverns. *Tunnelling and Underground Space Technology*. 20: 390-399.

Liu, T., Shen, M., Tao, B., He, Z. & Yuan, Y., 2006. Model test and 3d numerical simulation study on excavation of double-arch tunnel. *Yanshilixue Yu Gongcheng Xuebao/Chinese Journal of Rock Mechanics and Engineering*. Academia Sinica. 25(9): 1802-1808.

Ma, M. & Brady, B.H., 1999. Analysis of the dynamic performance of an underground excavation in jointed rock under repeated seismic loading. *Geotechnical and Geological Engineering*. 17(1): 1-20.

Pangpetch, P. & Fuenkajorn, K., 2007. Simulation of rock slope failure using physical model. In *Proceedings of the First Thailand Symposium on Rock Mechanics*. Suranaree University of Technology, Nakhon Ratchasima. pp. 227-243.

Richter, C., 1958. *Elementary Seismology*. San Francisco: W.H. Freeman and Co.

Sterpi, D. & Cividini, A. 2004. A physical and numerical investigation on the stability of shallow tunnels in strain softening media. *Rock Mechanics and Rock Engineering*. 37 (4): 277–298.

Stimpson, B., 1979. Simple physical modelling technique for the demonstration of interaction between underground openings. *International Journal of Rock Mechanics and Mining Sciences & Geomechanics Abstracts*. 16(3): 217-219.

Wald, D.A., Quitoriano, V., Heaton, T.H. & Kanamori, H., 1999. Relationships between peak ground acceleration, peak ground velocity, and modified Mercalli intensity in California. *Earthquake Spectra*. 15: 557-564.

Zhu, H., Zhang, F., Drumm, E.C., Chin, C.T. & Zhang, D., 2006. 2D model tests and numerical simulation in shallow tunneling considering existing building load. *Underground Construction and Ground Movement (GPS 155). In Proceedings of Sessions of GeoShanghai 2006*. pp. 304-311.

Zhu, W. & Zhao, J., 2004. *Stability analysis and modelling of underground excavations in fractured rocks*. Elsevier Geo-Engineering Book Series Volume 1, Series Editor: Hudson, J.A. Netherlands: Elsevier.

BIOGRAPHY

Mr. Chatkun Sakulnitichai was born on November 17, 1985 in Nakhon Ratchasima province, Thailand. He received his Bachelor's Degree in Engineering (Geotechnology) from Suranaree University of Technology in 2007. For his post-graduate, he continued to study with a Master's degree in the Geological Engineering Program, Institute of Engineering, Suranaree university of Technology. During, 2007-2009, he was a research assistant at the Geomechanics Research Unit, Institute of Engineering, Suranaree University of Technology. He published technical papers related to rock mechanics as; "*Simulation of Shallow Opening in Jointed Rock Mass under Static and Dynamic Loading using Physical Model*" in the 14th National Convention on Civil Engineering. Nakhon Ratchasima, Thailand *"Physical model simulation of shallow openings in jointed rock mass under static and dynamic loads"*. Bangkok, Thailand, and *"Physical model simulation of shallow openings in jointed rock mass under static and dynamic loads*" in the proceeding of the second Thailand symposium on rock mechanics. Chonburi, Thailand.